UNIVERSIDADE FEDERAL DO PARANÁ

LUNA RHAINE NASCIMENTO OLIVEIRA

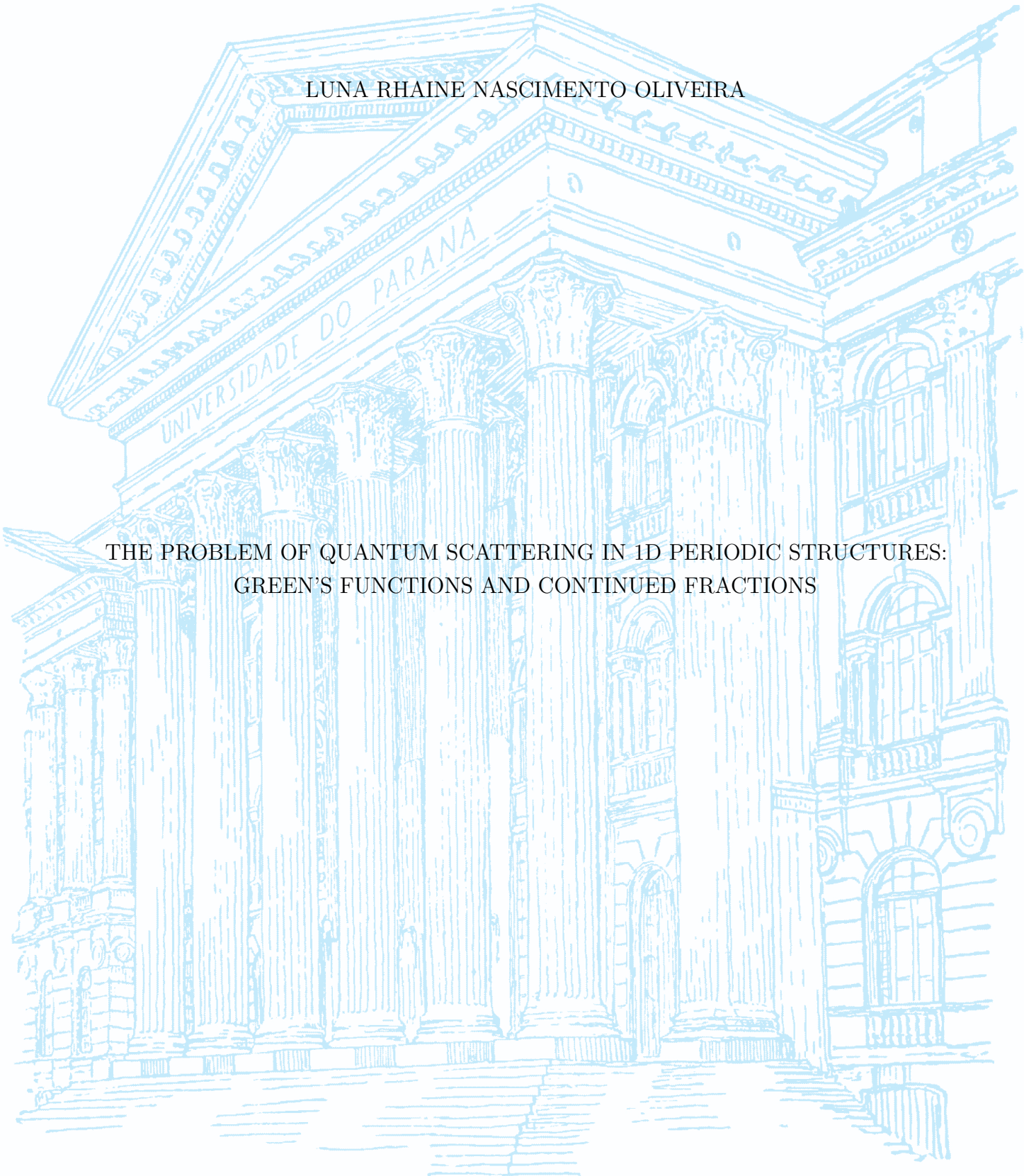

THE PROBLEM OF QUANTUM SCATTERING IN 1D PERIODIC STRUCTURES: GREEN'S FUNCTIONS AND CONTINUED FRACTIONS

CURITIBA

2023

LUNA RHAINE NASCIMENTO OLIVEIRA

THE PROBLEM OF QUANTUM SCATTERING IN 1D PERIODIC STRUCTURES: GREEN'S FUNCTIONS AND CONTINUED FRACTIONS

Dissertação apresentada ao *Programa de Pós-graduação em Física* do *Setor de Ciências Exatas* da *Universidade Federal do Paraná*, como parte dos requisitos necessários à obtenção do grau de Mestre em Física.

Supervisor: Prof. Dr. Marcos Gomes E. da Luz.

CURITIBA
2023

DADOS INTERNACIONAIS DE CATALOGAÇÃO NA PUBLICAÇÃO (CIP)
UNIVERSIDADE FEDERAL DO PARANÁ
SISTEMA DE BIBLIOTECAS – BIBLIOTECA CIÊNCIA E TECNOLOGIA

Oliveira, Luna Rhaine Nascimento.
The problem of quantum scattering in 1D periodic structures : Green's functions and continued fractions. / Luna Rhaine Nascimento Oliveira. – Curitiba, 2023.
1 recurso on-line : PDF.

Dissertação (Mestrado) – Universidade Federal do Paraná, Setor de Ciências Exatas, Programa de Pós-Graduação em Física.
Orientador: Prof. Dr. Marcos Gomes E. da Luz.

1. Física. 2. Teoria quântica. 3. Espalhamento quântico. 4. Delta de Dirac. I. Luz, Marcos Gomes E. da. II. Universidade Federal do Paraná. Programa de Pós-Graduação em Física. III. Título.

Bibliotecário: Nilson Carlos Vieira Júnior CRB-9/1797

TERMO DE APROVAÇÃO

Os membros da Banca Examinadora designada pelo Colegiado do Programa de Pós-Graduação FÍSICA da Universidade Federal do Paraná foram convocados para realizar a arguição da dissertação de Mestrado de **LUNA RHAINE NASCIMENTO OLIVEIRA** intitulada: **"The problem of quantum scattering in 1D periodic structures: Green's functions and continued fractions"**, sob orientação do Prof. Dr. MARCOS GOMES ELEUTÉRIO DA LUZ, que após terem inquirido a aluna e realizada a avaliação do trabalho, são de parecer pela sua APROVAÇÃO no rito de defesa.

A outorga do título de mestra está sujeita à homologação pelo colegiado, ao atendimento de todas as indicações e correções solicitadas pela banca e ao pleno atendimento das demandas regimentais do Programa de Pós-Graduação.

CURITIBA, 27 de Fevereiro de 2023.

Assinatura Eletrônica
27/02/2023 22:22:20.0
MARCOS GOMES ELEUTÉRIO DA LUZ
Presidente da Banca Examinadora

Assinatura Eletrônica
28/02/2023 08:48:07.0
LUIS GUILHERME DE CARVALHO REGO
Avaliador Externo (UNIVERSIDADE FEDERAL DE SANTA CATARINA)

Assinatura Eletrônica
28/02/2023 17:49:04.0
CRISTIANO FRANCISCO WOELLNER
Avaliador Interno (UNIVERSIDADE FEDERAL DO PARANÁ)

À Zeni e Lana, as mulheres da minha vida.

AGRADECIMENTOS

Ao meu orientador, Prof. Dr. Marcos Gomes E. da Luz, pela paciência e dedicação.

À todas as professoras e professores que de alguma forma contribuíram com a minha formação, desde antes do ingresso na UFPR. Em especial agradeço aos professores que compuseram a banca de pré-defesa: Prof. Dr. Marlus Koehler e Prof. Dr. Milton Massumi Fujimoto, pelas sugestões e ideias, e aos professores que compõe a banca de defesa: Prof. Dr. Luis Guilherme de Carvalho Rego, Prof. Dr. Cristiano Francisco Woellner, Prof. Dr. Claudionor Gomes Bezerra e Prof. Dr. Marlus Koehler, pelo aceite.

À minha família (Zeni, Lana e Fabiano) que sempre esteve ao meu lado me apoiando ao longo de toda a minha trajetória. Vocês são a razão da minha existência e a minha motivação nos momentos mais difíceis. Muito obrigada.

Ao amigo e companheiro, Jaderson Guilherme Polli, por todas as conversas sobre física e por todo o suporte e carinho. Sua presença foi fundamental nessa jornada.

Ao amigo, Marcos Vinícius W. Barcote, pelas sugestões sobre possíveis aplicações e pela companhia em praticamente todas refeições no RU.

Ao Programa de Pós-Gradução em Física e à Universidade Federal do Paraná pela oportunidade e suporte.

À CAPES pelo apoio financeiro.

Por fim, agradeço a Deus por ter me guiado através de caminhos inimagináveis.

"Nothing in life is to be feared. It is only to be understood. Now is the time to understand more, so that we may fear less." — Marie Curie

RESUMO

Um problema essencial em física é o espalhamento quântico não-relativístico em redes unidimensionais. Uma vez que o problema de espalhamento pode ser empregado para investigar a transmissão através de uma rede cristalina, há um grande número de aplicações em matéria condensada. Para estudar o espalhamento quântico através de potenciais localmente periódicos, a técnica mais implementada é o método da matriz de transferência. Neste trabalho, propomos uma abordagem alternativa que usa a função de Green exata para obter relações de recorrência para as amplitudes de espalhamento. As relações de recorrência são construídas de forma que é possível utilizar frações contínuas para determinar os coeficientes de reflexão e transmissão para qualquer potencial periódico formado por uma sequência de N blocos de construção localizados, apenas conhecendo as amplitudes de espalhamento de um único bloco. Uma grande vantagem desta abordagem é que ela pode ser aplicada a potenciais periódicos compostos por um grande número de células. Além disso, potenciais contínuos podem ser modelados com a técnica desenvolvida nesse trabalho. Considerando o número substancial de aplicações, empregamos como base três potenciais resolvidos analítica e exatamente: delta de Dirac, barreiras quadradas e barreiras trapezoidais, e estudamos os efeitos de espalhamento de suas possíveis combinações, especialmente o comportamento da probabilidade de transmissão para diferentes parâmetros de potencial e números de onda incidentes.

Palavras-chave: Problema de espalhamento quântico unidimensional, potenciais localmente periódicos, função de Green, fração contínua, probabilidade de transmissão.

ABSTRACT

An essential problem in physics is the nonrelativistic quantum scattering in one-dimensional networks. Since the scattering problem can be employed to investigate the transmission through a crystal lattice, there are a vast number of applications in condensed matter area. To study quantum scattering through locally periodic potentials, the most implemented technique is the transfer matrix method. In this work, we propose an alternative approach that uses the exact Green's function to obtain recurrence relations for the scattering amplitudes. The recurrence relations are constructed in such a way that is possible to utilize continued fractions to determine the transmission and reflection coefficients for any periodic potential formed by a sequence of N localized building blocks, just by knowing the scattering amplitudes of a single block. A great advantage of this approach is that it can be implemented to periodic potentials composed of a large number of cells. In addition, continuous potentials can be modeled with the technique developed in this work. Considering the substantial number of applications, we employ three analytically and exactly solved potentials as a basis: Dirac delta, square wall, and trapezoidal wall, and we study the scattering effects of the possible combinations of them, especially the behavior of the transmission probability for different potential parameters and incident wavenumbers.

Keywords: One-dimensional quantum scattering problem, periodic localized potentials, Green's function, continued fraction, transmission probability.

LIST OF FIGURES

LIST OF TABLES

CONTENTS

Chapter 1

Introduction

A key feature in Nature is periodicity. This can be seen in the movement of celestial bodies, the seasons and all climatic and biological periodicities generated by it [1], the harmonic oscillator-like systems, the periodic table of the (chemical) elements, and several more examples. An important periodic phenomenon is the formation of crystal lattices in solid materials, deeply studied nowadays due to the applications on the condensed matter area, which allowed great technological advances in recent years [2].

One-dimensional crystal lattice can be investigated, in the simplest way, as a 1D network where the atoms (or ions) are represented by (equally spaced) localized potentials [3]. Therefore the electron movement, considering this approximation, gave rise to a scattering problem. The first work about this kind of problem was published in 1928, in which the Bloch theorem was proposed [4]. In few words, this theorem states that the eigenfunctions of the wave equation for a periodic potential are the product of a plane wave and a function with the periodicity of the crystal lattice. The next important work, published in 1931, is the [5], which originates the so-applied Kronig-Penney model, where the atoms are idealized as square (rectangular) potential barriers. Only in the 70s, other relevant approaches emerged, due to the growing need for new materials in the computing area [6]. To study quantum scattering through locally periodic potentials, Kiang [7], Griffiths and Taussing [8], and Sprung et al. [9] developed the most applied technique: the transfer matrix method.

The scattering problem was also studied with different mathematical approaches, such as the continued fraction methodology (CF). For instance, starting with the discretization of the one-dimensional Schrödinger equation [10, 11] utilized continued fractions to calculate the transmission coefficient. Similarly, the Lippmann-Schwinger scattering integral equations was also solved with CF [12, 13, 14]. The scattering by a continued fraction potential is presented in [15].

The use of continued fractions in the study of physical problems is not restricted to scattering. For instance, the dynamical properties of macroscopic systems (e.g. electrical systems) can be described as time-correlation functions. Their Laplace transform can

be written as a CF expansion, hence the generalized susceptibilities and the transport coefficients can be expressed in terms of the static correlation functions [16]. Indeed continued fractions are encountered in the memory function approaches to the theory of relaxation [17]. In the field of equilibrium and non-equilibrium statistical mechanics [18] employed CF for the calculation of response functions, correlations, and their derivatives

Moreover, CF was also employed at Rayleigh-Schrödinger perturbation theory, especially to investigate the problems of the quartic anharmonic oscillator and the hydrogen atom in a linear radial potential [19]. Completely integrable systems, such as Painlevé equations, monodromy, and Stokes parameters were studied under the continued fraction technique as well, where an idea of quantum gravity in 2D arises from a topological point of view [20].

There are CF applications in the electromagnetic theory too. Infinite resistor network puzzles are solved with continued fractions methodology [21]. Since it is possible to expand the real part of the dielectric function as a T-fraction (a fractional series of a function), which can be written as a CF, the dielectric response of collisionless plasmas can be fitted by continued fractions [22].

Some coupled periodic processes of the solar system are explained with the physics of irrational numbers and CF [23]. The opposite direction was also explored: the physical interpretation of a massless singularity of a ferromagnetic Gaussian was used to understand the singularity behavior of a continued fraction and a time decay rate of a random walk on the field of positive integers [24].

In this work, we aim to develop an analytic method that uses the exact Green's function to obtain recurrence relations for the scattering coefficients of a general lattice. Then we want to employ continued fractions to determine the transmission and reflection amplitudes for any periodic potential composed of a sequence of N localized building blocks (BB, or cells), just knowing the scattering coefficients of the BB. Another objective is that such an approach allows modeling BBs formed by any combination of compact support potentials in an intuitive way. In addition, we desire to study large networks and simulate continuous potentials. Due to the considerable number of applications, we crave to use three exact solved potentials as a basis for the BBs: Dirac delta, square wall, and trapezoidal wall.

The present dissertation is organized as follows. In Chapter 2 we show the fundamental concepts, defining the one-dimensional quantum scattering problem and the mathematical tools that will be employed: Green's functions and continued fractions. In Chapter 3 we propose a novel approach for the scattering study, demonstrating the recurrence relations found for the transmission and reflection amplitudes of a general lattice (formed by barriers with arbitrary shapes, not necessarily equally spaced). Moreover, in this section we expose how continued fractions can be employed to obtain these quantities for periodic localized potentials, where the only requirement is to know the individual potential coefficients.

In Chapter 4 we present several applications for the method developed in Chapter 3.

Initially, we focus on the elementary barriers or single building blocks: Dirac delta, square wall, and trapezoidal wall showing the transmission probabilities behaviors and successfully comparing them with the literature. Thus we explore some examples of periodic lattices whose BBs are p-tuple, that is, whose cells are formed by a combination of the elementary barriers. Finally, in Chapter 5, we conclude the work by summarizing all the obtained results and presenting the prospects.

Chapter 2

Fundamental concepts

As said before, the electron movement in a crystal lattice can be (approximately) investigated as a scattering problem. Such an approach is fundamental in condensed matter since, for instance, the conductance of some materials can be predicted before continuing an experiment. To understand how this can be done, let us begin by answering a more fundamental question: what is a scattering process? In summary, a general scattering process can be described as follows: a beam of particles (A) is directed to a target (B), and after the scattering, there is a resulting beam of particles (C) [25], as schematized in Figure 2.1. It is common to assume that the properties of (A) and (B) are known and the goal is to discover the characteristics of (C).

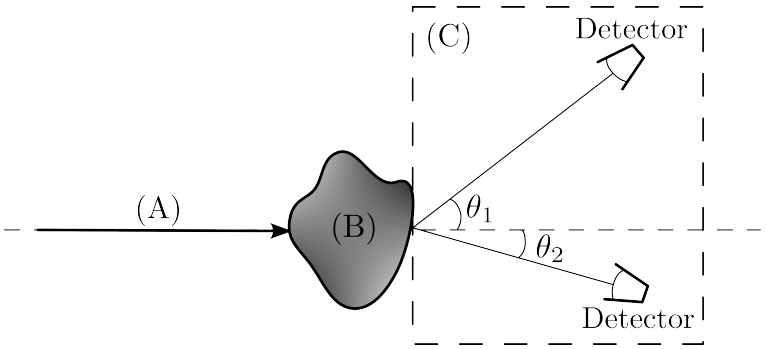

Figure 2.1: Scheme of a scattering process: a beam of particles (A) collides against a target (B) that, for now, has an arbitrary shape. The result is a different beam (C) that can be observed by the detectors localized inside the dashed box, as exemplified above. The main goal is to determine the properties of (C).

If this type of process could be studied under the gaze of classical mechanics would be sufficient to evaluate the deviation caused by the target onto the incident beam. But, once the particles live on a microscopic scale, quantum mechanics is required, and then the phenomena can become very complex. To simplify, we often consider the following hypothesis:

(i) The process occurs in a non-relativistic regime.

(ii) Although the spins are important in a collision study, here the spin will not be considered[1].

(iii) Only elastic process will be considered, where the internal structure of the particles does not change during the phenomenon[2].

(iv) What happens inside the target area (B) is not the purpose of this study, but rather what occurs inside the dashed box (C) (the scattering result)[3].

(v) The interaction between the incident beam of particles (A) and the target particles (B) is given by a potential $V(\mathbf{r})$, where $\mathbf{r} = \mathbf{r_A} - \mathbf{r_B}$ and $\mathbf{r_A}$, $\mathbf{r_B}$ are, respectively, the positions of (A) and (B).

Moreover, in the quantum picture, it is clear that a beam of incident particles (A) corresponds to an incident wave. Then, when we study a scattering process, the main goal is to discover the characteristics of the resulting wave (C). Despite quantum scattering phenomena happening (in Nature) more often in two or three dimensions, this work focuses on the most fundamental one: the *one-dimension quantum scattering*.

2.1 1D quantum scattering

Before analyzing the main subject of this section, the 1D scattering process, let us remind some elementary principles of quantum mechanics. For a general (and therefore three-dimensional) quantum problem, in which the associated wave function is ψ, it is known that $|\psi|^2$ has a probabilistic interpretation since, for example, in the representation basis $|\psi(\mathbf{r})|^2 d\mathbf{r}^3$ is the probability of finding the particle in the infinitesimal volume $d\mathbf{r}^3$. Moreover, due the *conservation of probability* it is possible to define the *probability density* ρ and the *probability current density* $\mathbf{J}$ that satisfies the continuity equation $\partial\rho/\partial t + \nabla\cdot\mathbf{J} = 0$, which implies $\rho = \psi^*\psi$ and

$$\mathbf{J}(\mathbf{r}) = \frac{\hbar}{2mi}[\psi^*(\nabla\psi) - (\nabla\psi^*)\psi], \tag{2.1}$$

where ∇ is the gradient operator [26, 27].

Now returning to the one-dimensional scattering problem, consider that there is an incident beam coming far from the left (right), i.e., from $x \to -\infty$ ($x \to \infty$) which is spread by a single potential $V(x)$. Also, assume that the coordinate system is such that

[1]Actually, it is assumed that all the particles involved are in a spin singlet state, that is not affected by the scattering.

[2]Otherwise, if the process is inelastic, part of the kinetic energy of (A) can be absorbed in the final state of the system [25].

[3]As will be shown further, when a block of scatters is considered as a target, it is not possible to know what happens inside the individual scatters, nevertheless, it is tangible to study what happens between them.

$V(x) \to 0$ when $|x| \to \infty$. One may ask what is the probability amplitude $\mathcal{T}$ of this wave to be *transmitted* through the barrier, and what is the probability amplitude $\mathcal{R}$ of this wave to be *reflected* by it. In other words, we desire to know what fraction of the incident wave is transmitted and what fraction is reflected.

If the barrier is a compact support potential (which means that it is nonzero only in an interval, say $a \leq x \leq b$) and if the incident wave is a planar wave, the statement of the last paragraph can be written mathematically as

$$\psi^{(\pm)}(x) = \frac{1}{\mathcal{N}} \begin{cases} A^{(\pm)}(k)\exp[\pm ikx] + B^{(\pm)}(k)\exp[\mp ikx], & x < a\,(x > b) \\ C^{(\pm)}(k)\exp[\pm ikx], & x > b\,(x < a) \end{cases}, \tag{2.2}$$

where $\mathcal{N}$ is a normalization constant, $k = \sqrt{2mE}/\hbar$ is the wavenumber, m is the mass and E is the energy of the incident beam. The indices $(+)$ and $(-)$ indicate that the incident wave is coming from, respectively, the left and the right.

Furthermore, the incident, reflected, and transmitted partial wave functions are, respectively, $\psi_{\text{inc}} = A^{(\pm)}(k)\exp[\pm ikx]$, $\psi_{\text{ref}} = B^{(\pm)}(k)\exp[\mp ikx]$, and $\psi_{\text{trans}} = C^{(\pm)}(k)\exp[\pm ikx]$. From probability conservation, the current density is such that $|\mathbf{J}_{\text{inc}}| = |\mathbf{J}_{\text{ref}}| + |\mathbf{J}_{\text{trans}}|$, thus

$$\frac{|\mathbf{J}_{\text{ref}}|}{|\mathbf{J}_{\text{inc}}|} + \frac{|\mathbf{J}_{\text{trans}}|}{|\mathbf{J}_{\text{inc}}|} = 1. \tag{2.3}$$

Since the ratios between the reflected (transmitted) and incident currents are the reflection (transmission) probabilities, denoted as, respectively, $|\mathcal{R}^{(\pm)}(k)|^2$ and $|\mathcal{T}^{(\pm)}(k)|^2$, we conclude that

$$|\mathcal{R}^{(\pm)}(k)|^2 + |\mathcal{T}^{(\pm)}(k)|^2 = 1. \tag{2.4}$$

Finally, employing the Equation (2.1) for each current density (using the 1D form for the gradient operator), it is easy to see that

$$\mathcal{R}^{(\pm)}(k) = \frac{B^{(\pm)}(k)}{A^{(\pm)}(k)} \quad \text{and} \quad \mathcal{T}^{(\pm)}(k) = \frac{C^{(\pm)}(k)}{A^{(\pm)}(k)}. \tag{2.5}$$

When, for simplicity, $A^{(\pm)} = 1$, $\mathcal{R}^{(\pm)}(k) = B^{(\pm)}(k)$ and $\mathcal{T}^{(\pm)}(k) = C^{(\pm)}(k)$ and the quantum scattering process is summarized in Figure 2.2. The expressions for $A^{(\pm)}(k)$, $B^{(\pm)}(k)$, and $C^{(\pm)}(k)$ — and hence for the total wave function $\psi^{(\pm)}(x)$ — can be calculated using the time-independent Schrödinger equation and the boundary conditions.

The difficulty level for solving the problem described above will depend on the barrier shape. If the intention is to find an exact and analytical solution, only three types of potentials can be investigated: the Dirac delta, the square wall, and the trapezoidal wall. The first two have a well-known resolution, shown in detail in several famous textbooks as [28, 29, 27, 30]. The last case is demonstrated in Appendix A, although already resolved in some papers like [31, 32, 33].

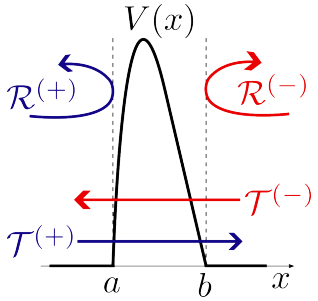

Figure 2.2: Summarizing a one-dimensional quantum scattering process: when $A^{(\pm)} = 1$ there are a reflection ($\mathcal{R}^{(\pm)}(k) = B^{(\pm)}(k)$) and a transmission ($\mathcal{T}^{(\pm)}(k) = C^{(\pm)}(k)$) amplitudes associated with the probabilities of the incident wave be, respectively, reflected and transmitted by the barrier. In blue, some arrows schematize the problem when the incident beam is coming from the left and in red when it is coming from the right.

Up to this point, the incident wave is spread across only one compact support potential. Naturally, the next question must be: what if the incident wave is spread by two or more sequential compact support potentials? Suppose that the one-dimensional lattice formed by these localized barriers is periodic, i.e., all the potentials are identical and equally spaced. This condition, despite being somewhat restrictive, agrees with the periodic behavior of crystalline materials, where each barrier of this network corresponds with a crystal site (an atom, ion, etc.). Several techniques were developed to study these localized periodic potentials.

2.1.1 Previous methodologies for periodic potentials

In 1992 Griffiths and Taussing [8] used the M *matrix method* to confirm the results already obtained by Kiang in 1974 [7] about the *Dirac comb*, a periodic lattice formed by N Dirac delta barriers[4]. In the next year, Sprung *et al.*. [9] employed the *transfer matrix technique*[5] to express the transmission and reflection coefficients for two kinds of periodic potentials: the Dirac delta and square wall[6]. This last work became the main reference in the area and started a sequence of articles that improved the same methodology [36, 37, 38, 39, 40, 41], which even today is implemented in several papers, as will be pointed out in the next subsection.

The transfer matrix is more general than the M matrix method, although they are

[4]Studying especially the transmission probability for $N = 1, 2, 3, 5, 9$ and 101.

[5]This technique was utilized by Kalotas and Lee in 1991 [34] to study arbitrary potential cells, and it was applied to the square wall and parabolic potential examples (numerically). A few years before, in 1986, Vezzetti and Cahay [35] already showed a general transfer matrix method and presented a compact expression for the transmission probability and the Bloch phase (which was implemented by Sprung *et al.*. to study more deeply the 1D quantum scattering).

[6]Focusing again on the transmission probability but for $N = 6, 10$ and 51.

almost the same[7] because both are based on the same principle: the scattering amplitudes can be found by solving the Schrödinger equation for the different regions — defined by the potential values on each interval — and applying the boundary conditions. These methodologies are briefly described and discussed below, starting with the M matrix method.

Initially, consider a general and localized potential $V(x)$ such that pictured in Figure 2.3(a). If a particle, with mass m and incident energy E, reaches such potential, the associated time-independent Schrödinger equation is

$$-\frac{\hbar^2}{2m}\frac{d^2\varphi(x)}{dx^2} + V(x)\varphi(x) = E\varphi(x), \tag{2.6}$$

where φ is the associated wave function. Since in regions I and III, $V(x) = 0$, the general solution for the above equation is

$$\varphi(x) = \begin{cases} A_0 \exp[ikx] + B_0 \exp[-ikx], & x < a \\ A_1 \exp[ikx] + B_1 \exp[-ikx], & x > b \end{cases}, \tag{2.7}$$

where $k = \sqrt{2mE}/\hbar$.

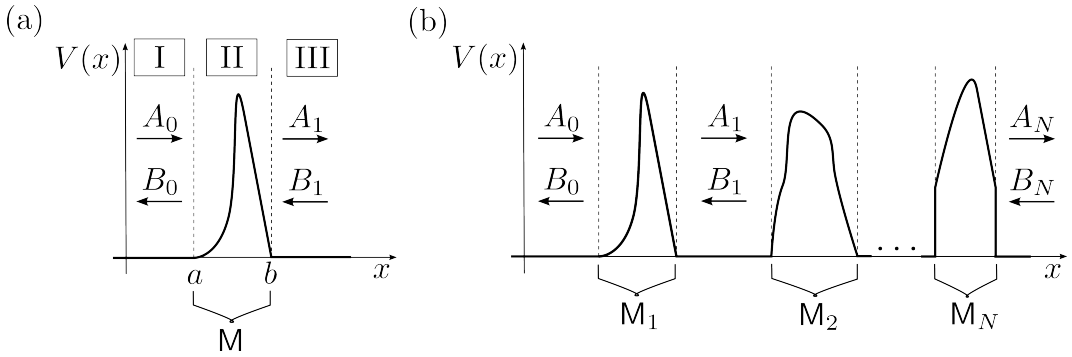

Figure 2.3: 1D quantum scattering by (a) one and by (b) N compact support potentials.

Notice that $\exp[\pm ikx]$ represents a wave traveling from the left (right)[8]. Thus, it is clear that A_0 and B_1 are the amplitudes of a wave incident coming from, respectively, left and right. Hence B_0 and A_1 are the reflected and transmitted amplitudes, depending on the case. It is common to assume that, for simplicity, the incident wave is coming from the left ($B_1 = 0$). So, from the Equation (2.5), the transmission probability is

$$|T|^2 = \left|\frac{A_1}{A_0}\right|^2, \tag{2.8}$$

so that the transmission coefficient is the ratio between the transmitted and the incident

[7] Despite Sprung *et al.*. [9] call the M matrix method (used in the Griffiths and Taussing paper [8]) as transfer matrix method, here, due to the differences between the techniques, it will be alternatively called (as in [8]).

[8] Combined with the $\exp[-iEt/\hbar]$, the time-dependent factor [8].

amplitudes of the wave fraction.

In order to find the scattering amplitudes — and hence $|T|^2$ — it is necessary to solve the Schrödinger's equation in region II and then use the boundary conditions at a and b. Typically this procedure results in a system of equations that has the following matrix form [8]

$$\begin{pmatrix} A_1 \\ B_1 \end{pmatrix} = \mathsf{M} \begin{pmatrix} A_0 \\ B_0 \end{pmatrix}, \quad \mathsf{M} = \begin{pmatrix} \mathsf{M}_{11} & \mathsf{M}_{12} \\ \mathsf{M}_{21} & \mathsf{M}_{22} \end{pmatrix}. \tag{2.9}$$

Since $B_1 = 0$, it is trivial to deduce that $|T|^2 = |\det(\mathsf{M})/\mathsf{M}_{22}|^2$.

Following this reasoning, if there are N compact support potentials, as shown in Figure 2.3(b), the M matrix for each part is such that

$$\begin{pmatrix} A_1 \\ B_1 \end{pmatrix} = \mathsf{M}_1 \begin{pmatrix} A_0 \\ B_0 \end{pmatrix}, \quad \begin{pmatrix} A_2 \\ B_2 \end{pmatrix} = \mathsf{M}_2 \begin{pmatrix} A_1 \\ B_1 \end{pmatrix}, \quad \cdots \quad \begin{pmatrix} A_N \\ B_N \end{pmatrix} = \mathsf{M}_N \begin{pmatrix} A_{N-1} \\ B_{N-1} \end{pmatrix}, \tag{2.10}$$

so,

$$\begin{pmatrix} A_N \\ B_N \end{pmatrix} = \mathsf{M}_N \mathsf{M}_{N-1} \mathsf{M}_{N-2} \cdots \mathsf{M}_1 \begin{pmatrix} A_0 \\ B_0 \end{pmatrix}, \tag{2.11}$$

finally, in this case,

$$\mathsf{M} = \prod_{j=1}^{N} \mathsf{M}_j, \tag{2.12}$$

namely, the M matrix for N barriers is simply the product of all M matrices for the scattering by each individual potential.

Notice that, if there is a set of identical and equally spaced potentials (i.e. a periodic lattice, as the one in Figure 2.4) the problem becomes easier since now $\mathsf{M}_1 = \mathsf{M}_i$ for every i. Then, to calculate the M $(= \mathsf{M}_1^N)$ matrix for the whole system, it is enough to know the scattering coefficients of a single barrier. However, we still need to calculate the Nth potency of M_1, which could be difficult for some potential shapes. Fortunately, for the Dirac comb, the M_1 format is simple, making this operation easy — what does not happen with more complicated barriers such as the square and trapezoidal walls (even though these barriers have exact solutions). This provided the core of the Griffiths and Taussing work [8], but another methodology is required to explain a more general scattering process.

As mentioned, the transfer matrix method is a generalization of the M matrix technique. Consider N periodic compact support potentials as shown in Figure 2.4, with $b - a = d$ (i.e. with width d), spaced by L. Again, one wants to solve the time-independent Schrödinger's equation shown in Equation (2.6), but now assuming that the incident wave is coming only from the left and that $A_0 = 1$ and $B_1 = 0$. Besides that, renaming $B_0 = R_N$ and

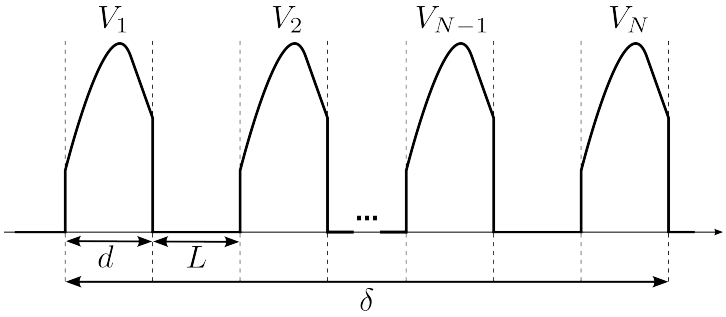

Figure 2.4: A periodic structure composed of N identical potentials, notice that the total lattice width is $\delta = N(d + L) - L$.

$A_1 = T_N$, the total wave function can be written as

$$\varphi(x) = \begin{cases} \exp[ikx] + R_N \exp[-ikx], & x < 0 \\ T_N \exp[ik(x - \delta)], & x > \delta \end{cases}, \tag{2.13}$$

with $\delta = N(d + L) - L$ (see Figure 2.4), and the first potential of the lattice begins at $x = 0$.

Once more, the coefficients R_N and T_N can be calculated by applying the boundary conditions for the solutions of the Schrödinger's equation in the different regions. Therefore, the following pair of linear equations is obtained

$$\begin{pmatrix} T_N \\ 0 \end{pmatrix} = \mathsf{M}^N \begin{pmatrix} 1 \\ R_N \end{pmatrix}, \tag{2.14}$$

where M is the M matrix for each individual (identical) potential.

Remember that the equation above emerged from the Equations (2.10), where $(A_i\ B_i)^T = \mathsf{M}_i(A_{i-1}\ B_{i-1})^T$ and the index T indicates the matrix transpose. One could look to analogous relations, say $(A_{i-1}\ B_{i-1})^T = \mathsf{T}_i(A_i\ B_i)^T$, so naturally

$$\begin{pmatrix} 1 \\ R_N \end{pmatrix} = \mathsf{T}^N \begin{pmatrix} T_N \\ 0 \end{pmatrix}, \tag{2.15}$$

with $\mathsf{T}^N = (\mathsf{M}^N)^{-1}$, and then it is evident that the coefficients are given by

$$1 = (\mathsf{T}^N)_{11} T_N\,, \quad R_N = (\mathsf{T}^N)_{21} T_N, \tag{2.16}$$

where $(\mathsf{T}^N)_{ij}$ is the element ij of T^N.

As demonstrated by induction in [9], it is possible to obtain that

$$\mathsf{T}^N = \frac{1}{\sin\phi}\{\mathsf{T}\sin(N\phi) - \mathbf{1}\sin[(N-1)\phi]\}, \tag{2.17}$$

where $\mathbf{1}$ is the 2×2 identity matrix and the T eigenvalues are of the form $\lambda_1 = 1/\lambda_2 = \exp[i\phi]$. Besides that, the T^N matrix has determinant equal to one and the trace is equal to $2\cos(N\phi)$ $(= \mathrm{tr}(\mathsf{T}^N))$. Additional information is that $\phi = \phi(k)$ is the Bloch phase (which is wavenumber dependent) associated with the unit cell potential $V(x)$ when $N \to \infty$ (i.e. when there is an infinitely periodic potential).

Then, with the Equations (2.16) and (2.17) we can demonstrate the following relation

$$\frac{1}{T_N} = \frac{1}{\sin\phi}\left\{\frac{1}{T_1}\sin(N\phi) - \sin[(N-1)\phi]\right\}. \tag{2.18}$$

Observe that if $\sin(N\phi)$ $(\sin[(N-1)\phi])$ vanishes the transmission probability is $|T_N|^2 = 1$ $(= |T_1|^2)$. To rephrase it, these conditions imply that the total transmitted wave (through the N barriers) has probability equal to one to pass (if $\sin(N\phi) \longrightarrow 0$) or has the same probability of passing through just one barrier (if $\sin[(N-1)\phi] \longrightarrow 0$). If N is large, $N\phi(k) \approx (N-1)\phi(k)$ so $T_N(k)$ is a very fluctuating function of k (or $\phi(k)$) [9].

Since $\mathsf{T}_{21} = R_1/T_1$, $(\mathsf{T}^N)_{21} = R_N/T_N$, and from Equation (2.17) it easy to see that

$$\frac{R_N}{T_N} = \frac{\sin(N\phi)}{\sin\phi}\frac{R_1}{T_1}. \tag{2.19}$$

Moreover, using Equation (2.18) in Equation (2.19)

$$R_N = R_1\left\{1 - T_1\frac{\sin[(N-1)\phi]}{\sin(N\phi)}\right\}^{-1}, \tag{2.20}$$

and all the scattering coefficients can be written in terms of N, $\phi(k)$, R_1, and T_1. Supposing that N, R_1, and T_1 are known, we just have to find $\phi(k)$.

In the literature, it is established that T^{-1} can be decomposed as $\mathsf{T}^{-1} = \mathsf{L}^{-1}\mathsf{W}\mathsf{L}$, where

$$\mathsf{L} = \begin{pmatrix} 1 & 1 \\ ik & -ik \end{pmatrix} \tag{2.21}$$

and is W is a real matrix [9]. This condition and the Equation (2.16) can be combined to show that

$$\mathsf{T} = \begin{pmatrix} \frac{1}{T_1} & \frac{R_1^*}{T_1^*} \\ \frac{R_1}{T_1} & \frac{1}{T_1^*} \end{pmatrix}. \tag{2.22}$$

The above matrix is called *transfer matrix*.

With the trace of T it is possible to discover the ϕ, since $\mathrm{tr}(\mathsf{T}^N) = 2\cos(N\phi)$ and adopting the property $2\Re(z) = z + z^*$, where $\Re(z)$ is the real part of z, we find

$$\cos\phi = \frac{\mathrm{tr}(\mathsf{T})}{2} = \frac{1}{2}\left(\frac{1}{T_1} + \frac{1}{T_1^*}\right) = \Re\left(\frac{1}{T_1}\right). \tag{2.23}$$

Finally, looking at the relations above and Equations (2.18) and (2.20), we conclude that to determine R_N and T_N, the scattering amplitudes for the entire periodic lattice, it is enough to know T_1 and R_1, the scattering amplitudes for a single cell of the lattice.

Although the transfer matrix method is a very applicable tool — what explains a large number of simulations (most made with numerical calculations) and experiments that use it as a theoretical method, as will be exemplified in the next section — this technique has a flaw: in Equations (2.18) and (2.20) we can notice that the scattering amplitudes are calculated taking the number of cells as parameters of sine functions. Thus, if N is large these functions are very oscillating and the computational calculations are time-consuming. The current work proposes a method that avoids this problem. In addition, our technique allows the analytical study of scattering processes in which the incident wave is spread by more complicated periodic potentials (i.e. more complicated than the periodic structures whose cells are simply Dirac deltas or square walls).

At the moment, only techniques involving matrices were cited. Nonetheless, the scattering problem has been studied with different and mathematically interesting approaches, like the Grossel and Vigoureux [42] paper that employed Einstein's addition law of velocities to calculate the scattering coefficients. Moreover, the works of Vigneron and Lambin [11, 10] presented a method that discretizes 1D Schrödinger equation and then uses *continued fractions (CF)* to calculate the transmission coefficient. Similarly, Horáček and Sasakawa [12, 13, 14] solved the Lippmann-Schwinger scattering integral equations using CF. The method introduced in the last works was widely applied, for instance, it was used to study the electron(positron)-atom scattering [43], the electron scattering by linear molecules [44], and the low-energy electron scattering by the hydrogen molecule [45]. As will be shown in the next chapter, continued fractions play an important role in the procedure developed in this dissertation.

In order to understand the relevance of nonrelativistic 1D scattering processes, next we expose some theoretical and experimental applications of the problem.

2.1.2 A few applications of the 1D quantum scattering

An important phenomenon that occurs when two particles collide against each other is entanglement. If the interaction potential is such that $V(x_1 - x_2) = V(x)$, where x_i is the i particle position ($i = 1, 2$), the Hamiltonian can be divided into two parts: one dependent on the center of mass (CM) coordinate and one dependent on the relative coordinate. Therefore, the time-independent Schrödinger's equation can be factorized as well, and one part will have a free particle behavior (the CM component) whereas another will correspond to a single particle, of position x, that is scattered by a potential $V(x)$.

The entanglement mechanisms for just one collision between two particles of equal and unequal masses are studied by [46]. Similarly [47] analyses quantum interference

and entanglement induced by multiple scattering of light. With this kind of procedure, more complicated processes can be examined, for example, [48] investigate numerically the entanglement between a beam of free fermions and a 1D lattice. [49] also employed these scattering-like mechanisms to calculate analytically the entanglement for some models, as systems consisting of qubits or oscillators.

Regarding theoretical research, there are several more applications. For instance, [50] deals with graphene superlattices as one-dimensional periodic potentials of square barriers and studies its electronic band gaps and transport properties. Moreover, to examine topological edge modes in one-dimensional photonic systems, [51] considers the interface between two different finite crystals, that constitute an open scattering system.

Regarding the experimental research, quantum interference and conduction through a one-dimensional silicon nanowire — which is 10 nm wide and 500 nm long — was studied in [52]. In this field, electron scattering in intrananotube quantum dots was also investigated, as in [53], where the quantum dots are realized in metallic single-walled carbon nanotubes by means of low-dose medium energy argon ion irradiation.

In acoustic, wave propagation and diffraction are essential phenomena. To analyze trapped modes and resonance wave transmission in a plate with a system of notches, [54] used a 1D quantum scattering system for the theoretical modeling and the numerical simulation, which are experimentally validated with laser Doppler vibrometry. Also in acoustic, a lattice of Helmholtz resonators connected to a tube was experimentally explored and compared with a 1D quantum scattering phenomenon [55].

Superlattices were investigated as well. For example, in [56] superlattices in one-dimensional nanoscale semiconductors are reviewed. These types of materials are of fundamental importance for developing potential nanoelectronic and optoelectronic devices. Other types of equipment in vogue can be treated as superlattices, as multi-junction solar cells[9], whose conversion efficiencies are quickly increasing due to works like [57], that used the transfer matrix method to simulate the experimental procedure before it is performed.

Therefore it is possible to conclude that, although be the simplest case, one-dimensional scattering is a very rich phenomenon, which can be investigated in a considerable number of simulations and experiments. To create a connection with more complex problems outside the current work's sphere, the next subsection gives a short outline for quantum scattering in a higher dimension.

2.1.3 Quantum scattering in three dimensions

Consider an incident beam of particles, of mass m, whose direction movement is the z axis, as shown in Figure 2.5. This beam is then spread by a potential $V(\mathbf{r})$, localized around the origin O. Defining Φ_{inc} as the incident flux of particles, i.e., Φ_{inc} is the number

[9]Solar cells formed by multiple junctions composed of different semiconductor materials.

of particles per unit of time that pass through a unit surface perpendicular to z axis in the region where $z \to -\infty$ (far from the potential region).

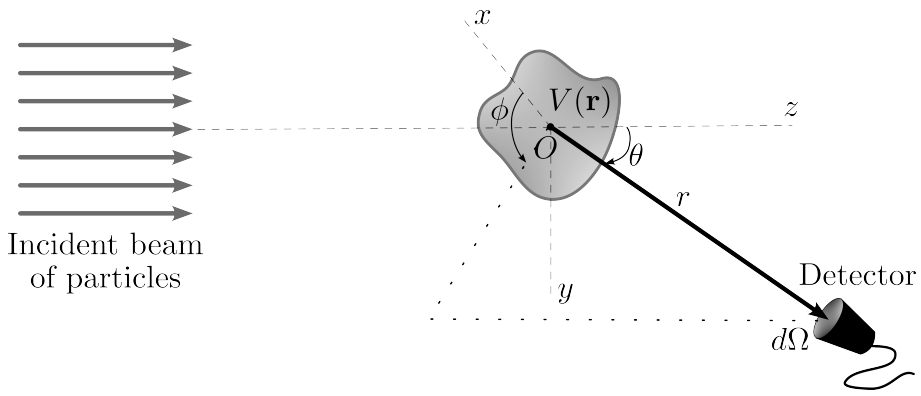

Figure 2.5: A three-dimensional scattering process, where the incident beam (coming from $z \to -\infty$) is spread by a potential $V(\mathbf{r})$, and the outgoing wave is measured by the solid angle detector, $d\Omega$, placed far from the barrier influence (at the polar angles θ and ϕ).

Also, assume that there is a detector far away from the potential region, placed in the polar angles θ and ϕ, and that spans a solid angle reading $d\Omega$. One may ask how many particles are measured by the detector per unit of time. It is clear that this quantity, say dn, is directly proportional to Φ_{inc} and $d\Omega$. Let $\sigma(\theta, \phi)$ be the coefficient of proportionality between dn and $\Phi_{inc} d\Omega$, then

$$dn = d\sigma(\theta, \phi)\Phi_{inc} d\Omega, \tag{2.24}$$

as can be seen in the equation above, $d\sigma(\theta, \phi)$ has an area dimension, and it is called *differential scattering cross section*.

It is expected that the overall wave function for the problem can be written as

$$\psi(\mathbf{r}) = \exp[ikz] + f_k(\theta, \phi)\frac{\exp[ikr]}{r}, \tag{2.25}$$

far from the potential actuation zone, where the first term corresponds to an incident planar wave and the second one to the scattered wave[10]. The function $f_k(\theta, \phi)$ is called *scattering amplitude*, and it is the only part of the above equation that depends on the potential $V(\mathbf{r})$. The $f_k(\theta, \phi)$ is the 3D function analogous to the transmission and reflection amplitudes, so discussed in the one-dimensional case.

Inspecting the expression for the probability current (see Equation (2.1)) of the incident and scattered waves, it is possible to demonstrate that $d\sigma(\theta, \phi)/d\Omega = |f_k(\theta, \phi)|^2$

[10]Notice that in the scattered wave, there is a $1/r$ factor. It results from the following: the time-independent Schrödinger's equation can be rewritten, when there is no potential, as $(\nabla^2 + k^2)\psi(\mathbf{r}) = 0$, and in three spatial dimensions $(\nabla^2 + k^2)\exp[ikr]$ is not zero, but $(\nabla^2 + k^2)\exp[ikr]/r$ is. Observe that ∇^2 is the Laplace operator [25].

[28, 27, 30, 26]. The left-hand side is measured experimentally — by knowing the device reading angle and the number of particles that reach the detector — whereas the right-hand side is a theoretical quantity — which can even be calculated analytically for simple scattering potentials[11].

2.2 Green's function

In all Physics research topics, there are a considerable number of problems that are solved by differential equations. To solve those equations, several mathematical methods were developed. When the differential equation in question contains an inhomogeneous term, often called a *source term*, the most effective technique that can be implemented is the *Green's function*. A widely known example is the problem of finding the electrical potential $\Phi(\mathbf{r})$ generated by a charge density $\rho(\mathbf{r})$. One of Maxwell's equations gives rise to Poisson's equation,

$$-\nabla^2\Phi(\mathbf{r}) = \frac{1}{\epsilon_0}\rho(\mathbf{r}), \tag{2.27}$$

where the right-hand side is the source, and ϵ_0 is the vacuum permittivity.

Applying Coulomb's law, it is known that the potential in $\mathbf{r}$ generated by each element of charge $\rho(\mathbf{r}')d^3\mathbf{r}'$ is [58]

$$\Phi(\mathbf{r}) = \frac{1}{4\pi\epsilon_0}\int d^3\mathbf{r}'\frac{\rho(\mathbf{r}')}{|\mathbf{r}-\mathbf{r}'|}, \tag{2.28}$$

with the integration being made in all the spaces where there is charge distribution. The above equation can be interpreted as follows: the charge density is converted to a potential through an integral operator, also called *kernel*, which is a two-variable function,

$$G(\mathbf{r},\mathbf{r}') = \frac{1}{4\pi\epsilon_0}\frac{1}{|\mathbf{r}-\mathbf{r}'|}, \tag{2.29}$$

the Green's function of this problem, and then,

$$\Phi(\mathbf{r}) = \int d^3\mathbf{r}'G(\mathbf{r},\mathbf{r}')\rho(\mathbf{r}'). \tag{2.30}$$

Consider now a more general problem. Let $\mathcal{L}$ be a linear second-order differential operator. So Green's function has the properties [59, 60]:

(i) The inhomogeneous differential equation $\mathcal{L}\Phi(\mathbf{r}) = s(\mathbf{r})$, with its boundary conditions,

[11] The *total scattering cross section* is such that

$$\sigma = \int d\sigma(\theta,\phi) = \int |f_k(\theta,\phi)|^2 d\Omega, \tag{2.26}$$

where the integration is calculated over all space.

has the solution

$$\Phi(\mathbf{r}) = \int d^3\mathbf{r}' G(\mathbf{r}, \mathbf{r}') s(\mathbf{r}'), \tag{2.31}$$

where the integration is made in all the relevant spaces.

(ii) The Green's function that appears in item (i) is the solution of

$$\mathcal{L}G(\mathbf{r}, \mathbf{r}') = \delta(\mathbf{r} - \mathbf{r}'), \tag{2.32}$$

that is associated with the homogeneous differential equation $\mathcal{L}\Phi(\mathbf{r}) = 0$, which has the same boundary conditions of $\mathcal{L}\Phi(\mathbf{r}) = s(\mathbf{r})$.

(iii) Assume that $\mathcal{L} = z - \tilde{\mathcal{L}}$, where z is a complex variable and $\tilde{\mathcal{L}}$ is other linear second-order differential operator. If $\tilde{\mathcal{L}}$ define a Hermitian eigenvalue problem as $\tilde{\mathcal{L}}\phi = \lambda\phi$, whose discrete and continuous eigenvalues λ_n and λ_c are associated, respectively, with the eigenfunctions $\phi_n(\mathbf{r})$ and $\phi_c(\mathbf{r})$, it is possible to affirm that:

(iii.a) The Green's function is a z dependent function $G(\mathbf{r}, \mathbf{r}'; z)$.

(iii.b) $G(\mathbf{r}, \mathbf{r}'; z)$ is a symmetric function, i.e.,

$$G(\mathbf{r}, \mathbf{r}'; z) = G^*(\mathbf{r}', \mathbf{r}; z^*), \tag{2.33}$$

where the index $*$ denotes the complex conjugate operation.

(iii.c) $G(\mathbf{r}, \mathbf{r}'; z)$ can be written as an eigenfunction expansion such that

$$G(\mathbf{r}, \mathbf{r}'; z) = \sum_n \frac{\phi_n(\mathbf{r})\phi_n^*(\mathbf{r}')}{z - \lambda_n} + \int dc \frac{\phi_c(\mathbf{r})\phi_c^*(\mathbf{r}')}{z - \lambda_c}. \tag{2.34}$$

(iv) $G(\mathbf{r}, \mathbf{r}')$ is continuous and differentiable at all points where $\mathbf{r} \neq \mathbf{r}'$.

Returning to the electrostatic example commented before, notice that, using the properties above it is easy to see that Green's function for the problem is given by the Equation (2.29). This happens because we need to solve $-\epsilon_0 \nabla^2 G(\mathbf{r}, \mathbf{r}') = \delta(\mathbf{r} - \mathbf{r}')$, with the boundary condition $G(\mathbf{r}, \mathbf{r}') = 0$ when $\mathbf{r} \to \infty$[12]. Integrating it over a spherical volume of radius R, whose the center is in $\mathbf{r}'$ and employing the Gauss' theorem,

$$\int_{\tilde{r}<R} d^3\mathbf{r} \nabla \cdot \nabla G(\mathbf{r}, \mathbf{r}') = \int_{\tilde{r}=R} \nabla G(\mathbf{r}, \mathbf{r}') \cdot d^2\mathbf{r} = -\frac{1}{\epsilon_0}, \tag{2.35}$$

[12]In other words, far away from the origin the charge source does not originate potential, so there is no Green's function related [59].

where it was assumed that $G(\mathbf{r}, \mathbf{r}')$ depends only on[13] $\tilde{r} = |\mathbf{r} - \mathbf{r}'|$. Thus

$$4\pi R^2 \frac{dG}{d\tilde{r}}\Big|_{\tilde{r}=R} = -\frac{1}{\epsilon_0}, \tag{2.36}$$

once this relation must be valid for every R,

$$\frac{dG}{d\tilde{r}} = -\frac{1}{4\pi\epsilon_0}\frac{1}{\tilde{r}^2}, \tag{2.37}$$

and the Equation (2.29) is easily recovered.

At this point, it is clear that Green's function form is built upon the linear operator $\mathcal{L}$ and the boundary conditions. Adopting the recipe described above, Green's functions for different operators and boundary conditions can be constructed, and some of the most important are presented in Table 2.1. Previously, we discussed that the scattering problem — like most quantum mechanical systems — can be solved by the Schrödinger's equation, a second-order differential equation. So Green's function for the solution of some quantum mechanical systems will certainly look like some of the expressions shown in the table, as will be seen further.

An alternative way to study a problem employing Green's function methodology is by the *Perturbation Theory*. Let us examine the following situation: the total Hamiltonian in question is such that $H(\mathbf{r}) = H_0(\mathbf{r}) + V(\mathbf{r})$, where the eigenvalues and the eigenfunctions associated with H_0 can be easily found and V contributes with a small part of the system energy[14]. For this reason, the $V(\mathbf{r})$ is a *perturbation* of a well-determined case. If the Green's function associated with $H_0(\mathbf{r})$ is $G_0(\mathbf{r}, \mathbf{r}'; z)$[15], the Green's function for the overall Hamiltonian is [60]

$$\begin{aligned} G(\mathbf{r}, \mathbf{r}'; z) = G_0(\mathbf{r}, \mathbf{r}'; z) &+ \int d\mathbf{r_1} G_0(\mathbf{r}, \mathbf{r_1}; z) V(\mathbf{r_1}) G_0(\mathbf{r_1}, \mathbf{r}'; z) \\ &+ \int\int d\mathbf{r_1} d\mathbf{r_2} G_0(\mathbf{r}, \mathbf{r_2}; z) V(\mathbf{r_2}) G_0(\mathbf{r_2}, \mathbf{r_1}; z) V(\mathbf{r_1}) G_0(\mathbf{r_1}, \mathbf{r}'; z) + \cdots. \end{aligned} \tag{2.38}$$

All the information described so far about Green's function technique composes the basis of the approach developed in this work, as will become clear in the next subsections.

2.2.1 Green's function in 3D scattering problem

In order to bring some intuition about Green's function for the one-dimensional case, let us start with Green's function for the 3D quantum scattering problem described in

[13] This hypothesis came from the fact that the boundary conditions are spherically symmetric at an infinite distance.

[14] Mathematically, if E_j^0 and $|j\rangle_0$ with $j = 1, 2, \ldots$ are, respectively, the eigenvalues and eigenfunctions of H_0, we must have $|_0\langle j-1|V|j\rangle_0| \ll E_j^0 - E_{j-1}^0$ and $|_0\langle j+1|V|j\rangle_0| \ll E_{j+1}^0 - E_j^0$.

[15] From Equation (2.34) it is clear that once the eigenvalues and the eigenfunctions of $H_0(\mathbf{r})$ are known, $G_0(\mathbf{r}, \mathbf{r}'; z)$ can be written as an eigenfunction expansion.

Table 2.1: Green's function for different linear operators and boundary conditions[a] [59].

	Laplace[b] $\mathcal{L} = \nabla^2$	Helmholtz[c] $\mathcal{L} = \nabla^2 + k^2$	Modified Helmholtz[d] $\mathcal{L} = \nabla^2 - k^2$
1D	$\frac{1}{2}\lvert x - x'\rvert$	$-\frac{i}{2k}\exp[ik\lvert x - x'\rvert]$	$-\frac{1}{2k}\exp[-k\lvert x - x'\rvert]$
2D	$\frac{1}{2\pi}\ln(\lvert\mathbf{r} - \mathbf{r}'\rvert)$	$-\frac{i}{4}H_0^{(1)}(k\lvert\mathbf{r} - \mathbf{r}'\rvert)$	$-\frac{1}{2\pi}K_0(k\lvert\mathbf{r} - \mathbf{r}'\rvert)$
3D	$-\frac{1}{4\pi}\frac{1}{\lvert\mathbf{r}-\mathbf{r}'\rvert}$	$-\frac{1}{4\pi}\frac{\exp[ik\lvert\mathbf{r}-\mathbf{r}'\rvert]}{\lvert\mathbf{r}-\mathbf{r}'\rvert}$	$-\frac{1}{4\pi}\frac{\exp[-k\lvert\mathbf{r}-\mathbf{r}'\rvert]}{\lvert\mathbf{r}-\mathbf{r}'\rvert}$

[a] The vector $\mathbf{r}$ can be either a two-dimensional or three-dimensional position vector.

[b] Laplace boundary conditions: for 1D and 2D are arbitrary and 3D is $G \to 0$ if $\mathbf{r} \to \infty$.

[c] Helmholtz boundary conditions: outgoing wave for all dimensions. $H_0^{(1)}$ is a Hankel function such that $H_0^{(1)}(x) = i\frac{2}{\pi}\ln(x) + 1 + i\frac{2}{\pi}\times$ $\times[\gamma - \ln(2)] + \ldots$, where γ is the Euler-Mascheroni constant.

[d] Modified Helmholtz boundary conditions: $G \to 0$ at infinity for all dimensions. K_0 is a modified Bessel function, i.e., $K_0(x) = -\ln(x) +$ $-\gamma + \ln(2) + \ldots$.

Subsection 2.1.3. The time-independent Schrödinger's equation for this case is

$$\Big[-\frac{\hbar^2}{2m}\nabla^2 + V(\mathbf{r})\Big]\psi(\mathbf{r}) = E\psi(\mathbf{r}), \tag{2.39}$$

where $V(\mathbf{r})$ is the scattering potential. Defining $E = (\hbar^2 k^2)/(2m)$ and $\mathcal{V}(\mathbf{r}) = (2m/\hbar^2)V(\mathbf{r})$, the above expression can be rewritten as

$$\Big[\nabla^2 + k^2\Big]\psi(\mathbf{r}) = \mathcal{V}(\mathbf{r})\psi(\mathbf{r}). \tag{2.40}$$

Then the associated Green's function is the solution of[16] $[\nabla^2 + k^2]G(\mathbf{r}) = \delta(\mathbf{r})$.

[16] The Green's function is always (at least) a two-variable function, but here the variable $\mathbf{r}'$ is omitted since the source term, the right-hand side of Equation (2.40) involves the scattering potential and it was assumed in the Subsection 2.1.3 that $V(\mathbf{r}')$ is centered at the origin. Then $\mathbf{r}' = 0$.

Notice that the linear operator in question is the Helmholtz operator thus, from Table 2.1, Green's function is given by [25]

$$G^{(\pm)}(\mathbf{r}) = -\frac{1}{4\pi}\frac{\exp[\pm ikr]}{r}, \tag{2.41}$$

where $r = |\mathbf{r}|$ and the ± 1 factor means that it is possible to consider the particles coming from both left $(+)$ and right $(-)$. Observe that here it is considered just one scattering process, but the wave could suffer more collisions after being spread for the first time. This is what happens with a free electron inside a crystal lattice. As imagined, this type of phenomenon is difficult to analyze. However, for the one-dimensional case, with localized potentials, there is an exact expression for Green's function.

2.2.2 The exact Green's function for 1D quantum scattering

Consider the following 1D problem: there is an incident wave coming from the left or the right, which will be spread by an arbitrary set of compact support potentials, as shown in Figure 2.6. If there are $N = n - l + 1$ barriers, the whole segmented potential is

$$V(x) = \sum_{i=l}^{n} V_i(x), \tag{2.42}$$

and we want to know how is Green's function associated with the one-dimensional time-independent Schrödinger equation

$$\Big[-\frac{\hbar^2}{2m}\frac{d^2}{dx^2} + V(x)\Big]\varphi(x) = E\varphi(x). \tag{2.43}$$

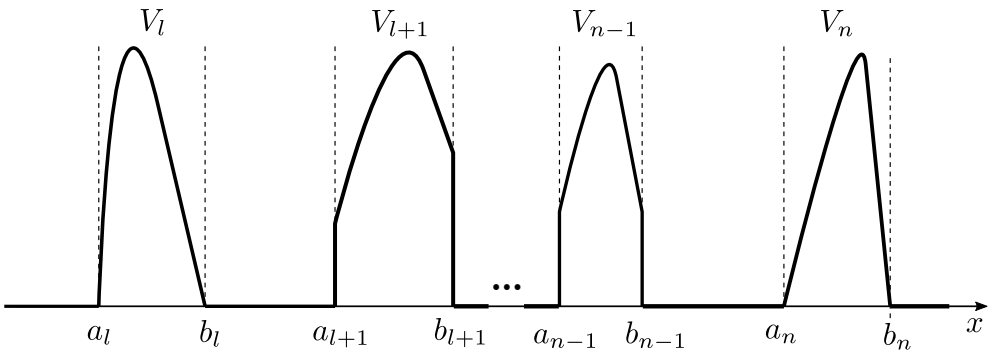

Figure 2.6: System formed by $N = n - l + 1$ arbitrary compact support potentials.

Let $\{\varphi_n, \varphi_k\}$ be the complete set of solutions for the above equation, in other words, φ_n and φ_k are, respectively, the bound and scattering states associated with energies E_n and $\hbar^2k^2/(2m)$. Therefore, as seen before, there are two ways to write Green's function

for this problem: as an eigenfunction expansion as given by the Equation (2.34)

$$G(x_f, x_i; E) = \sum_n \frac{\varphi_n(x_f)\varphi_n^*(x_i)}{E - E_n} + \int_0^\infty dk \frac{\varphi_k(x_f)\varphi_k^*(x_i)}{E - \frac{\hbar^2 k^2}{2m}}, \tag{2.44}$$

or by a perturbative expansion

$$\begin{aligned} G(x_f, x_i; E) = G_0(x_f, x_i; E) + \int dx_1 G_0(x_f, x_1; E) V(x_1) G_0(x_1, x_i; E) \\ + \int\int dx_1 dx_2 G_0(x_f, x_2; E) V(x_2) G_0(x_2, x_1; E) V(x_1) G_0(x_1, x_i; E) + \cdots, \end{aligned} \tag{2.45}$$

which corresponds to the Equation (2.38). Here the general vectors $\mathbf{r}$ and $\mathbf{r}'$ were replied by the wave initial and final positions, x_i and x_f.

Employing Equations (2.44) and (2.45), it is possible to prove that for such a system, the exact expression for Green's function — for an incident wave propagating from the right or the left — is a relation analogous to the *semiclassical formula*[17], which is given by [31]

$$G(x_f, x_i; k) = \frac{m}{i\hbar^2 k} \sum_{s.p.} W_{s.p.} \exp\left[\frac{i}{\hbar} S_{s.p.}(x_f, x_i; k)\right], \tag{2.47}$$

where *s.p.* means *scattering path*, that is, the path on which the particle starts in x_i and is spread between the potentials until it reaches x_f. Furthermore, $S_{s.p.}$ and $W_{s.p.}$ are, respectively, the *classical action* and the *amplitude* of the corresponding s.p..

Before exploring in more detail the equation above, let us state an important property of the scattering coefficients that is present in each $W_{s.p.}$ term. It is possible to demonstrate that the scattering amplitudes for any arbitrary compact support potential can be written as a product of a complex function and a general phase [31]. For example, if a wave collides against a potential $V(x)$, defined in the $[a, b]$ interval, the fraction of the wave that is reflected (if the wave comes from left or right) is $\mathcal{R}^{(\pm)} = r^{(\pm)} \exp[\pm ik2c^{\mp}]$ and the fraction that is transmitted is $\mathcal{T}^{(\pm)} = t^{(\pm)} \exp[-ik(b-a)]$, with $c^- = a$ and $c^+ = b$.

Returning to Equation (2.47), the classical action is such that $S_{s.p.} = kL_{s.p.}$, where $L_{s.p.}$ is the free scattering path, i.e., the total length of such s.p. *outside* of the potentials (that is, outside of the range where the compact support potentials are defined). The above definition may sound counterintuitive, since for different energies the effective separation between the potentials can change, as indicated in Figure 2.7. However, this separation

[17] The Van Vleck–Gutzwiller semiclassical approximation formula is [61]

$$G_{s.c.}(\mathbf{r}_f, \mathbf{r}_i; k) = \frac{2\pi}{(2\pi i\hbar)^{\frac{n+1}{2}}} \sum_c ((-1)^{n+1} D_c)^{\frac{1}{2}} \exp\left[-\frac{i\pi}{2}\eta_c\right] \exp\left[iS_c(\mathbf{r}_f, \mathbf{r}_i; k)\right], \tag{2.46}$$

where S_c is the classical action, D_c is the semiclassical amplitude (if $n = 1$, $D_c = 1/(|x_f||x_i|)$), the Morse index η_c is the number of conjugate points at constant energy and the sum is over all the trajectories, between the positions $\mathbf{r}_i$ and $\mathbf{r}_f$, with energy E.

depends on the potential shape, and therefore this information is present in the scattering coefficients that appear in the amplitude $W_{s.p.}$ described next.

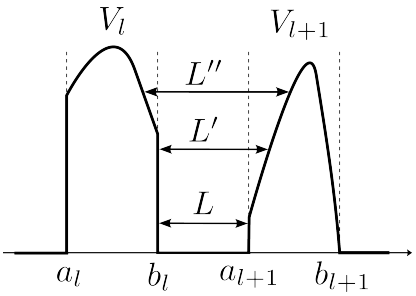

Figure 2.7: A example that for different energies the effective separation between two potentials can change ($L \neq L' \neq L''$), however, the width that appears in the total length is the width $L = a_{l+1} - b_l$, defined from the compact support potentials ranges.

Moreover, each time the particle reaches a potential it can be either reflected or transmitted, then the partial amplitude is equal to a reflection or transmission coefficient. Therefore, the total $W_{s.p.}$ is the product of the complex functions, $r^{(\pm)}$ and $t^{(\pm)}$, of all partial amplitudes in that specific s.p.. For simplicity, in this work, unless stated otherwise, whenever scattering coefficients are mentioned we are referring to $r^{(\pm)}$ and $t^{(\pm)}$ (and not $\mathcal{R}^{(\pm)}$ and $\mathcal{T}^{(\pm)}$). To create more intuition about the last equation, the technique required to write Green's function is shown in Appendix B.

The exact Green's function for 1D quantum scattering, introduced in Equation (2.47), is a quite useful formula. A few reasons are:

(i) The shape of each potential is arbitrary, as the width between them. Thus, Equation (2.47) is suitable for the most general (and multi-)scattering process involving compact support potentials.

(ii) The Equation (2.47) can be interpreted as a *multiple scattering expansion* or a *planar wave expansion* since each term of the sum has a very clear physical interpretation: each collision in an s.p. adds a new amplitude product in the correspondent $W_{s.p.}$, whereas the length traveled is accounted by an exponential argument in $S_{s.p.}$. Since the time-independent Schrödinger's equation for such a problem has a Helmholtz-like operator, from Table 2.1, the planar wave presence was already predicted[18].

[18]The exact expression is given in the Equation (2.47) also remembers Feynman's path integral, given by

$$K(x_N, x_1; t_N, t_1) = \langle x_N, t_N | x_1, t_1 \rangle = \int_{x_1}^{x_N} \mathcal{D}[x(t)] \exp\left[\frac{i}{\hbar} dt S_c(x, \dot{x})\right], \tag{2.48}$$

where $K(x_N, x_1; t_N, t_1)$ is the quantum propagator and $\mathcal{D}[x(t)]$ is an infinite-dimensional integral operator over all the possible paths of the system [27, 30]. This connection is a intuitive since the propagator is the inverse Fourier Transform of the Green's function, as will be commented in item (iv).

(iii) As demonstrated in [62], a general barrier $V(x)$ can be written as a compact support potentials set $\{V_i(x)\}$, such that $a_{i+1} = b_i$ for all $i = 1, 2, \ldots, N$, that is, the $V_i(x)$s are "glued" to each other. Thus the exact Green's function for this potential $V(x)$ can also be calculated with the Equation (2.47) (by dividing $V(x)$ into pieces $V_i(x)$, which will depend on the whole potential shape).

(iv) From the literature it is known that the quantum propagator K is the inverse Fourier transform of the Green's function [27, 30]. So the Equation (2.47) enables the investigation of the wave propagation with the relations $\varphi(x,t) = \int dx_0 K(x, x_0; t)\varphi_0(x_0) = \int dx_0 (i/2\pi) \int_{-\infty}^{\infty} dE \exp[-itE/\hbar] G(x, x_0; E)\varphi_0(x_0)$. This approach is used in [63], where a classification scheme for the complete family of 1D point interactions is proposed.

(v) As can be seen in the Equation (2.44), if Green's function for such a phenomenon is well established, the energy eigenvalues can be found with the G poles, while the eigenfunctions with the G residues.

The last advantage that could be included in the above list is that Equation (2.47) makes it possible to construct recurrence relations for the reflection and transmission amplitudes of an arbitrary scattering process. As mentioned before, in the scattering study, discovering these coefficients, and the associated probabilities are of fundamental importance. The demonstration of the statement made in this paragraph is the initial step for the development of this work and is shown in the next chapter. But first, we present the required aspects of the other key idea for the methodology developed in this dissertation: the continued fractions.

2.3 Continued Fractions

As seen in Chapter 1, continued fractions have applications in several fields of physics. In addition, there are so many more in mathematics and chemistry [64]. By definition, a CF is an ordered pair $\{\{\{a_n\}, \{b_n\}\}, \{f_n\}\}$, such that $a_1, a_2, \ldots \neq 0$ and $b_1, b_2, \ldots$ are complex numbers, and $\{f_n\}$ is a sequence in the extended complex plane, where f_n is called the nth *approximant* and is given by [65, 66]

$$f_n = b_0 + \cfrac{a_1}{b_1 + \cfrac{a_2}{b_2 + \cfrac{a_3}{\ddots \; + \frac{a_n}{b_n}}}}, \tag{2.49}$$

with $n = 1, 2, \ldots$. Therefore, the continued fraction $\{\{\{a_n\}, \{b_n\}\}, \{f_n\}\}$ is often written as

$$b_0 + \mathbf{K}(a_n/b_n) = b_0 + \cfrac{a_1}{b_1 + \cfrac{a_2}{b_2 + \cfrac{a_3}{\ddots}}}. \tag{2.50}$$

When $a_n = 1$ for all n, the CF is called *simple* (or *regular*).

Moreover, it is known that the nth approximant can be given as

$$f_n = \frac{X_n}{Y_n}, \qquad n = 0, 1, \ldots, \tag{2.51}$$

such that there is a sequence of complex numbers $\{X_n\}$ and $\{Y_n\}$ defined by the system of second-order linear difference equations,

$$\begin{cases} X_n = b_n X_{n-1} + a_n X_{n-2} \\ Y_n = b_n Y_{n-1} + a_n Y_{n-2} \end{cases}, \tag{2.52}$$

with $n = 0, 1, 2, \ldots$ and the initial conditions $X_{-1} = 1$, $X_0 = b_0$, $Y_{-1} = 0$ and $Y_0 = 1$. The quantities X_n and Y_n are called, respectively, as nth *numerator* and *denominator* of the continued fraction [67, 65]. The above properties provide a simplification for the methodology proposed in this work.

Chapter 3

The Green's function method allied to continued fractions

3.1 Exact Green's function and recurrence relations

When the scattering structure in the analysis is composed of an arbitrary number of localized potentials, and such a number is large, determining the exact expression for Green's function via Equation (2.47) can be an arduous task. To simplify it we evaluate a set of potentials as a block, scrutinizing them as a single potential. Hence we aim to find an expression for this block's reflection and transmission coefficients.

3.1.1 Recurrence relations for compact support potentials

Let us investigate the simplest case first and then proceed to generalization by induction. Initially take two potentials of arbitrary format and compact support, V_l and V_{l+1}, whose domains are, respectively, $[a_l, b_l]$ and $[a_{l+1}, b_{l+1}]$, as schematized in Figure 3.1. Consider that the transmission and reflection coefficients are, respectively, $T_j^{(\pm)}$ and $R_j^{(\pm)}$, with $j = l,\, l+1$, where the signals $\pm$ indicates that the wave is coming from the left or right. Writing $G(x_f, x_i; k) = \frac{m}{i\hbar^2 k} g_{--}(x_f, x_i; k)$ when $x_i, x_f < a_l$ (that is, when the endpoints of all possible s.p. lie before both potentials, as indicated by the circles in the axis of Figure 3.1), we see that the exact Green's function will be such that

$$g_{--}(x_f, x_i; k) = \exp(ik|x_f - x_i|) + R_l^{(+)} \exp[-ik(x_i + x_f - 2a_l)] + T_l^{(+)} P_l^{(+)} \exp[ik(a_l - x_i)], \tag{3.1}$$

where $P_l^{(+)}$ represents an infinite set of all possible trajectories between the potentials V_l and V_{l+1}, which culminate in x_f after being transmitted through V_l by the left.

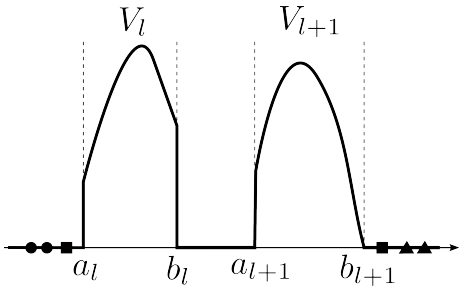

Figure 3.1: System formed by two different compact support potentials.

Analyzing the possible trajectories between the potentials, we obtain

$$\begin{aligned} P_l^{(+)} = T_l^{(-)} \exp[ik(a_l - x_f)] \Big\{ & R_{l+1}^{(+)} \exp[2ik(a_{l+1} - b_l)] \\ & + (R_{l+1}^{(+)})^2 R_l^{(-)} \exp[4ik(a_{l+1} - b_l)] + (R_{l+1}^{(+)})^3 (R_l^{(-)})^2 \exp[6ik(a_{l+1} - b_l)] + \dots \Big\}. \end{aligned} \tag{3.2}$$

Since the term in braces is equal to

$$\sum_{n=0}^{\infty} (R_{l+1}^{(+)})^{n+1} (R_l^{(-)})^n \exp[2ik(a_{l+1} - b_l)]^{n+1} = \frac{R_{l+1}^{(+)} \exp[2ik(a_{l+1} - b_l)]}{1 - R_l^{(-)} R_{l+1}^{(+)} \exp[2ik(a_{l+1} - b_l)]}, \tag{3.3}$$

i.e., a *geometric series*,

$$P_1^{(+)} = \frac{R_{l+1}^{(+)} T_l^{(-)} \exp[ik(a_l - x_f)] \exp[2ik(a_{l+1} - b_l)]}{1 - R_l^{(-)} R_{l+1}^{(+)} \exp[2ik(a_{l+1} - b_l)]}. \tag{3.4}$$

Substituting (3.4) into (3.1),

$$\begin{aligned} g_{--}(x_f, x_i; k) = \exp(ik|x_f - x_i|) + R_l^{(+)} \exp[-ik(x_i + x_f - 2a_l)] \\ + \frac{R_{l+1}^{(+)} T_l^{(-)} T_l^{(+)} \exp[2ik(a_{l+1} - b_l)] \exp[-ik(x_i + x_f - 2a_l)]}{1 - R_l^{(-)} R_{l+1}^{(+)} \exp[2ik(a_{l+1} - b_l)]}. \end{aligned} \tag{3.5}$$

From Figure 3.1 we notice that, excluding the case where the particle leaves the initial position and reaches the final position before "touching" the first potential, there is a *mandatory path* for any s.p.: leave x_i and "cross" V_l (to thus develop reflections between the potentials) and "cross" V_l again to reach x_f. This mandatory path is given by the factor $\exp[ik(a_l - x_i)] \exp[ik(a_l - x_f)] = \exp[-ik(x_i + x_f - 2a_l)]$. For this reason, from Equation (3.5) we define the reflection coefficient (+) of the block formed by both potentials as

$$R_{l+1,l}^{(+)} = R_l^{(+)} + \frac{R_{l+1}^{(+)} T_l^{(-)} T_l^{(+)} \exp[2ik(a_{l+1} - b_l)]}{1 - R_l^{(-)} R_{l+1}^{(+)} \exp[2ik(a_{l+1} - b_l)]}, \tag{3.6}$$

so we can write

$$g_{--}(x_f, x_i; k) = \exp(ik|x_f - x_i|) + R_{l+1,l}^{(+)} \exp[-ik(x_i + x_f - 2a_l)]. \tag{3.7}$$

In order to determine the reflection coefficient $(-)$ we consider the case where $x_i, x_f > b_{l+1}$ (indicated by the two triangles in Figure 3.1). Similarly, we get

$$g_{++}(x_f, x_i; k) = \exp(ik|x_f - x_i|) + R_{l+1}^{(-)} \exp[ik(x_i + x_f - 2b_{l+1})] + \frac{R_l^{(-)} T_{l+1}^{(-)} T_{l+1}^{(+)} \exp[2ik(a_{l+1} - b_l)] \exp[ik(x_i + x_f - 2b_{l+1})]}{1 - R_l^{(-)} R_{l+1}^{(+)} \exp[2ik(a_{l+1} - b_l)]}, \tag{3.8}$$

but now the mandatory path is represented by the factor $\exp[ik(x_i - b_{l+1})] \exp[ik(x_f - b_{l+1})] = \exp[ik(x_i + x_f - 2b_{l+1})]$, so

$$R_{l+1,l}^{(-)} = R_{l+1}^{(-)} + \frac{R_l^{(-)} T_{l+1}^{(-)} T_{l+1}^{(+)} \exp[2ik(a_{l+1} - b_l)]}{1 - R_l^{(-)} R_{l+1}^{(+)} \exp[2ik(a_{l+1} - b_l)]}. \tag{3.9}$$

Finally we evaluate $g(x_f, x_i; k)$ when $x_i < a_l$ and $x_f > b_{l+1}$ and when $x_i > b_{l+1}$ and $x_f < a_l$ (both cases represented by the squares in Figure 3.1), obtaining respectively

$$g_{+-}(x_f, x_i; k) = \frac{T_l^{(+)} T_{l+1}^{(+)} \exp[ik(a_{l+1} - b_l)] \exp[ik(x_f - x_i - (b_{l+1} - a_l)]}{1 - R_l^{(-)} R_{l+1}^{(+)} \exp[2ik(a_{l+1} - b_l)]}, \tag{3.10}$$

and,

$$g_{-+}(x_f, x_i; k) = \frac{T_{l+1}^{(-)} T_l^{(-)} \exp[ik(a_{l+1} - b_l)] \exp[ik(x_i - x_f - (b_{l+1} - a_l)]}{1 - R_l^{(-)} R_{l+1}^{(+)} \exp[2ik(a_{l+1} - b_l)]}. \tag{3.11}$$

Since the mandatory paths are represented by $\exp[ik(a_l - x_i + x_f - b_{l+1})]$ and $\exp[ik(x_i - x_f - (b_{l+1} - a_l)]$, we define

$$T_{l+1,l}^{(+)} = \frac{T_l^{(+)} T_{l+1}^{(+)} \exp[ik(a_{l+1} - b_l)]}{1 - R_l^{(-)} R_{l+1}^{(+)} \exp[2ik(a_{l+1} - b_l)]}, \tag{3.12}$$

and,

$$T_{l+1,l}^{(-)} = \frac{T_{l+1}^{(-)} T_l^{(-)} \exp[ik(a_{l+1} - b_l)]}{1 - R_l^{(-)} R_{l+1}^{(+)} \exp[2ik(a_{l+1} - b_l)]}. \tag{3.13}$$

Observe that in both reflections and transmission coefficients, the exponential depends only on k and the width between the potential constituents of the block, that is, on $a_{l+1} - b_l$.

Now consider a system formed by three compact support potentials of arbitrary formats, as schematized in Figure 3.2. In this case, we treat the first two potentials as a block (the shaded area of Figure 3.2), whose coefficients are: $R_{l+1,l}^{(\pm)}$ and $T_{l+1,l}^{(\pm)}$ given by Equations (3.6) to (3.13). Thus it is evident that, for example, the reflection coefficient $(+)$ for the block formed by the three potentials is as follows

$$R_{l+2,l}^{(+)} = R_{l+1,l}^{(+)} + \frac{R_{l+2}^{(+)} T_{l+1,l}^{(-)} T_{l+1,l}^{(+)} \exp[2ik(a_{l+2} - b_{l+1})]}{1 - R_{l+1,l}^{(-)} R_{l+2}^{(+)} \exp[2ik(a_{l+2} - b_{l+1})]}. \tag{3.14}$$

Lastly, let us examine the most general case, the system formed by $N = n - l + 1$ arbitrary localized potentials (Figure 2.6). Treating the first $N - 1$ barriers as a first block,

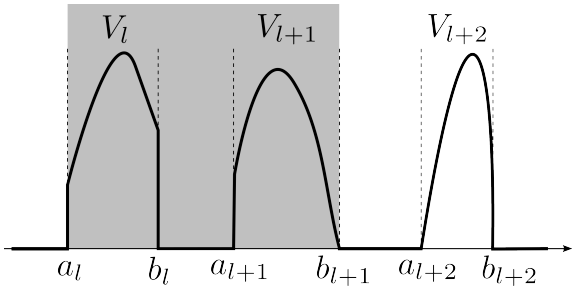

Figure 3.2: System formed by three different compact support potentials.

of coefficients $R^{(\pm)}_{n-1,l}$ and $T^{(\pm)}_{n-1,l}$, the amplitudes of the block consisting of all N potentials are

$$R^{(+)}_{n,l} = R^{(+)}_{n-1,l} + \frac{R^{(+)}_n T^{(-)}_{n-1,l} T^{(+)}_{n-1,l} \exp[2ik(a_n - b_{n-1})]}{1 - R^{(-)}_{n-1,l} R^{(+)}_n \exp[2ik(a_n - b_{n-1})]}, \tag{3.15}$$

$$R^{(-)}_{n,l} = R^{(-)}_n + \frac{R^{(-)}_{n-1,l} T^{(-)}_n T^{(+)}_n \exp[2ik(a_n - b_{n-1})]}{1 - R^{(-)}_{n-1,l} R^{(+)}_n \exp[2ik(a_n - b_{n-1})]}, \tag{3.16}$$

$$T^{(+)}_{n,l} = \frac{T^{(+)}_{n-1,l} T^{(+)}_n \exp[ik(a_n - b_{n-1})]}{1 - R^{(-)}_{n-1,l} R^{(+)}_n \exp[2ik(a_n - b_{n-1})]}, \tag{3.17}$$

and,

$$T^{(-)}_{n,l} = \frac{T^{(-)}_{n-1,l} T^{(-)}_n \exp[ik(a_n - b_{n-1})]}{1 - R^{(-)}_{n-1,l} R^{(+)}_n \exp[2ik(a_n - b_{n-1})]}. \tag{3.18}$$

The above equations are the recurrence relations for the scattering amplitudes of a set of compact support potentials with arbitrary formats. These relations are already known in the literature (as in [42, 68]), which were previously obtained by the employment of the transfer matrix method. It demonstrates how powerful the use of exact Green's function is, since such relations can be rigorously demonstrated in a very intuitive way — because the general structure of the Equations (3.15) to (3.18) emerges from a geometric series originated from the sum over all possible scattering paths.

If the potentials are point interactions, that is, if $a_j = b_j = y_j$ for all j, the recurrence relations of Equations (3.15) to (3.18) become the same as those obtained in [69]. We notice that it is counterintuitive to imagine that the recurrence relations for compact support potentials and point potentials are practically the same, i.e., that the exponentials in both cases depend only on the width between the block (formed by the potentials V_l a V_{n-1}) and the last potential (V_n). However, this is a consequence of the following fact: in the construction of Green's function, the total length of each s.p. is accounted only *outside* of the potentials, as said before. The width of each cell is present inside the scattering coefficients $T^{(\pm)}_j$ and $R^{(\pm)}_j$, with $j = l, l+1, \ldots, N$.

3.2 Scattering coefficients and continued fractions

3.2.1 The relation between reflection and transmission coefficients

The recurrence relations found in Subsection 3.1.1 enable obtaining new relations between the scattering coefficients. For this, let us investigate the elementary properties of general amplitudes. From [31, 70] we known that $t^{(+)} = t^{(-)} = t$, and due the probability conservation, it is clear that $|r^{(\pm)}|^2 + |t|^2 = 1$. Thus $|r^{(+)}|^2 = |r^{(-)}|^2 \Rightarrow r^{(+)} r^{(+)^*} = r^{(-)} r^{(-)^*}$. For a complex z it holds that $z^* = |z| \exp[-i \arg(z)]$, so

$$r^{(+)} = \frac{r^{(-)^*}}{r^{(+)^*}} r^{(-)} = \left| \frac{r^{(-)}}{r^{(+)}} \right| \exp\left[-i \arg\left(\frac{r^{(-)}}{r^{(+)}} \right) \right] r^{(-)}, \tag{3.19}$$

as $\left| \frac{r^{(-)}}{r^{(+)}} \right| = 1$ and setting $\phi = -\arg\left(\frac{r^{(-)}}{r^{(+)}} \right)$, we found that

$$r^{(+)} = r^{(-)} \exp(i\phi), \tag{3.20}$$

in other words, between the coefficients $r^{(+)}$ and $r^{(-)}$ there is only a phase. Furthermore, it is evident that if the barrier is symmetric, that is, if $r^{(+)} = r^{(-)}$, the phase between such coefficients is zero (or a multiple of 2π).

Now consider a periodic lattice composed of localized potentials, i.e., a network formed by N identical barriers spaced by a length L $(= a_{l+1} - b_l)$, as in Figure 3.3. First assume the *barrier-block set* (see Figure 3.3(a)), that is, that we know the coefficients of the first barrier, given by $r^{(+)} = r$, $r^{(-)} = r \exp(-i\phi)$ and t, and of the block formed by the following $N-1$ potentials, given by $R_{N-1}^{(+)} = R_{N-1}$, $R_{N-1}^{(-)} = R_{N-1} \exp(-i\Phi_{N-1})$ and T_{N-1}. From Subsection 3.1.1 (Equations (3.15) to (3.18)) the coefficients for the block composed of all N potentials are

$$R_N = r + \frac{R_{N-1} t^2 \exp(2ikL)}{1 - r R_{N-1} \exp[i(2kL - \phi)]}, \tag{3.21}$$

$$R_N \exp(-i\Phi_N) = R_{N-1} \exp(-i\Phi_{N-1}) + \frac{r T_{N-1}^2 \exp[i(2kL - \phi)]}{1 - r R_{N-1} \exp[i(2kL - \phi)]}, \tag{3.22}$$

and,

$$T_N = \frac{t T_{N-1} \exp(ikL)}{1 - r R_{N-1} \exp[i(2kL - \phi)]}. \tag{3.23}$$

On the other hand, when analyzing the *block-barrier set* (see Figure 3.3(b)), the coefficients of the N potentials will be

$$R_N = R_{N-1} + \frac{r T_{N-1}^2 \exp(2ikL)}{1 - r R_{N-1} \exp[i(2kL - \Phi_{N-1})]}, \tag{3.24}$$

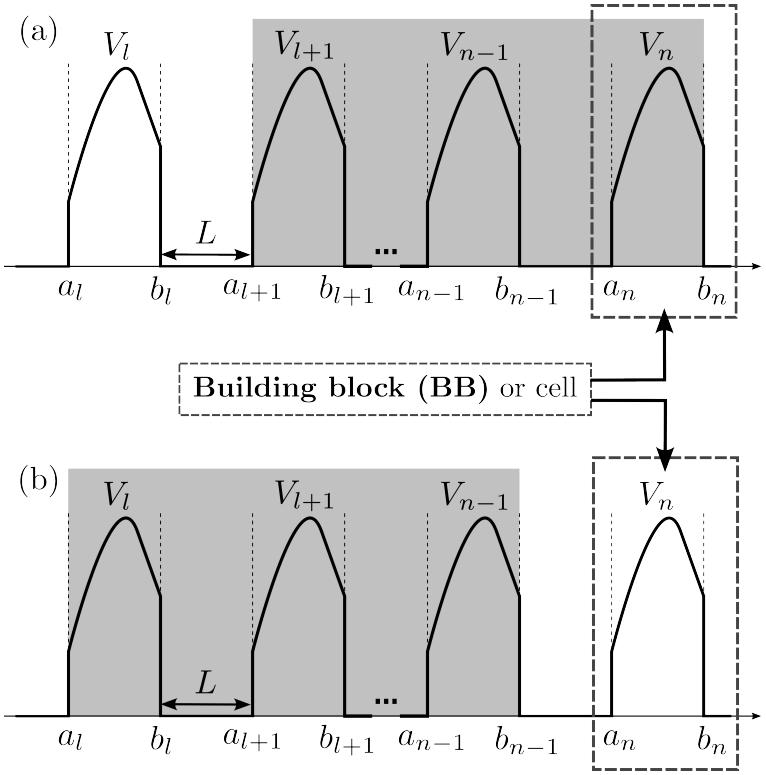

Figure 3.3: A general periodic structure, highlighting the (a) barrier-block set and the (b) block-barrier set. The dashed box highlights the building block (BB, or cell) of a such periodic structure.

$$R_N \exp(-i\Phi_N) = r\exp(-i\phi) + \frac{R_{N-1}t^2\exp[i(2kL-\Phi_{N-1})]}{1 - rR_{N-1}\exp[i(2kL-\Phi_{N-1})]}, \tag{3.25}$$

and,

$$T_N = \frac{tT_{N-1}\exp(ikL)}{1 - rR_{N-1}\exp[i(2kL-\Phi_{N-1})]}. \tag{3.26}$$

Since the barriers are identical, Equations (3.21) to (3.23) correspond, respectively, to Equations (3.24) to (3.26). Then, comparing Equations (3.23) and (3.26), we notice that $\exp(i\phi) = \exp(i\Phi_{N-1})$, in words, the phase between the reflection coefficients (+) and (−) of only one barrier is the same phase of such coefficients for a block with $N-1$ potentials. Since we know $r^{(\pm)}$, and hence ϕ and Φ_{N-1}, if it is possible to determine $R^{(+)}_{N-1} = R_{N-1}$, $R^{(-)}_{N-1} = R_{N-1}\exp(-i\Phi_{N-1})$ is found too.

Moreover, using the above result ($\phi = \Phi_{N-1}$) in Equation (3.24) and doing some manipulations, we can write

$$\sqrt{\frac{(R_N - R_{N-1})}{r}}t = \frac{T_{N-1}t\exp(ikL)}{\sqrt{1 - rR_{N-1}\exp[i(2kL-\phi)]}}, \tag{3.27}$$

or yet,

$$T_{N-1}t\exp(ikL) = \sqrt{1 - rR_{N-1}\exp[i(2kL-\phi)]}\sqrt{\frac{(R_N - R_{N-1})}{r}}t. \tag{3.28}$$

From Equation (3.23) — or (3.26) — we see that

$$T_N(1 - rR_{N-1}\exp[i(2kL - \phi)]) = \sqrt{1 - rR_{N-1}\exp[i(2kL - \phi)]}\sqrt{\frac{(R_N - R_{N-1})}{r}}t \quad (3.29)$$

therefore

$$T_N = \sqrt{\frac{R_N - R_{N-1}}{r(1 - rR_{N-1}\exp[i(2kL - \phi)])}}t, \quad (3.30)$$

hence it is possible to calculate the transmission coefficient if $R_N = R_N^{(+)}$ is known.

3.2.2 The (+) reflection coefficient and continued fractions

Consider again a system formed by N identical barriers spaced by a length L, where we know the coefficients $r^{(\pm)}$ and t of the composing cells. It was demonstrated that just by calculating $R_N^{(+)}$ we can obtain the other coefficients of the block, $R_N^{(-)}$ and T. For this reason, we aim to find $R_N^{(+)}$ in a simple way for an arbitrary number of potentials. Treating the potentials V_{l+1} to V_n as a block of coefficients $R_{N-1}^{(\pm)}$ and T_{N-1}, the total reflection coefficient (+), of the N potentials, is given by Equation (3.21).

To simplify the notation, some definitions are made. First let $A_N = r^{(-)}R_N^{(+)}\times \exp(2ikL)$. Using Equation (3.21), we see that

$$A_N = r^{(-)}r^{(+)}\exp(2ikL) + \frac{A_{N-1}t^2\exp(2ikL)}{1 - A_{N-1}}. \quad (3.31)$$

Setting $v^{(\pm)} = r^{(\pm)}\exp(ikL)$ and $u = t\exp(ikL)$, we obtain

$$A_N = v^{(-)}v^{(+)} + \frac{A_{N-1}u^2}{1 - A_{N-1}}. \quad (3.32)$$

Now let $B_N = 1 - A_N$, then

$$B_N = 1 - v^{(-)}v^{(+)} - \frac{(1 - B_{N-1})u^2}{B_{N-1}} = 1 + u^2 - v^{(-)}v^{(+)} - \frac{u^2}{B_{N-1}}. \quad (3.33)$$

Finally, making $C_N = B_N/iu$, we have

$$C_N = \frac{1 + u^2 - v^{(-)}v^{(+)}}{iu} - \frac{u}{iB_{N-1}} = \frac{1 + u^2 - v^{(-)}v^{(+)}}{iu} + \frac{iu}{B_{N-1}}, \quad (3.34)$$

and, defining

$$\gamma = \frac{1 + u^2 - v^{(-)}v^{(+)}}{iu} \quad (3.35)$$

we concluded that

$$C_N = \gamma + \frac{1}{C_{N-1}}, \quad (3.36)$$

and this expression is valid for an arbitrary number of potentials.

Accordingly, we notice that

$$C_{N-1} = \gamma + \frac{1}{C_{N-2}}\,, \quad C_{N-2} = \gamma + \frac{1}{C_{N-3}}\,, \quad \cdots \quad , \quad C_1 = \gamma + \frac{1}{C_0}\,, \tag{3.37}$$

that is, C_N is an *approximant of a simple* (or *regular*) *continued fraction* given by

$$C_N = \gamma + \cfrac{1}{\gamma + \cfrac{1}{\gamma + \cfrac{1}{\ddots \;\; \gamma + \frac{1}{C_0}}}} \tag{3.38}$$

in which there are N γs diagonally and its last denominator is C_0, where

$$C_0 = \frac{B_0}{iu} = \frac{1 - A_0}{iu} = \frac{1 - r^{(-)} R_0^{(+)} \exp(2ikL)}{iu} = \frac{1}{iu}, \tag{3.39}$$

since for $N = 0$ there is no barrier, $R_0^{(+)} = 0$.

Furthermore, we observe that

$$C_N = \frac{B_N}{iu} = \frac{1 - A_N}{iu} = \frac{1 - r^{(-)} R_N^{(+)} \exp(2ikL)}{iu}, \tag{3.40}$$

thus,

$$R_N^{(+)} = \frac{1 - iuC_N}{r^{(-)} \exp(2ikL)} = \frac{1 - iuC_N}{r^{(+)} \exp[i(2kL - \phi)]}. \tag{3.41}$$

In Equation (3.38) note that C_N depends only on $v^{(\pm)}$ and u, or rather, on the spacing L between the block barriers, the incident wavenumber k, and the coefficients of a single barrier, $r^{(\pm)}$ and t, which are known. Hence C_N can be easily determined. Finally, with the equation above we calculate $R_N^{(+)}$, and consequently $R_N^{(-)}$ and T_N. Therefore, all the coefficients of the block formed by N potentials are determined.

As said before, the scattering problem has been already solved by using continued fractions. The most applied methodology, in this case, is the one developed in the Horáček and Sasakawa papers [12, 13, 14]. In these works, they show that the partial scattering amplitudes can be written as continued fractions (that is why they call their technique as *method of continued fractions*[1]), and the calculations are realized in an iteration fashion. The iteration procedure stops when the first partial scattering amplitude does not change anymore. That is, the continued fractions are employed in order to discard the scattering information that is considered insignificant. Our method acts oppositely since the continued fractions are used to accumulate all the information about the scattering. In other words,

[1]Since the main mathematical tool used in the technique developed in this dissertation is also the continued fractions, we will also call our method as *method of continued fractions*.

what the function C_N do is count all the length paths and all the partial scattering amplitudes that the wave founds in its trajectory. The physical meaning of C_N is an *accumulated transmission*, since it depends on C_{N-1} and hence, on all the others C_is ($i < N$). Therefore, although C_N is an auxiliary function — because we are usually interested in $R_N^{(\pm)}$ and T_N, it carries all the scattering information (notice that calculating C_N, it is easy to calculate $R_N^{(\pm)}$ and T_N). Further the applications will bring some light to this statement.

Lastly, notice that a periodic structure (with N cells) becomes transparent when $|T_N|^2 = 1$ (and the wave will certainly pass through the lattice), i.e., when $|R_N^{(\pm)}|^2 = 0$. Looking at the Equation (3.41), since $C_0 = 1/(iu)$, we obtain

$$|R_N^{(+)}|^2 = |R_N^{(-)}|^2 = \left|\frac{1 - C_N/C_0}{r^{(+)}}\right|^2 = 0. \tag{3.42}$$

Moreover, we know that $0 \leq |r^{(\pm)}|^2 \leq 1$, so, ignoring the case $|r^{(\pm)}|^2 = 0$, we will have $|1 - C_N/C_0|^2 = 0$. Hence, the condition required for a transparent lattice is $C_N = C_0$. This is other important information about the scattering process that is present in the auxiliary function C_N.

3.2.3 The C_N convergent function

Notice that in Equation (3.38) the number of cells is not an explicit parameter. However, recalling the properties of continued fractions, the auxiliary function C_N can be written explicitly in terms of N. From Equations (2.49) to (2.52), notice that for $n = N$, $C_N = f_N = X_N/Y_N$, we have

$$\begin{cases} X_N = C_0 X_{N-1} + X_{N-2} \\ Y_N = C_0 Y_{N-1} + Y_{N-2} \end{cases}. \tag{3.43}$$

One crucial observation is that $C_n \neq f_n$ for any $n \neq N$ because, for example,

$$C_3 = \gamma + \cfrac{1}{\gamma + \cfrac{1}{\gamma + \cfrac{1}{C_0}}}, \tag{3.44}$$

while

$$f_3 = \gamma + \cfrac{1}{\gamma + \cfrac{1}{\gamma + \cfrac{1}{\gamma}}}. \tag{3.45}$$

In words, for the continued fraction $1 + \mathbf{K}(1/b_n)$, where $b_n \in \{\gamma, C_0\}$, f_N uses $N+1$ γs, while C_N uses N γs and the C_0.

However, due the repetition of γs on the diagonal of Equation (3.38), for any $n \neq N$, $f_n = X_n/Y_n$ is such that

$$\begin{cases} X_n = \gamma X_{n-1} + X_{n-2} \\ Y_n = \gamma Y_{n-1} + Y_{n-2} \end{cases}. \tag{3.46}$$

The equations above are *second-order homogeneous linear recurrence relations* that can be easily solved using the recurrence relation techniques.

Associated with $X_n = \gamma X_{n-1} + X_{n-2}$ — or with $Y_n = \gamma Y_{n-1} + Y_{n-2}$ — we have the *characteristic equation* $x^2 - \gamma x - 1 = 0$ [71, 72], which has two different roots

$$x_1 = \Gamma_1 = \frac{\gamma + \sqrt{\gamma^2+4}}{2} \quad \text{and} \quad x_2 = \Gamma_2 = \frac{\gamma - \sqrt{\gamma^2+4}}{2}, \tag{3.47}$$

then, the solutions for the Equations in (3.46) are,

$$X_n = c_1(\Gamma_1)^n + c_2(\Gamma_2)^n \quad \text{and} \quad Y_n = \tilde{c}_1(\Gamma_1)^n + \tilde{c}_2(\Gamma_2)^n, \tag{3.48}$$

where $c_1, c_2, \tilde{c}_1$ and $\tilde{c}_2$ are constants to be calculated.

Applying the initial conditions for X_n (see the conditions below Equation (2.52)),

$$\begin{cases} \gamma = c_1 + c_2 \\ 1 = \frac{c_1}{\Gamma_1} + \frac{c_2}{\Gamma_2} \end{cases}, \tag{3.49}$$

solving this system and making some manipulations we obtain

$$c_1 = \frac{(\Gamma_1)^2}{\sqrt{\gamma^2+4}} \quad \text{and} \quad c_2 = -\frac{(\Gamma_2)^2}{\sqrt{\gamma^2+4}}. \tag{3.50}$$

Repeating this procedure for Y_n's initial conditions we find

$$\begin{cases} 1 = \tilde{c}_1 + \tilde{c}_2 \\ 0 = \frac{\tilde{c}_1}{\Gamma_1} + \frac{\tilde{c}_2}{\Gamma_2} \end{cases}, \tag{3.51}$$

thus,

$$\tilde{c}_1 = \frac{\Gamma_1}{\sqrt{\gamma^2+4}} \quad \text{and} \quad \tilde{c}_2 = -\frac{\Gamma_2}{\sqrt{\gamma^2+4}}. \tag{3.52}$$

Once Equations (3.48) to (3.52) are valid when $n \neq N$ — for example when $n = N-1$ or $n = N-2$ — we can write $C_N = X_N/Y_N$ with X_N and Y_N given by Equation (3.46) such that

$$C_N = \frac{C_0 X_{N-1} + X_{N-2}}{C_0 Y_{N-1} + Y_{N-2}} = \frac{C_0[c_1(\Gamma_1)^{N-1} + c_2(\Gamma_2)^{N-1}] + c_1(\Gamma_1)^{N-2} + c_2(\Gamma_2)^{N-2}}{C_0[\tilde{c}_1(\Gamma_1)^{N-1} + \tilde{c}_2(\Gamma_2)^{N-1}] + \tilde{c}_1(\Gamma_1)^{N-2} + \tilde{c}_2(\Gamma_2)^{N-2}}, \tag{3.53}$$

therefore,

$$C_N = \frac{C_0[(\Gamma_1)^{N+1} - (\Gamma_2)^{N+1}] + (\Gamma_1)^N - (\Gamma_2)^N}{C_0[(\Gamma_1)^N - (\Gamma_2)^N] + (\Gamma_1)^{N-1} - (\Gamma_2)^{N-1}}. \tag{3.54}$$

Again, notice that C_N depends on the scattering coefficients of only one barrier (the lattice cell), the wavenumber, and the space between them, but, in addition, here the dependence of the number of cells is explicit (and is not a parameter of a sine function, as in the transfer matrix method, making calculations faster).

Using the equation above — or the Equation (3.38) — on the Equation (3.41) it is possible obtain the reflection probability for N barriers as

$$|R_N^{(+)}|^2 = |R_N^{(-)}|^2 = \left|\frac{1 - it\exp(ikL)C_N}{r^{(+)}}\right|^2, \tag{3.55}$$

since the reflection coefficients differ just by one phase. Furthermore, with the Equations (3.30) and (3.41), we can calculate the transmission probability as

$$\begin{aligned} |T_N|^2 &= \left| \left[\frac{R_N^{(+)} - R_{N-1}^{(+)}}{r^{(+)}(1 - r^{(+)}R_{N-1}^{(+)}\exp[i(2kL - \phi)])}\right]^{\frac{1}{2}} t \right|^2, \\ &= \left| \frac{\frac{(1-iuC_N)-(1-iuC_{N-1})}{r^{(-)}\exp(2ikL)}}{r^{(+)}(1 - r^{(-)}\frac{1-iuC_{N-1}}{r^{(-)}\exp(2ikL)}\exp(2ikL))} \right| |t|^2 \end{aligned} \tag{3.56}$$

or simply,

$$|T_N|^2 = \left| \frac{C_{N-1} - C_N}{C_{N-1}} \right| \left|\frac{t}{r^{(+)}}\right|^2. \tag{3.57}$$

In short, the Equations (3.55) and (3.57) can be employed to study the scattering problem where an incident wave is spread by a periodic structure composed of localized potentials, and it is enough to know the scattering amplitudes of just one lattice component. This lattice component, highlighted by the dashed box of Figure 3.3, which we call *building block* (BB, or cell), can be a composition of potentials, and its reflections and transmission coefficients are determined employing the recurrence relations presented in Subsection 3.1.1. Such a study will be made in the next chapter.

Chapter 4

Applications

4.1 Single Building blocks

In order to investigate the scattering process in which a wave is spread by a potential composition, we use as a base three analytically and exactly solved potentials: Dirac delta, square wall, and trapezoidal wall. These potentials are called *single* (or *elementary*) *building blocks*. All the combinations that can be made with p of these potentials are called *p-tuple building blocks*, and some of them are shown in the next section. Moreover, in all the graphics present in this chapter it was agreed, for simplicity, that the incident beam mass and the reduced Planck constant are equal to the unit ($m = \hbar = 1$).

4.1.1 Dirac delta barrier

As an initial example, consider a set of N Dirac delta potentials, where the scatter potentials are such that $V(x) = \lambda\delta(x)$ and they are spaced by a length L, as shown in Figure 4.1. It is evident that such a potential corresponds to a point interaction, besides that, it is symmetric. Therefore, the transmission and reflection coefficients of a single barrier are such that $r^{(+)} = r^{(-)} = r$ and $t^{(+)} = t^{(-)} = t$, where, if the incident particle has a mass m, we have

$$r = \frac{\beta}{ik - \beta}, \quad t = \frac{ik}{ik - \beta} \text{ and } \beta = \frac{m\lambda}{\hbar^2}, \tag{4.1}$$

relations well-known in the literature [29]. Although it represents a simple case, the Dirac delta barrier is widely studied, especially in scattering-like mechanisms — since this potential can characterize the interaction between two particles (in movement) that collides against each other [46]. Moreover, a Dirac comb (1D network of delta functions) was employed to investigate the entanglement of free fermions with different parts of an empty one-dimensional lattice [48].

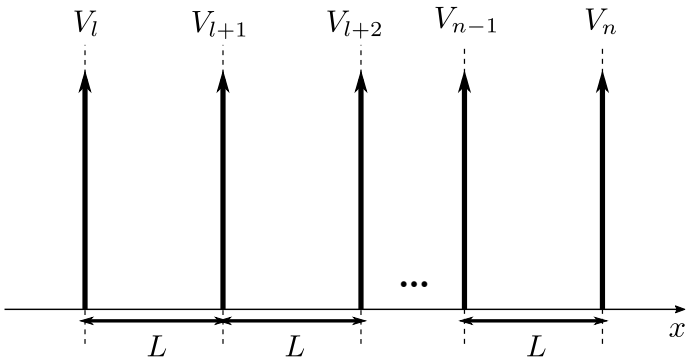

Figure 4.1: System formed by $N = n - l + 1$ Dirac delta potentials ($V(x) = \lambda\delta(x)$) spaced by a length L.

Using Equation (4.1), we can calculate C_0 from Equation (3.39), obtaining

$$C_0 = \frac{1}{iu} = \frac{1}{it\exp(ikL)} = -\frac{ik-\beta}{k\exp(ikL)}. \tag{4.2}$$

Furthermore, employing Equation (4.1) in Equation (3.35) we determine γ as

$$\gamma = \frac{1+u^2-v^{(-)}v^{(+)}}{iu} = \frac{1+(t^2-r^2)\exp(2ikL)}{it\exp(ikL)} = \frac{1-\frac{(-k^2-\beta^2)}{(ik-\beta)^2}\exp(2ikL)}{-\frac{k\exp(ikL)}{ik-\beta}}, \tag{4.3}$$

or yet,

$$\gamma = \frac{(ik-\beta)-(ik+\beta)\exp(2ikL)}{-k\exp(ikL)} = -\frac{1}{k}[(ik-\beta)\exp(-ikL)-(ik+\beta)\exp(ikL)], \tag{4.4}$$

so, from Euler's formula

$$\gamma = -2\Big[i\cos(kL) + \frac{\beta}{k}\sin(kL)\Big]. \tag{4.5}$$

Finally, using the approximant of a continued fraction from Equation (3.38) — or the convergent function form from Equation (3.54) — together with the expressions of C_0 and γ it is possible to calculate the C_Ns for a lattice with an arbitrary number of cells. To illustrate it, we observe that for a single barrier

$$C_1 = -\frac{1}{k(ik-\beta)}[-(k^2+2ik\beta)\cos(kL) + i(k^2+2i\beta-2\beta^2)\sin(kL)]. \tag{4.6}$$

Thus, we can determine $C_2 = \gamma + 1/C_1$, $C_3 = \gamma + 1/C_2$, etc., until reaching the desired number of BBs. Figure 4.2 shows, in logarithmic scale, the plot of $|C_N|^2$ for $N = 1$ to $N = 4$ for $\beta = L = 1$.

Figure 4.3 shows the graphics of $|T_N|^2$ and $|R_N|^2$ for $N = 1$ to $N = 4$ with $\beta = L = 1$, where we observe the same curves obtained for the transmission probability in previous

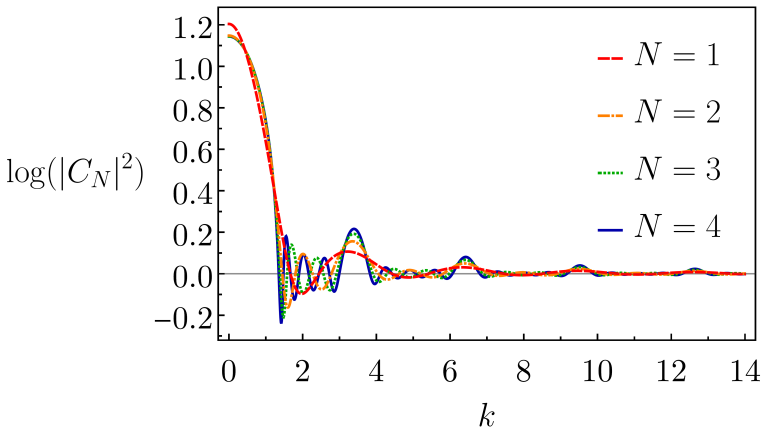

Figure 4.2: Log-scale graphic of $|C_N|^2$ for a system formed by $N = 1, 2, 3$ and 4 Dirac delta barriers, with $\beta = L = 1$.

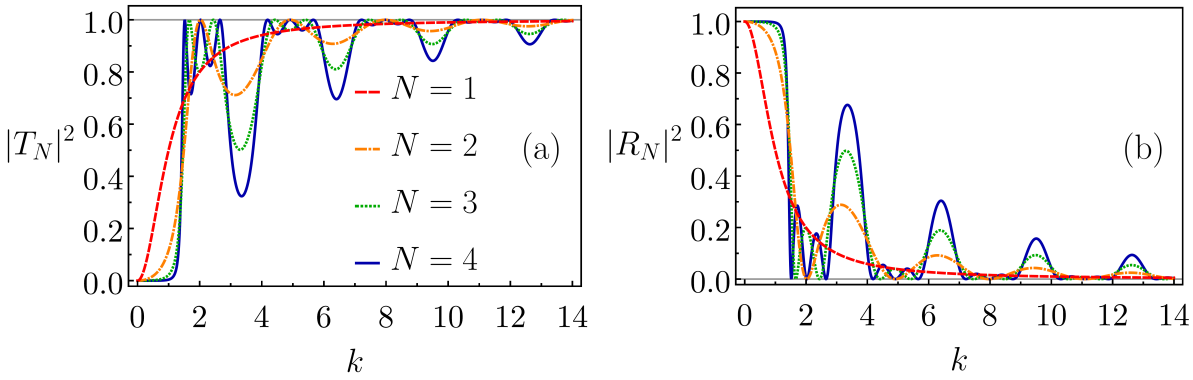

Figure 4.3: Graphic of (a) transmission and (b) reflection probabilities for a system formed by $N = 1, 2, 3$ and 4 Dirac delta barriers, with $\beta = L = 1$.

works [8, 7, 9]. A comparison between two results, one obtained with the continued fraction method and the other obtained with the transfer matrix method [9] is presented in Figure 4.4. Moreover, in Figure 4.3 we also notice that the number of *quasi-bound states*[1], that is, the number of peaks where $|T_N|^2 = 1$, in each *allowed band* (or *allowed zone*)[2] is equal to $N - 1$, as expected. Lastly, it is evident that $|T_N|^2 + |R_N|^2 = 1$ for any N, as desired, and that the greater the incident energy, the greater the probability of transmission.

Comparing the graphics of Figures 4.2 and 4.3(b), we see that the curves are similar, even the allowed bands of $|R_N^{(+)}|^2$ can be seen in the plot of $\log(|C_N|^2)$ (the "bands" of

[1]Since all the potential used in this work are purely repulsive, there are no bound states [73]. However, according with [30]:

> The particle can be trapped inside (the barrier), but it cannot be trapped forever. Such a trapped state has a finite lifetime as a consequence of quantum-mechanical tunneling. In other words, a particle leaks through the barrier to the outside region. Let us call such a state a quasi-bound state because it would be an honest bound state if the barrier were infinitely high.

Moreover, the peaks in which $|T_N|^2 = 1$, coincide with the quasi-bound state energies [74].

[2]They are bands where the transmission is different from zero. The bands where there is no transmission are called *forbidden band* (or *forbidden zone*).

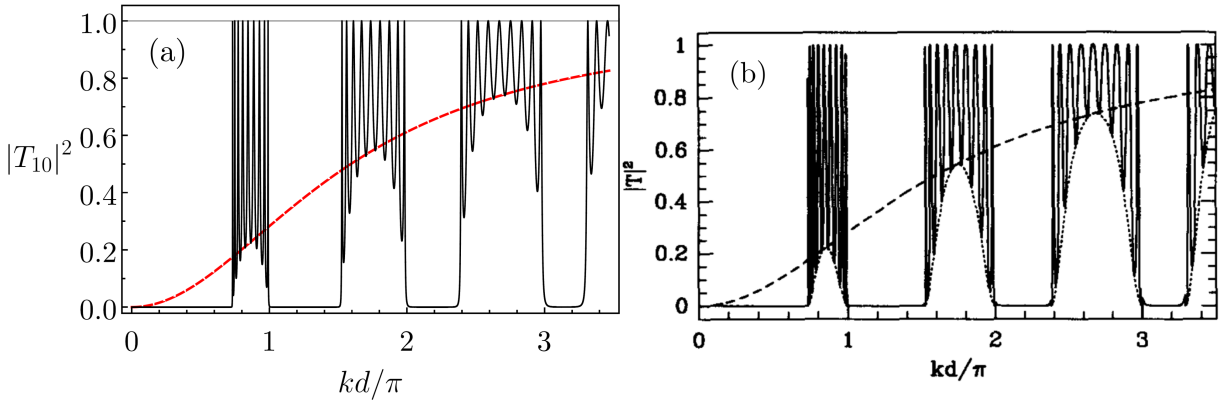

Figure 4.4: Graphics of transmission probability for a Dirac comb composed of $N = 10$ cells, obtained by employing (a) the continued fraction method and (b) the transfer matrix method (adapted from [9]). The parameters are: $\beta = 5$ and $L = d = 1$ for (a) and $\beta/d = 5$ for (b). Here, just for comparison, $d = L$.

$\log(|C_N|^2)$ do not coincide exactly with the real bands of $|R_N^{(+)}|^2$, but they are analogue). Of course, this is due to the proportional relation between $R_N^{(+)}$ and C_N, as can be observed in Equation (3.41). In addition, we point out that the number of oscillations in each "allowed band" of $\log(|C_N|^2)$ is N, one unity more than the number of peaks in each allowed band of $|T_N|^2$.

Figure 4.5 highlights another information about the scattering process that can be investigated with the auxiliary function C_N. As said before, a lattice formed by N cells is transparent ($|T_N|^2 = 1$) when $C_N = C_0$. To understand this statement let us do a thought experiment. Assume that we are studying a scattering process where we know the following parameters: the energy of the incident particle ($k = 2.5$), the potential strength ($\beta = 1$), and the distance between two adjacent cells ($L = 2$), and our goal is to discover how many cells the lattice must have to become transparent (the cells are Dirac delta functions). For this, we plot a C_N graph in terms of N (see Figure 4.5). Notice that in Figure 4.5, the dotted-red and the dashed-dotted-blue horizontal lines indicate, respectively, the values of $\Re[C_0]$ and $\Im[C_0]$. All the *pairs* of $\Re[C_N]$ red triangles and $\Im[C_N]$ blue circles that fall (respectively) upon these lines, is associated with a number of cells that makes the lattice transparent. In this case when $N = 15, 32, 47, 62, 79, 94$ (see the vertical dashed-gray lines), we have $|T_N|^2 = 1$.

An advantage of our method is that it can be easily applied to any number of barriers, even for large numbers[3]. For instance, in Figure 4.6, the solid-black line represents a plot of $|T_N|^2$ for $N = 10^{10}$ Dirac delta potentials and we compare it with the graphic of $|t|^2 = |T_1|^2$, the dashed red line, both with the parameters $\beta = L = 1$. It can be seen that the transmission probability for one BB bounds the lower border of the allowed bands

[3]Due to the continued fraction, C_N, it is not intuitive to assume that such calculations are easy, however, when implemented, all the functions present in the method become numbers (given a k), and is a straightforward task to realize a recurrence table of continued fraction in any programming language.

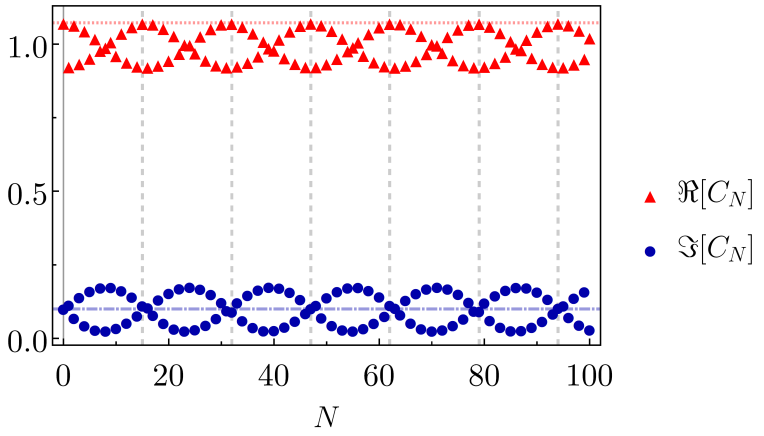

Figure 4.5: C_N's real and imaginary parts in terms of N (number of cells). When $\Re[C_N] = \Re[C_0]$ and $\Im[C_N] = \Im[C_0]$ the periodic structure is transparent ($|T_N|^2 = 1$). The parameters are: $k = 2.5$, $\beta = 1$, and $L = 2$. The vertical dashed lines correspond to $N = 15, 32, 47, 62, 79, 94$, where $|T_N|^2 = 1$.

(in both Figures 4.3(a) and 4.6). This behavior is present in the graphics for any shape of the cell. Comparing the graphics of Figure 4.3(a) and 4.6, we see that as the number of barriers increases, the allowed bands get fuller while the forbidden (where there is no transmission) get more well-defined and the transmission probability is closer to zero. This phenomenon is often called *filling of allowed bands* [8, 9].

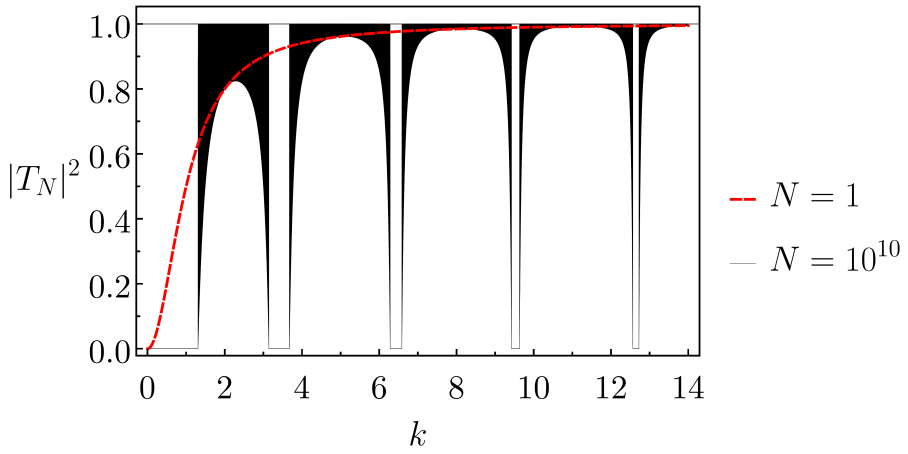

Figure 4.6: Transmission probability for one (in red-dashed) and $N = 10^{10}$ (in solid-black) Dirac delta potentials, with $\beta = L = 1$.

Another relevant investigation is the one shown in Figure 4.7, where we plotted a contour graphic of the transmission probability as a function of k and β with $L = 1$ for $N = 10^{10}$ barriers. One can see that even for strong potentials (λ or β large) and low incident energies (k small) there are points where $|T_N|^2$ is different from zero and even equal to one[4]. The most special case is introduced in Figure 4.7(b), where there is a

[4]Note that our classical intuition predicts the general behavior: the stronger (weaker) the potential and the lower (higher) the incident energy, the less (more) transmission will take place.

quasi-state ($|T_N|^2 = 1$) for the lowest wavenumber ($k \simeq 3.1$) and the highest potential strength ($\beta \simeq 82.4$) possible. In this configuration, the incident particle passes through the ten billion Dirac delta barriers, as if they were simply not there, which is a good application for the study of 1D networks in condensed matter.

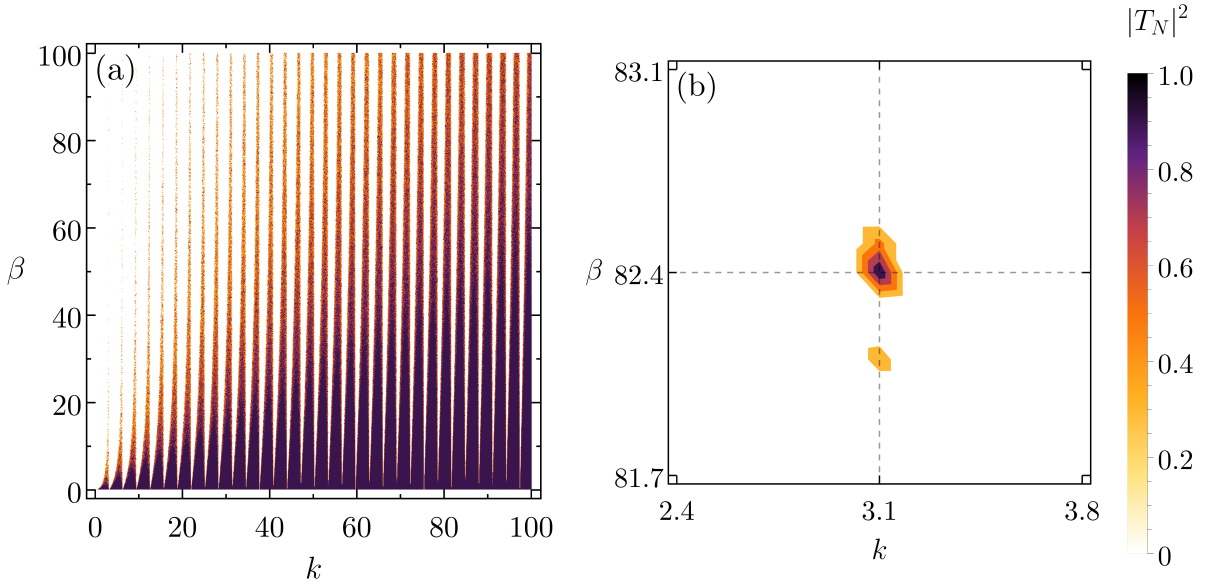

Figure 4.7: Transmission probability contour graphic for $N = 10^{10}$ Dirac delta barriers in terms of k and β for two different ranges (with $L = 1$).

With the Equations (4.2) to (4.6) we notice that the C_N is a bit complicated function for large N. However, for certain values of k, C_N's will become simpler. Analyzing Figure 4.1, we can see that the set of N delta potentials coincides with $N-1$ infinite square wells. For the latter, only the k's such that

$$k = \frac{n\pi}{L}, \qquad n = 0, 1, \ldots \tag{4.7}$$

are valid. So, in this case, from Equation (4.5), we get that $\gamma = (-1)^{n+1}2i$ and

$$C_0 = (-1)^{n+1}\frac{ik - \beta}{k}. \tag{4.8}$$

As a consequence, using Equation (3.38) we have

$$C_1 = \gamma + \frac{1}{C_0} = (-1)^{n+1}\left(2i + \frac{k}{ik - \beta}\right) = (-1)^{n+1}\frac{ik - 2\beta}{k + i\beta}, \tag{4.9}$$

and

$$C_2 = \gamma + \frac{1}{\gamma + \frac{1}{C_0}} = (-1)^{n+1}\left(2i + \frac{k + i\beta}{ik - 2\beta}\right) = (-1)^{n+1}\frac{ik - 3\beta}{k + 2i\beta}. \tag{4.10}$$

Continuing with these calculations, we see that in general

$$C_N = (-1)^{n+1}\frac{ik-(N+1)\beta}{k+Ni\beta}. \tag{4.11}$$

Thus, from Equation (3.41), the reflection coefficient is

$$R_N = R_N^{(\pm)} = \frac{1+(-1)^{n+1}itC_N}{r} = \frac{1}{r}+\left(\frac{it}{r}\right)\frac{ik-(N+1)\beta}{k+Ni\beta}, \tag{4.12}$$

with r and t given by Equations (4.1).

To find an expression for T_N we use Equation (3.30). For this, it is necessary to determine

$$R_N - R_{N-1} = \left(\frac{it}{r}\right)\left[\frac{ik-(N+1)\beta}{k+Ni\beta} - \frac{ik-N\beta}{k+(N-1)i\beta}\right], \tag{4.13}$$

i.e,

$$\begin{aligned} R_N - R_{N-1} = \left\{\frac{it}{r(k+Ni\beta)[k+(N-1)i\beta]}\right\}[ik^2-(N+1)k\beta-(N-1)k\beta \\ -(N+1)(N-1)i\beta^2-ik^2+Nk\beta+Nk\beta+iN^2\beta^2], \end{aligned} \tag{4.14}$$

therefore,

$$R_N - R_{N-1} = -\frac{t\beta^2}{r(k+Ni\beta)[k+(N-1)i\beta]}. \tag{4.15}$$

Furthermore, as the barriers are symmetric $\phi = 0$, hence

$$1 - rR_{N-1} = 1 - r\left[\frac{1}{r}+\left(\frac{it}{r}\right)\frac{ik-N\beta}{k+(N-1)i\beta}\right] = -it\left[\frac{ik-N\beta}{k+(N-1)i\beta}\right]. \tag{4.16}$$

Then the transmission coefficient for N potentials is

$$T_N = \sqrt{\frac{t\beta^2}{r(k+Ni\beta)[k+(N-1)i\beta]}}\sqrt{\frac{k+(N-1)i\beta}{irt(ik-N\beta)}}t, \tag{4.17}$$

that is,

$$T_N = \frac{t}{r}\frac{\beta}{(ik-N\beta)}. \tag{4.18}$$

Briefly, for the case where $k = n\pi/L$ with integer n, we can easily calculate general expressions for R_N and T_N from C_N. These relations are given by Equations (4.12) and (4.18). Rewriting them in terms of k and β (applying Equation (4.1)), we get that

$$R_N = \frac{N\beta}{ik-N\beta} \quad \text{and} \quad T_N = \frac{ik}{ik-N\beta}. \tag{4.19}$$

Analyzing Equations (4.1) and (4.19) we observe that such coefficients of a block formed by N Dirac delta barriers are very similar to the coefficients of a single delta barrier. In

other words, there is only the exchange of β for $N\beta$ (or λ for $N\lambda$). Figure 4.8 compares the probabilities discrete plots for this situation with the graphs of $|t|^2 = |T_1|^2$ and $|r|^2 = |R_1|^2$, respectively. As we can see, the higher N, the more slowly $|T_N|^2$ ($|R_N|^2$) tends to 1 (zero).

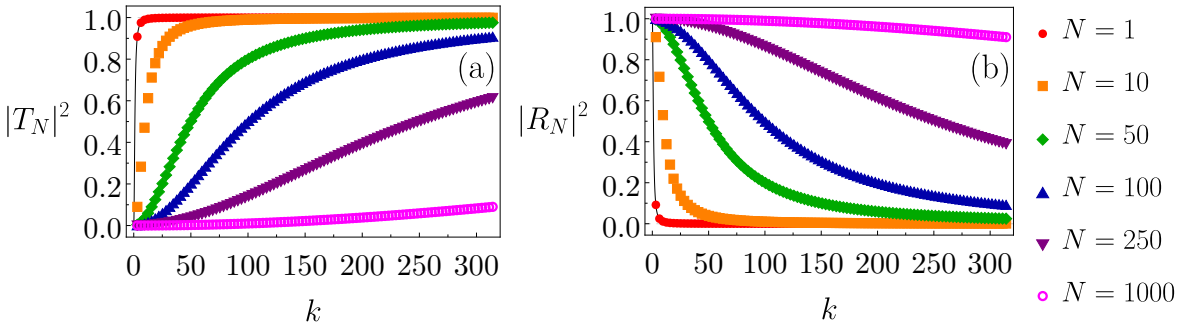

Figure 4.8: Discrete plot of (a) transmission and (b) reflection probabilities for systems composed of $N = 1, 10, 50, 100, 250$ and 1000 Dirac delta barriers when $k = n\pi/L$, for n integer (with $\beta = L = 1$). The curves in (a) and (b) are the graphics of $|t|^2 = |T_1|^2$ and of $|r|^2 = |R_1|^2$, respectively.

4.1.2 Square barrier

To increase the complexity of the problem, we will consider a symmetrical but not point interaction: the square barrier. From the literature, we know that for a potential of height V_0 and width $2a$, the transmission and reflection coefficients of a single barrier are (for $E < V_0$) [27]

$$t = \frac{2\kappa k}{2\kappa k \cosh(2\kappa a) + i(\kappa^2 - k^2)\sinh(2\kappa a)}, \tag{4.20}$$

and,

$$r = -\frac{i(\kappa^2 + k^2)\sinh(2\kappa a)}{2\kappa k \cosh(2\kappa a) + i(\kappa^2 - k^2)\sinh(2\kappa a)}, \tag{4.21}$$

where

$$k = \frac{\sqrt{2mE}}{\hbar} \quad \text{and} \quad \kappa = \frac{\sqrt{2m(V_0 - E)}}{\hbar} \tag{4.22}$$

are, respectively, the wavenumbers outside and inside the potential. It is evident that, since this is a symmetric barrier, $r^{(+)} = r^{(+)} = r$ and $\phi = 0$. Also, notice that, if the energy of the incident wave is greater than the barrier energy ($E > V_0$), it is sufficient to perform the exchange $\kappa \to i\tilde{\kappa}$, with $\tilde{\kappa} = \sqrt{2m(E - V_0)}/\hbar$.

The lattice composed of this barrier was first studied a long time ago in [5], where the Kronig-Penny model was proposed. Since then, several applications emerged. For example, in [75] an experimental study of a 1D semiconductor superlattice constituted by a GaAs (gallium arsenide) chip is simulated as a square network. [76] uses the Kronig-Penny model to experimentally analyze impurity effects in a ring, where there is a microwave guide with Teflon pieces that are treated as square walls. The already cited works [57, 50] developed

similar approaches, to investigate the conductance along, respectively, multi-junction solar cells and lattices of graphene layers.

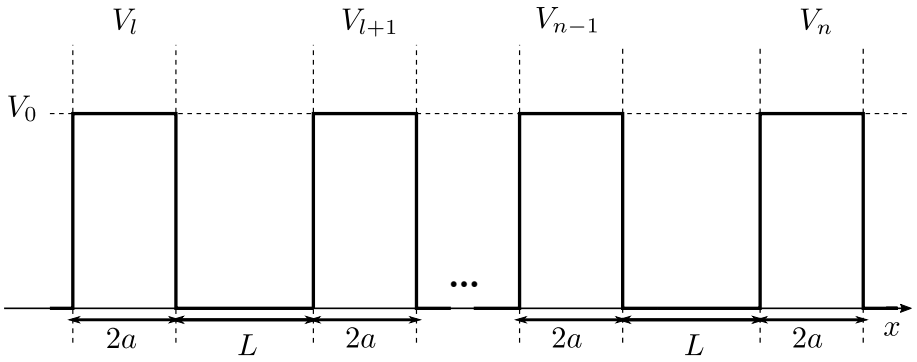

Figure 4.9: System formed by $N = n - l + 1$ square barriers of height V_0 and width $2a$, spaced by a length L.

Similarly as made in the last subsection, let us now consider a set of N identical square barriers spaced by a length L, as in Figure 4.9. To find C_N it is first necessary to determine C_0 and γ. Using Equation (3.39) we see that

$$C_0 = -\frac{i}{t\exp(ikL)} = -i\exp(-ikL)\Big[\cosh(2\kappa a) + i\frac{(\kappa^2 - k^2)\sinh(2\kappa a)}{2\kappa k}\Big]. \tag{4.23}$$

Furthermore, using Equation (3.35) we have that

$$\gamma = \frac{1 + (t^2 - r^2)\exp(2ikL)}{it\exp(ikL)}. \tag{4.24}$$

Calculating initially

$$t^2 - r^2 = \frac{4\kappa^2k^2 + (\kappa^2 + k^2)^2\sinh^2(2\kappa a)}{[2\kappa k\ cosh(2\kappa a) + i(\kappa^2 - k^2)\sinh(2\kappa a)]^2}, \tag{4.25}$$

(employing Equations (4.20) and (4.21)) and setting $s = 2\kappa k\cosh(2\kappa a) + i(\kappa^2 - k^2)\sinh(2\kappa a)$, we get

$$\gamma = \frac{s}{2i\kappa k\exp(ikL)}\frac{s^2 + [4\kappa^2k^2 + (\kappa^2 + k^2)^2\sinh^2(2\kappa a)]\exp(2ikL)}{s^2}, \tag{4.26}$$

or yet,

$$\gamma = \frac{s^2\exp(-ikL) + [4\kappa^2k^2 + (\kappa^2 + k^2)^2\sinh^2(2\kappa a)]\ exp(ikL)}{2i\kappa ks}. \tag{4.27}$$

Since $(\kappa^2 + k^2)^2 - (\kappa^2 - k^2)^2 = 4\kappa^2k^2$, we can write

$$\begin{aligned} 4\kappa^2k^2 + (\kappa^2 + k^2)^2\sinh^2(2\kappa a) &= 4\kappa^2k^2\cosh^2(2\kappa a) - 4\kappa^2k^2\sinh^2(2\kappa a) \\ &\quad + (\kappa^2 + k^2)^2\sinh^2(2\kappa a) \\ &= 4\kappa^2k^2\cosh^2(2\kappa a) + (\kappa^2 - k^2)^2\sinh^2(2\kappa a), \end{aligned} \tag{4.28}$$

that is, $4\kappa^2k^2 + (\kappa^2 + k^2)^2 \sinh^2(2\kappa a) = ss^*$. Thus,

$$\gamma = \frac{s\exp(-ikL) + [s\exp(-ikL)]^*}{2i\kappa k}. \tag{4.29}$$

Finally, as for complex z, $z + z^* = 2\Re(z)$, and given that

$$\Re[s\exp(-ikL)] = 2\kappa k\cosh(2\kappa a)\cos(kL) + (\kappa^2 - k^2)\sinh(2\kappa a)\sin(kL), \tag{4.30}$$

we conclude that the γ is given by

$$\gamma = -2i\cosh(2\kappa a)\cos(kL) - i\frac{(\kappa^2 - k^2)}{\kappa k}\sinh(2\kappa a)\sin(kL), \tag{4.31}$$

and so it is possible to find C_N, and consequently R_N and T_N, for a network composed of any number of cells.

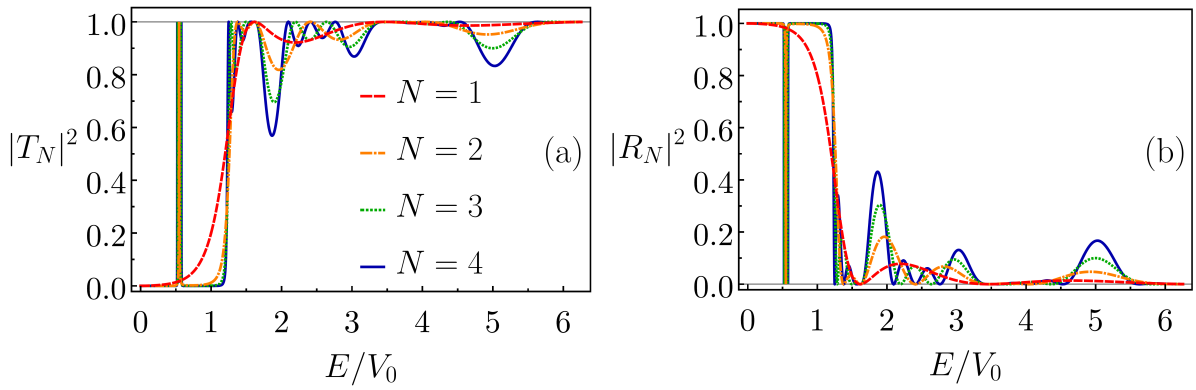

Figure 4.10: (a) Transmission and (b) reflection probability graphics for a system formed by $N = 1, 2, 3$ and 4 square walls (with $V_0 = 4$, $L = 1$ and $2a = 2$).

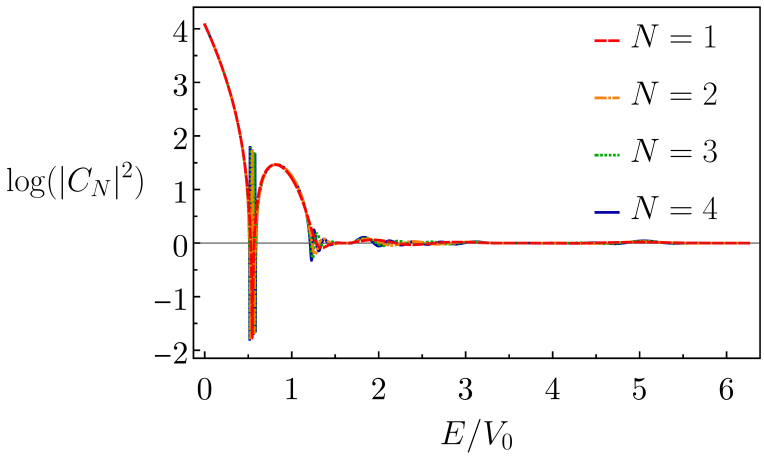

Figure 4.11: Log-scale plot of $\log(|C_N|^2)$ for a system formed by $N = 1, 2, 3$ and 4 square walls (with $V_0 = 4$, $L = 1$ and $2a = 2$).

Figures 4.10 and 4.11 present the graphics of scattering probabilities and $\log(|C_N|^2)$ for $N = 1, 2, 3$ and 4, where we find the patterns of transmission probability predicted in

the literature [77, 9] (see Figure 4.12). As imagined, again there is a formation of allowed and forbidden energy bands. Moreover, comparing Figures 4.10 and 4.11, it is possible to see that the curves of $\log(|C_N|^2)$ carry some information about the scattering process, although in this case (unlike the Dirac combs) the allowed and forbidden bands are not so visible because the thin band for $k < 1$ assumes high values.

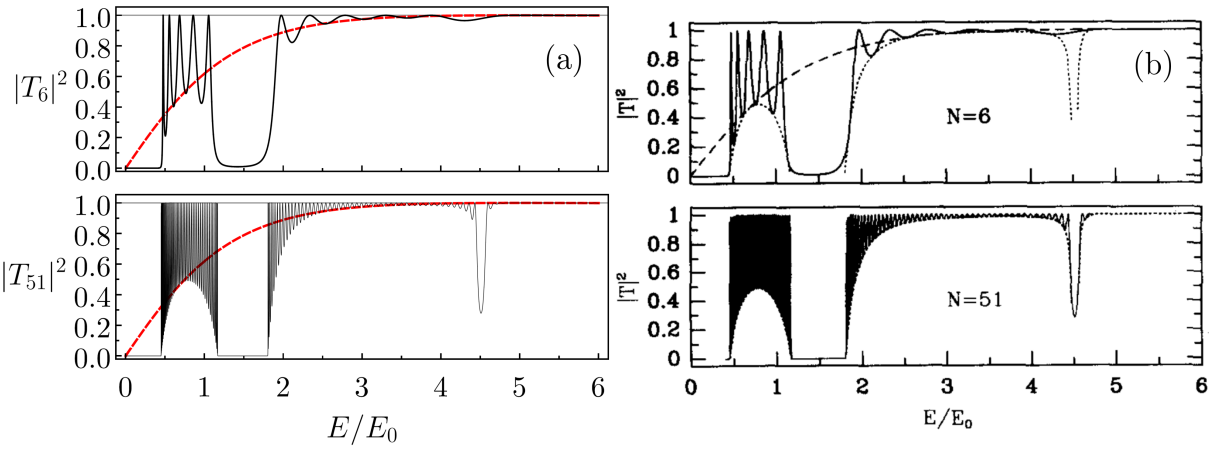

Figure 4.12: Graphics of transmission probability for periodic lattices whose cells are square walls, obtained by employing (a) the continued fraction method and (b) the transfer matrix method (adapted from [9]). In both cases, there are plots for $N = 1$ (dashed curve), $N = 6$, and $N = 51$, as indicated. The parameters are: $V_0 = E_0 = 1$ and $L = 2a = \pi/2$ for (a) and $V_0 = E_0$ and $L = 2a = \pi/(2\sqrt{V_0})$ for (b). Here, just for comparison, $V_0 = E_0$. Notice that the curves of (a) and (b) are the same.

Once more, an advantage of our method is that we can observe the behavior of the probabilities of systems composed of an expressive number of BBs. As an example, Figure 4.13 shows the plot of $|T_N|^2$ for $N = 10^6$ square barriers using the same parameters of Figure 4.10(a), where the filling of allowed bands is detected again (that is, in each allowed band of Figure 4.13 the solid-black curve oscillates $N - 1$ times, in other words, the solid-black curve touches the $|T_N|^2 = 1$ horizontal line $999,999$ times).

Again, by analyzing Equations (4.23) and (4.31), we see that a special case occurs if $k = n\pi/L$ with an integer n. In that case,

$$C_0 = (-1)^{n+1} i \Big[\cosh(2\kappa a) + w \sinh(2\kappa a) \Big], \tag{4.32}$$

and,

$$\gamma = (-1)^{n+1} 2i \cosh(2\kappa a), \tag{4.33}$$

where $w = i(\kappa^2 - k^2)/2\kappa k$.

Since with these specific values of wavenumber, γ and C_0 are simpler functions, it is

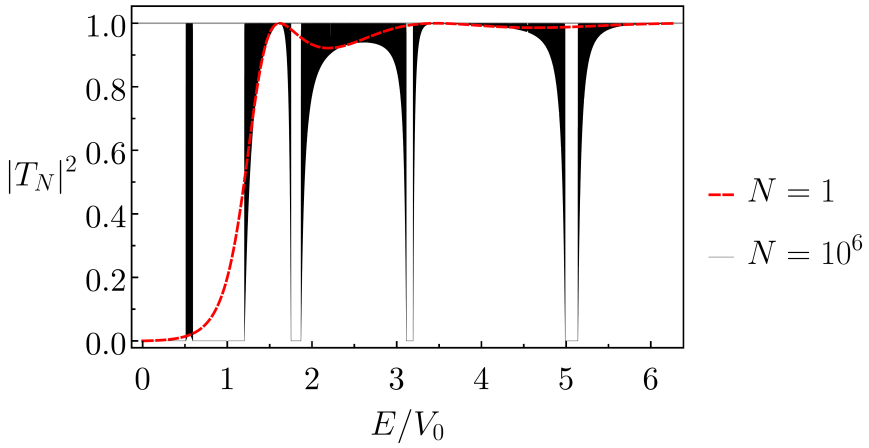

Figure 4.13: Transmission probability for one (in red-dashed) and $N = 10^6$ (in solid-black) square barriers (where $V_0 = 4$, $L = 1$ and $2a = 2$).

possible to determine $C_1 (= \gamma + 1/C_0)$ explicitly as

$$\begin{aligned} C_1 &= (-1)^{n+1} 2i \cosh(2\kappa a) - \frac{(-1)^{n+1} i}{\cosh(2\kappa a) + w\ sinh(2\kappa a)}, \\ &= (-1)^{n+1} i\ \frac{2\cosh^2(2\kappa a) + 2w\cosh(2\kappa a)\sinh(2\kappa a) - 1}{\cosh(2\kappa a) + w\sinh(2\kappa a)}, \\ &= (-1)^{n+1} i\ \frac{\cosh^2(2\kappa a) + \sinh^2(2\kappa a) + w\sinh(4\kappa a)}{\cosh(2\kappa a) + w\sinh(2\kappa a)}, \end{aligned} \tag{4.34}$$

or yet,

$$C_1 = (-1)^{n+1} \frac{i\cosh(4\kappa a) + iw\sinh(4\kappa a)}{\cosh(2\kappa a) + w\sinh(2\kappa a)}, \tag{4.35}$$

so,

$$C_1 = (-1)^{n+1} \frac{2\kappa k i\cosh(4\kappa a) - (\kappa^2 - k^2)\sinh(4\kappa a)}{2\kappa k\cosh(2\kappa a) + i(\kappa^2 - k^2)\sinh(2\kappa a)}. \tag{4.36}$$

Then, calculating $C_2 = \gamma + 1/C_1$ we get

$$C_2 = (-1)^{n+1}\left[2i\cosh(2\kappa a) + \frac{x}{y}\right] = (-1)^{n+1}\frac{x + 2iy\cosh(2\kappa a)}{y}, \tag{4.37}$$

where,

$$x = 2\kappa k\cosh(2\kappa a) + i(\kappa^2 - k^2)\sinh(2\kappa a), \tag{4.38}$$

and

$$y = 2\kappa k i\cosh(4\kappa a) - (\kappa^2 - k^2)\sinh(4\kappa a). \tag{4.39}$$

First, notice that

$$\begin{aligned} x + 2iy\cosh(2\kappa a) = {} & 2\kappa k\cosh(2\kappa a) + i(\kappa^2 - k^2)\sinh(2\kappa a) - 2\kappa k[2\cosh(2\kappa a)\cosh(4\kappa a)] \\ & - i(\kappa^2 - k^2)[2\cosh(2\kappa a)\sinh(4\kappa a)], \end{aligned} \tag{4.40}$$

since

$$2\cosh(2\kappa a)\cosh(4\kappa a) = \cosh(2\kappa a) + \cosh(6\kappa a), \tag{4.41}$$

$$2\cosh(2\kappa a)\sinh(4\kappa a) = \sinh(2\kappa a) + \sinh(6\kappa a), \tag{4.42}$$

we found that

$$C_2 = (-1)^{n+1}\frac{2\kappa k i\cosh(6\kappa a) - (\kappa^2 - k^2)\sinh(6\kappa a)}{2\kappa k\cosh(4\kappa a) + i(\kappa^2 - k^2)\sinh(4\kappa a)}. \tag{4.43}$$

Thus, continuing this procedure, we have that, in general,

$$C_N = (-1)^{n+1}\frac{2\kappa k i\cosh[2(N+1)\kappa a] - (\kappa^2 - k^2)\sinh[2(N+1)\kappa a]}{2\kappa k\cosh(2N\kappa a) + i(\kappa^2 - k^2)\sinh(2N\kappa a)}. \tag{4.44}$$

whatever the number of barriers, as long as $k = n\pi/L$. Once we know C_N we can find R_N. From Equation (3.41)

$$R_N = \frac{1 - it\exp(ikL)C_N}{r\exp(2ikL)} = \frac{1 + i(-1)^{n+1}tC_N}{r}. \tag{4.45}$$

For simplicity, we define $\alpha = 2\kappa a$, $\beta = 2\kappa k$, $\varepsilon = i(\kappa^2 - k^2)$ and

$$\mathcal{A}(N) = \beta\cosh(N\alpha) + \varepsilon\sinh(N\alpha), \tag{4.46}$$

thus, from Equations (4.20), (4.21) and (4.44), we obtain

$$t = \frac{\beta}{\mathcal{A}(1)}, \quad r = -\frac{i(\kappa^2 + k^2)\sinh(\alpha)}{\mathcal{A}(1)} \quad \text{and} \quad C_N = (-1)^{n+1}\frac{i\mathcal{A}(N+1)}{\mathcal{A}(N)}. \tag{4.47}$$

Therefore, the reflection coefficient (see Equation (4.45)) will be such that

$$\begin{aligned} R_N &= -\frac{\mathcal{A}(1)}{i(\kappa^2 + k^2)\sinh(\alpha)}\Big[1 - \frac{\beta\mathcal{A}(N+1)}{\mathcal{A}(1)\mathcal{A}(N)}\Big] \\ &= -\frac{1}{i\mathcal{A}(N)(\kappa^2 + k^2)\sinh(\alpha)}\Big[\mathcal{A}(1)\mathcal{A}(N) - \beta\mathcal{A}(N+1)\Big], \end{aligned} \tag{4.48}$$

using the definition of $\mathcal{A}(N)$ (Equation (4.46)),

$$\begin{aligned} R_N = -\frac{1}{i\mathcal{A}(N)(\kappa^2 + k^2)\sinh(\alpha)}\Big\{\Big[\beta\cosh(\alpha) + \varepsilon\sinh(\alpha)\Big]\Big[\beta\cosh(N\alpha) \\ + \varepsilon\sinh(N\alpha)\Big] - \beta^2\cosh[(N+1)\alpha] - \beta\varepsilon\sinh[(N+1)\alpha]\Big\}, \end{aligned} \tag{4.49}$$

$$\begin{aligned} R_N = -\frac{1}{i\mathcal{A}(N)(\kappa^2 + k^2)\sinh(\alpha)}\Big[\beta^2\cosh(\alpha)\cosh(N\alpha) + \beta\varepsilon\cosh(\alpha)\sinh(N\alpha) \\ + \beta\varepsilon\sinh(\alpha)\cosh(N\alpha) + \varepsilon^2\sinh(\alpha)\sinh(N\alpha) - \beta^2\cosh(\alpha)\cosh(N\alpha) \\ - \beta^2\sinh(\alpha)\sinh(N\alpha) - \beta\varepsilon\sinh(\alpha)\cosh(N\alpha) - \beta\varepsilon\cosh(\alpha)\sinh(N\alpha)\Big]. \end{aligned} \tag{4.50}$$

So,

$$R_N = -\frac{1}{i(\kappa^2+k^2)\mathcal{A}(N)}(\varepsilon^2-\beta^2)\sinh(N\alpha). \tag{4.51}$$

from the definitions of ε and β: $\varepsilon^2-\beta^2 = -(\kappa^2-k^2)^2 - 4k^2\kappa^2 = -(\kappa^2+k^2)^2$, then we see what

$$R_N = -\frac{i(\kappa^2+k^2)\sinh(N\alpha)}{\mathcal{A}(N)}, \tag{4.52}$$

then we conclude that

$$R_N = -\frac{i(\kappa^2+k^2)\sinh(2N\kappa a)}{2\kappa k\cosh(2N\kappa a)+i(\kappa^2-k^2)\sinh(2N\kappa a)}. \tag{4.53}$$

Starting from Equation (3.30) it is possible to determine the transmission coefficient in an analogous way, where we obtain

$$T_N = \frac{2\kappa k}{2\kappa k\cosh(2N\kappa a)+i(\kappa^2-k^2)\sinh(2N\kappa a)}. \tag{4.54}$$

Note that when $k = n\pi/L$ with an integer n, both scattering coefficients correspond to the coefficients of a single barrier with the exchange of $2a$ for $N(2a)$, similarly to what occurs for a Dirac comb.

Finally, if beyond $k = n\pi/L$, $V_0 = 2E$, that is, if[5] $\kappa = \sqrt{2m(V_0-E)}/\hbar = \sqrt{2mE}/\hbar = k$, we have

$$R_N = -i\tanh(2N\kappa a) \quad \text{and} \quad T_N = \operatorname{sech}(2N\kappa a), \tag{4.55}$$

or yet,

$$R_N = -i\tanh\left[\left(\frac{2a}{L}\right)Nn\pi\right] \quad \text{and} \quad T_N = \operatorname{sech}\left[\left(\frac{2a}{L}\right)Nn\pi\right]. \tag{4.56}$$

Hence, if the fraction $2a/L$ is small, the transmission probability can be different from zero even for a large number of cells, because the greater the spacing between the BBs, compared to their lengths, the easier the wave transmission becomes. Figure 4.14 presents such probabilities for different values of $2a/L$.

[5] I.e., when the incident energy is equal to half barrier energy, the wavenumbers inside and outside the potential are equal.

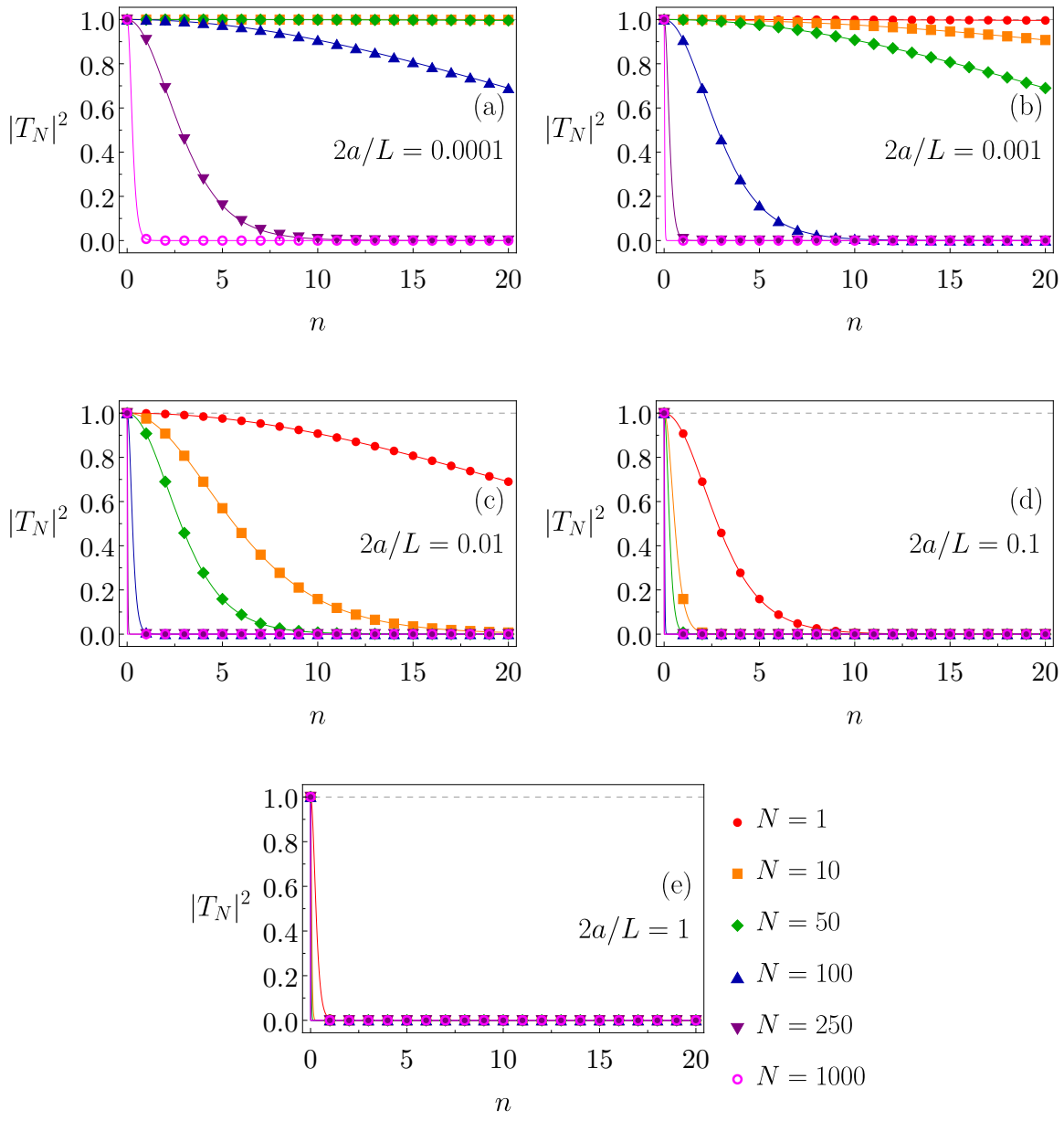

Figure 4.14: Transmission probability for N square barriers when $k = n\pi/L$ and $V_0 = 2E$ for different values of $2a/L$. The points are the actual graphic as the wavenumber is discrete, but the lines have been shown to aid understanding.

4.1.3 Trapezoidal barrier

As the last single building block, we present an anti-symmetrical barrier. The scattering problem though one trapezoidal barrier, whose potential is $V(x) = [-(V_a - V_b)x + (V_a b - V_b a)]/(b-a)$ (as shown in Figure 4.15), has already been exactly solved in some papers (as [31, 32, 33]). Here we use the reference [31] (see Appendix A), which finds the reflection and transmission coefficients as

$$r^{(\pm)}(k) = \frac{D^{(\pm)}(k)}{E(k)} \quad \text{and} \quad t(k) = -\frac{2\eta(k)}{\pi E(k)}, \tag{4.57}$$

where

$$D^{(\pm)}(k) = [\mathrm{Ai}(y_a) \mp \eta(k)\mathrm{Ai}'(y_a)][\mathrm{Bi}(y_b) \mp \eta(k)\mathrm{Bi}'(y_b)] - [\mathrm{Ai}(y_b) \mp \eta(k)\mathrm{Ai}'(y_b)][\mathrm{Bi}(y_a) \mp \eta(k)\mathrm{Bi}'(y_a)], \tag{4.58}$$

and

$$E(k) = [\mathrm{Ai}(y_a) + \eta(k)\mathrm{Ai}'(y_a)][\mathrm{Bi}(y_b) - \eta(k)\mathrm{Bi}'(y_b)] - [\mathrm{Ai}(y_b) - \eta(k)\mathrm{Ai}'(y_b)][\mathrm{Bi}(y_a) + \eta(k)\mathrm{Bi}'(y_a)], \tag{4.59}$$

with,

$$\alpha = \left(\frac{2m}{\hbar^2}\right)\frac{V_a - V_b}{b-a}, \quad \beta = \left(\frac{2m}{\hbar^2}\right)\frac{V_a b - V_b a}{b-a}, \quad \text{and} \quad \eta(k) = i\frac{\alpha^{\frac{1}{3}}}{k} \tag{4.60}$$

where $y_c = y|_{x=c}$, $F'(y_c) = dF(y_c)/dy_c$ and $\mathrm{Ai}, \mathrm{Ai}', \mathrm{Bi}$ and Bi' are the Airy functions and their derivatives, respectively. Notice that though Figure 4.15 suggests that $V_a > V_b$ the potential expression is valid even if $V_b > V_a$ (as the other expressions showed above).

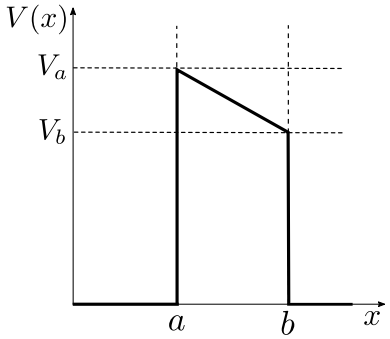

Figure 4.15: One trapezoidal barrier of width $(b-a)$ and slope $(V_b - V_a)/(b-a)$.

This potential shape has been used to simulate fictitious semiconductors [78]. Moreover, trapezoidal (and triangular, as will be presented next) barriers have been employed to study the charge transport in oxides. For instance, [79] investigate thin aluminum oxide films while [80] ultra-thin gate dielectrics. In addition, numerical approaches were developed for two-dimensional metal-oxide semiconductors [81] and good agreement between ferroelectric tunnel junctions based on perovskite tunnel barriers and the trapezoidal barrier modeling was also reported [82]. In a recent paper, the trapezoidal barrier was used to help in the conversion of raw data, provided by the scanning tunneling microscope (STM), into surface topographic images [83].

Consider now a system formed by $N = n - l + 1$ trapezoidal barriers with width $(b-a)$, spaced by L, as shown in Figure 4.16. We can employ the continued fraction method to find the plots of the reflection and transmission probabilities for different values of V_a and V_b. As a first example the Figures 4.17 and 4.18 present the graphics of $|T_N|^2$, $|R_N|^2$ and $\log(|C_N|^2)$ when $(b-a) = 3$ and $(V_a - V_b) = 5$, for $N = 1, 2, 3$ and 4. We point out that, similar to the last two BBs, the number of quasi-bound states (in which $|T_N|^2 = 1$) in each allowed band is equal to $N-1$, and that the curves of $\log(|C_N|^2)$ again carry the scattering properties. The behavior of $|t|^2 = |T_1|^2$'s curve (see Figure 4.17(a)) has been

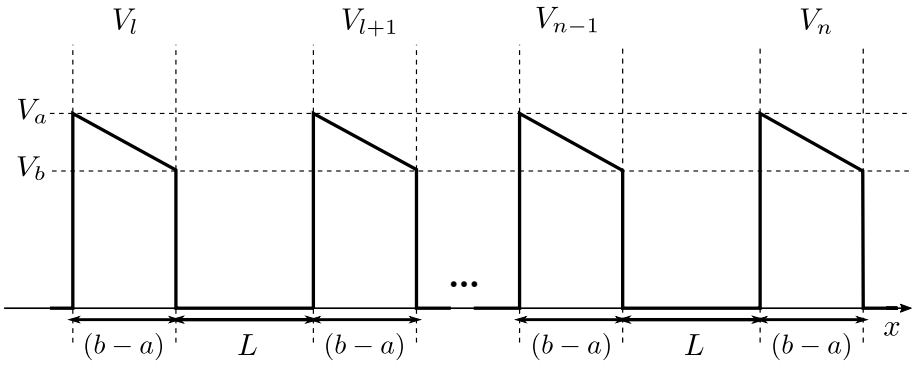

Figure 4.16: System composed of $N = n - l + 1$ trapezoidal barriers of width $(b - a)$ and slope $(V_b - V_a)/(b - a)$, spaced by L.

already described in the literature [32, 33], and it is the same shown here. However, similar analyzes are not found for a lattice with two or more trapezoidal cells.

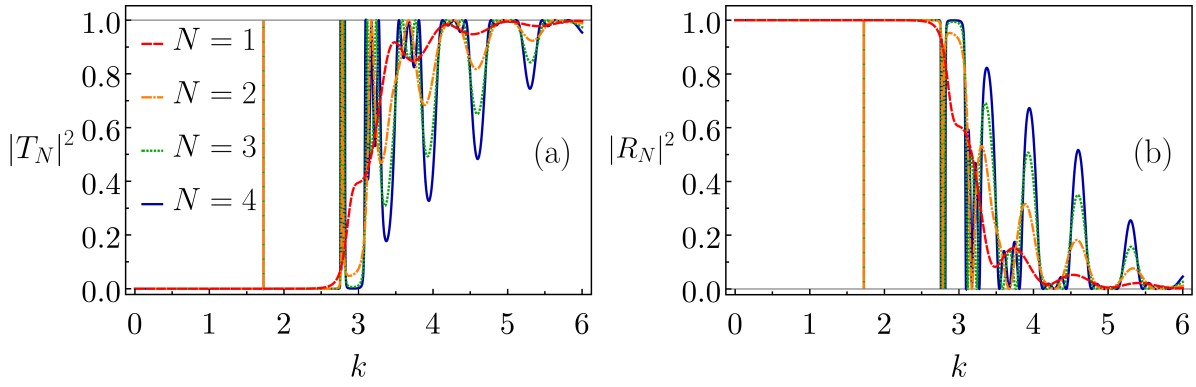

Figure 4.17: Graphic of (a) transmission and (b) reflection probabilities for a system formed by $N = 1, 2, 3$ and 4 trapezoidal barriers (with $(b - a) = 3$, $V_a = 10$, $V_b = 5$ and $L = 1$).

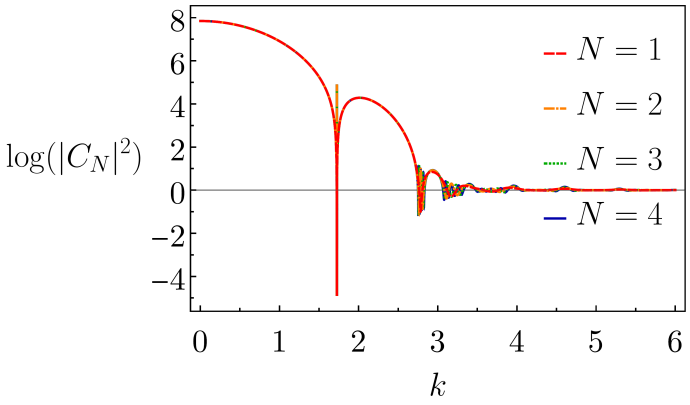

Figure 4.18: Log-scale graphic of $|C_N|^2$ for a system composed of $N = 1, 2, 3$ and 4 trapezoidal barriers (with $(b - a) = 3$, $V_a = 10$, $V_b = 5$ and $L = 1$).

Comparing the Figures 4.3(a) and 4.17(a), that is, the transmission graphics for, respectively, Dirac delta and trapezoidal BBs, we notice that here the curve of $|t|^2 = |T_1|^2$,

that delimits the bottom of the other N's lines, have some variations, i.e., does not converge to one too directly as the delta BB plots in Figure 4.3(a). In addition, Figure 4.19 shows again a great advantage of our method: the possibility to calculate the transmission probability for a large number of barriers, $N = 10^6$, even for a complicated BB[6], notice that the filling of allowed bands is detected again.

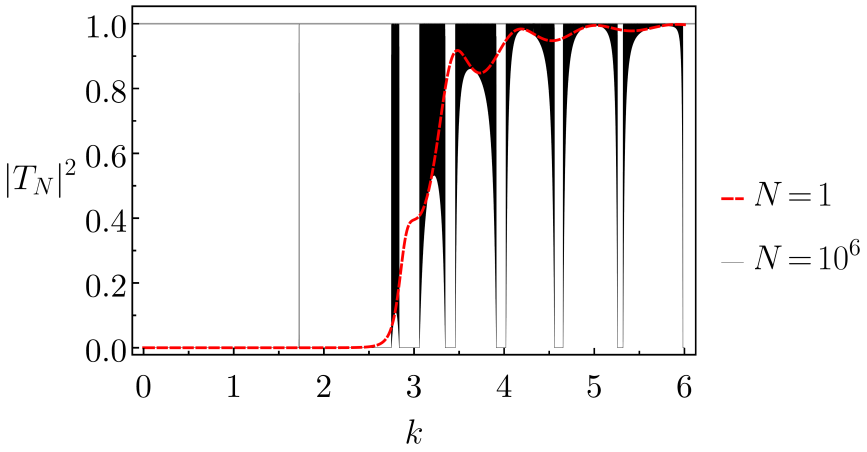

Figure 4.19: Transmission probability for a system formed by one (in dashed-red) and $N = 10^6$ (in solid-black) trapezoidal barriers (with $(b-a) = 3$, $V_a = 10$, $V_b = 5$ and $L = 1$).

Observe that as the trapezoidal barrier is not symmetric, a system composed of N of these potentials will not be either. To illustrate this we present in Figure 4.20 the plot of ϕ, and the real and imaginary parts of $(R_4^{(+)} - R_4^{(-)})$ (as seen in the Section 3.2) for $N = 4$ and the same parameters used above. It is evident that $R_4^{(+)} \neq R_4^{(-)}$, but $|R_4^{(+)}|^2 = |R_4^{(-)}|^2$ (both are the solid-dark blue curve of the Figure 4.17(b)). Furthermore, it would be a waste of time to study the differences between the transmission probability for systems composed of a single trapezoidal BB with slopes Δ and $-\Delta$, since the system with Δ corresponds to one with $-\Delta$ mirrored vertically, and for any potential $t^{(+)} = t^{(-)}$.

[6]Comparing the expressions of the reflection and transmission amplitudes of the three single BBs, we see how the trapezoidal is more complicated, but it is still possible to apply our technique for a large number of barriers.

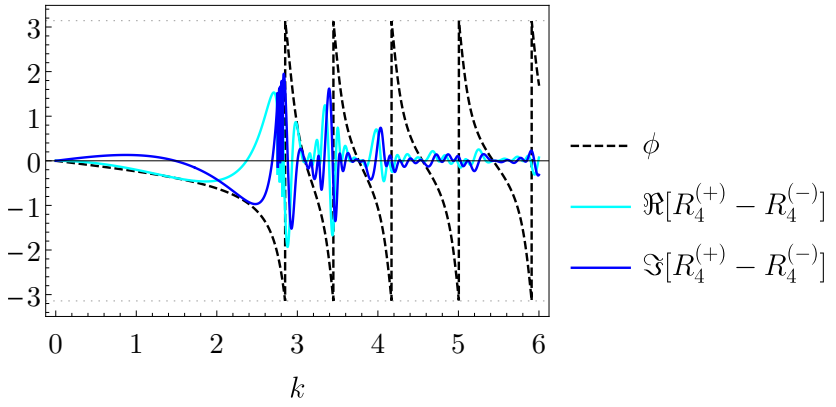

Figure 4.20: Comparison between the (+) and (−) reflection coefficients for four trapezoidal barriers (where $(b-a)=3$, $V_a=10$, $V_b=5$ and $L=1$).

Another interesting case is the one schematized in Figure 4.21, a system formed by $N=n-l+1$ trapezoidal barriers such that $V_b=0$ (could be $V_a=0$ as well). Here we call this type of potential, derived from a trapezoidal barrier, a *triangular barrier*[7], such that $V(x)=V_a[(b-x)/(b-a)]$. The graphic of the transmission probability for this case, when $V_a=5$ and $(b-a)=3$, is shown in Figure 4.22. We point out that the curves of Figure 4.22 are not the same ones shown in Figure 4.17(a), even though the slopes of the triangular BB and the trapezoidal BB are equal. This is evidently due to the different V_b heights, which makes the trapezoidal BB more "square". Lastly notice how the graphics of Figure 4.3(a) and Figure 4.22 are similar (we can say that when there is no V_b height the system composed of N trapezoidal barriers becomes more "sharp", and therefore similar to one formed by N delta barriers).

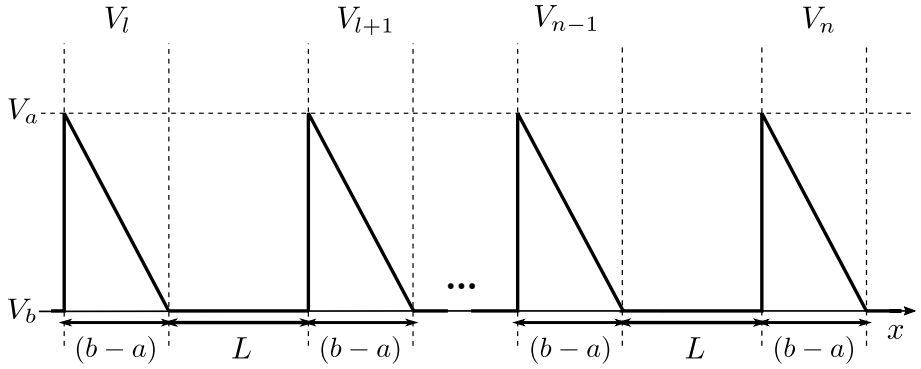

Figure 4.21: System formed by $N=n-l+1$ triangular barriers of width $(b-a)$ and slope $-V_a/(b-a)$, spaced by L.

[7]The scattering coefficients for this barrier were studied in [84], where they are written in terms of the Airy functions as well.

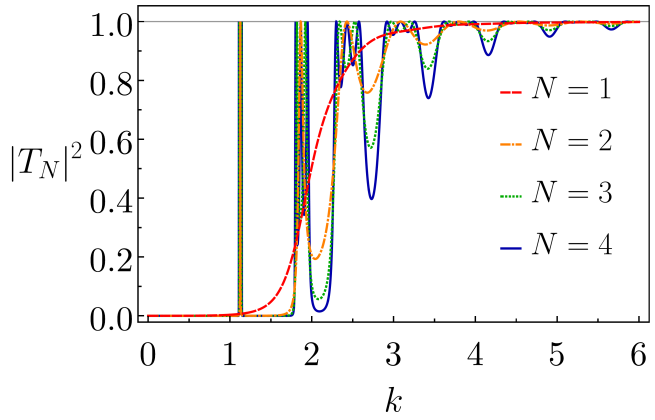

Figure 4.22: Transmission probability for a system composed of $N = 1, 2, 3$ and 4 triangular barriers (with $(b - a) = 3$, $V_a = 5$, $V_b = 0$ and $L = 1$).

As a last analysis, Figure 4.23(a) shows a comparison between a symmetric BB, the square wall, and an asymmetric BB, the trapezoidal wall. To understand such comparison consider a trapezoidal wall with parameters a, b, V_a, and $V_b (< V_a)$ (see Figure 4.15). Assume that we fix all the parameters except V_a, and then we decrease V_a until $V_a = V_b$, that is, until the trapezoidal becomes a square wall. In Figure 4.23(a) we see that as the absolute value of slope decreases (approaching zero) the curve of $|T_N|^2$ for a periodic lattice ($N = 10$) whose cell is a trapezoid becomes the curve of $|T_N|^2$ for a periodic lattice ($N = 10$) whose cell is a square.

In Figure 4.23(b) we present the contour graphic of transmission probability for a periodic network whose building block is a trapezoidal wall with a, b, and V_b fixed, and $0 \leq V_a \leq 12$ and $0 < k \leq 6$. First, notice that the curves of Figure 4.23(a) are represented by the dashed horizontal lines (with the same colors) in Figure 4.23(b), because if instead of a contour graphic, we had a 3D plot, the dashed horizontal lines in Figure 4.23(b) would represent the cross-section for each specific V_a in the 3D plot. In Figure 4.23(b) we also see that as the difference $V_a - V_b$ increases the allowed bands get thinner and more distant from the origin. These effects can be explained by the general increase in the BB's height.

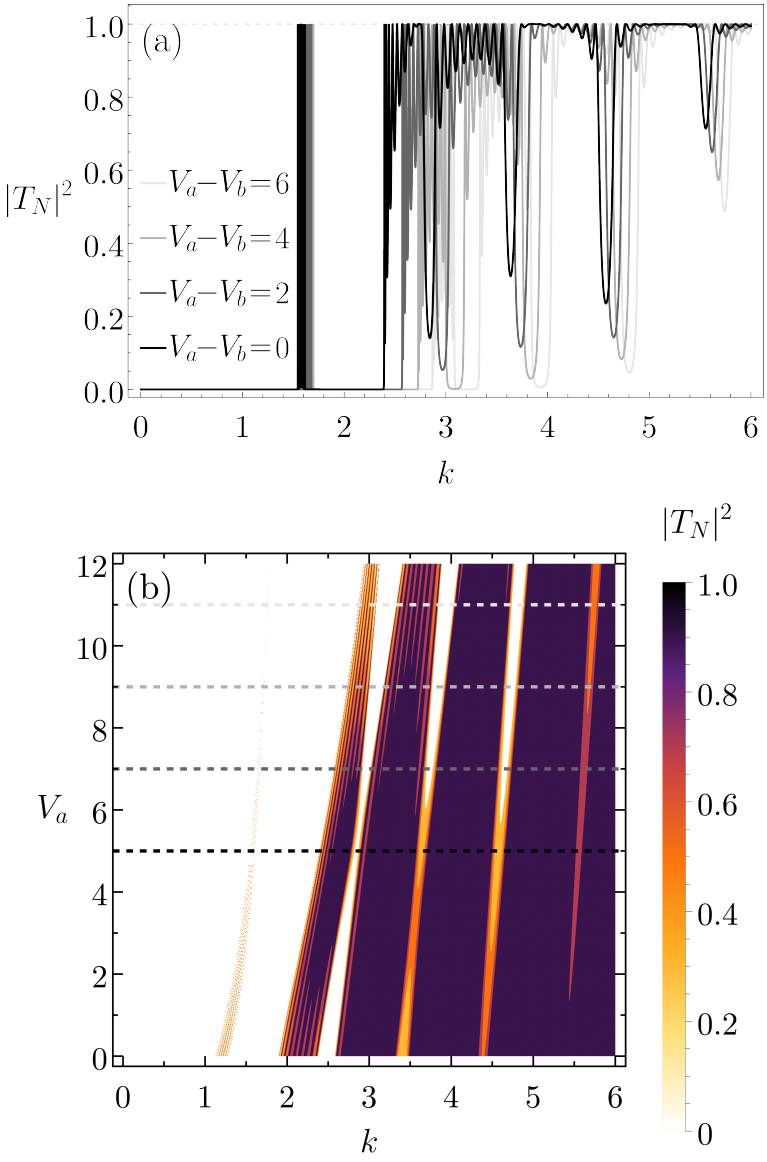

Figure 4.23: (a) Comparison between the transmission probabilities for ten trapezoidal barriers — in which the width is $(b-a)=2$, the right height is $V_b=5$, and the difference (V_a-V_b) change as indicated with $V_a > V_b$ — and ten square barriers — where the width is also two $(2a=2)$ and the height is five $(V_0=5)$. It is clear that the trapezoidal curves converge to square one as the absolute value of the slope gets smaller (in all the lines $L=1$). (b) Contour graphic of transmission probability in terms of k and V_a, with the same parameters of (a). In the black dashed line, the lattice BB is a square barrier, whereas above (below) the BBs are trapezoidal barriers with a negative (positive) slope. When $V_a=0$ the BB is triangular.

4.2 p-tuple building blocks

Once studied the periodic potentials composed of single building blocks, we can begin a more complex — and maybe more interesting — analysis: periodic potentials whose BBs are formed by more than one of our elementary potentials (Dirac delta, square and

trapezoidal walls). As explained in Chapter 3, to use the continued fraction method is necessary to know the reflections and transmission of the BB. These quantities are easily calculated with the recurrence relations of Equations (3.15) to (3.18). Therefore it is just needed to employ the Schrödinger equation once: to find the amplitudes for the elementary potentials. After that, all the calculations are described in the previous chapters of this work.

4.2.1 Some double building blocks

Since we have three elementary potentials, there are nine combinations for the *double building blocks*. Here we will focus on the BBs with the most curious transmission behaviors or the most interesting compositions (shapes). The same approach will be adopted in the next subsections.

Consider the BBs composed of a square followed by a trapezoidal barrier and vice versa. We call these building blocks *ST* and *TS*, respectively. As the trapezoidal potential is not symmetric, this BB will not be either. This characteristic causes exotic behavior. To understand this, first, let us look at a BB formed by a square barrier followed by a Dirac delta (SD). Once the transmission coefficients for this BB are such that $t^{(+)} = t^{(-)} = t$, if we mirror the BB, obtaining a DS (with the same parameters, Figure 4.24(a)), it is clear that the transmission coefficients for SD and DS are equal[8]. The same will be observed for the periodic potential formed by them.

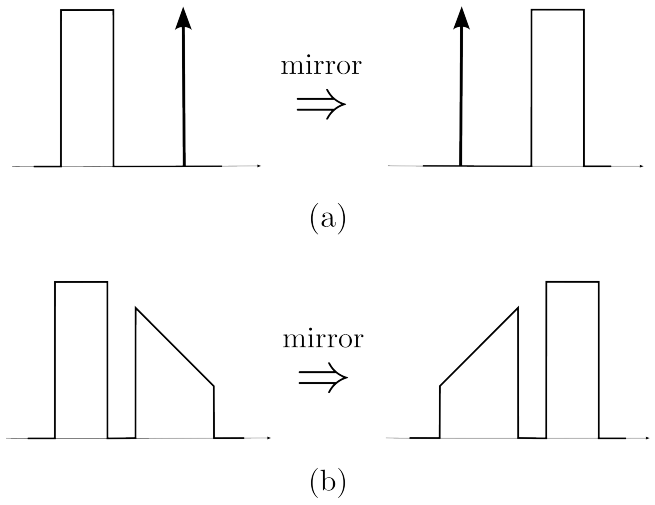

Figure 4.24: Comparison between the mirrored double building blocks formed by (a) symmetrical potentials and (b) at least an asymmetrical barrier. In (a) we show, from left to right, an SD and a DS building block, while in (b) we present a ST followed by a TS_m barrier.

However, this will not happen for the ST and TS building blocks, due to the trapezoidal

[8]Notice that this will occur with any combination of symmetrical barriers (two different deltas or squares).

asymmetry. If we mirror the ST BB we will obtain a building block composed of a trapezoidal wall followed by a square wall but with the trapezoidal slope inverted, as shown in Figure 4.24(b). This last BB is called as TS_m, i.e., a TS BB with the T mirrored. The ST and TS_m cells have the same transmission amplitude (as the lattices formed by them), whereas TS (with the original trapezoidal slope) will not have the same transmission coefficient[9].

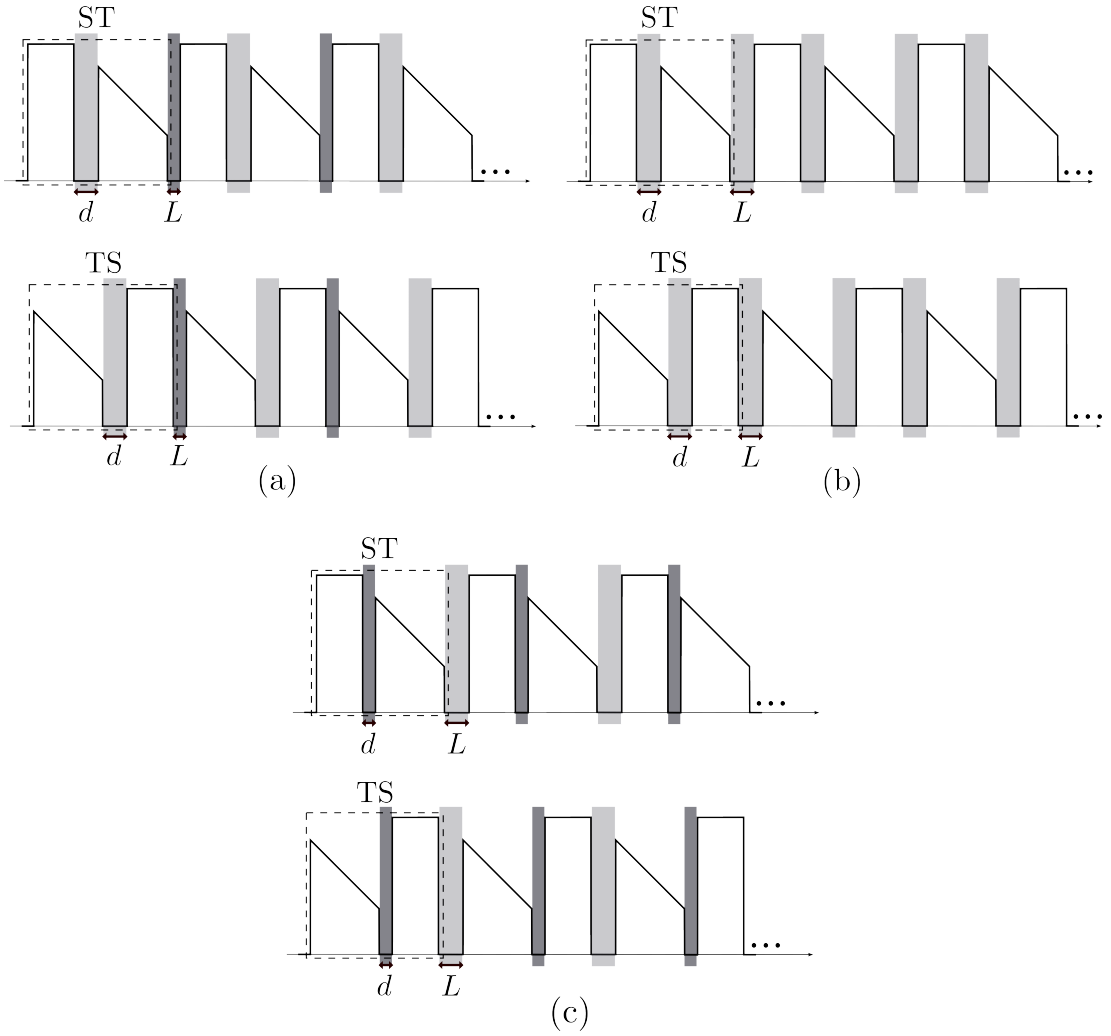

Figure 4.25: Different configurations of ST and TS building blocks. (a) $d > L$, (b) $d = L$ and (c) $d < L$.

To bring light, Figure 4.26 compares the transmission probabilities for the two lattices of Figure 4.25(a). In such a figure we present an ST and a TS building block in which the space between the elementary potentials is $d = 1$, and the space between adjacent BBs is $L = 0.5$. It is clear that for one BB ($N = 1$) the curves are very different, indeed the TS

[9]Consider ST and TS cells again. A wave coming from the left that encounters an ST BB "touches", in sequence (see Figure 4.24(b)): the square wall, the highest side of T, and then the lowest side of T. However, a wave coming from the left that encounters a TS BB "touches", in the sequence: the highest side of T, the lowest side of T, and then the square wall. The differences between these "touch" sequences are important because different resonances occur between the square wall and the highest or the lowest sides of T.

has a peak in which the transmission probability is near 0.8, while ST has a dislocated peak in which the transmission is next to 0.6. As the number of BBs increases, the behaviors of transmission probability get similar, but they are never equivalent. Looking at Figure 4.26(e), where $N = 10^6$, we may conclude that in this case there is a dependence on the borders. In other words, the $|T_N|^2$ changes if the lattice begins (or ends) with a square or a trapezoidal barrier.

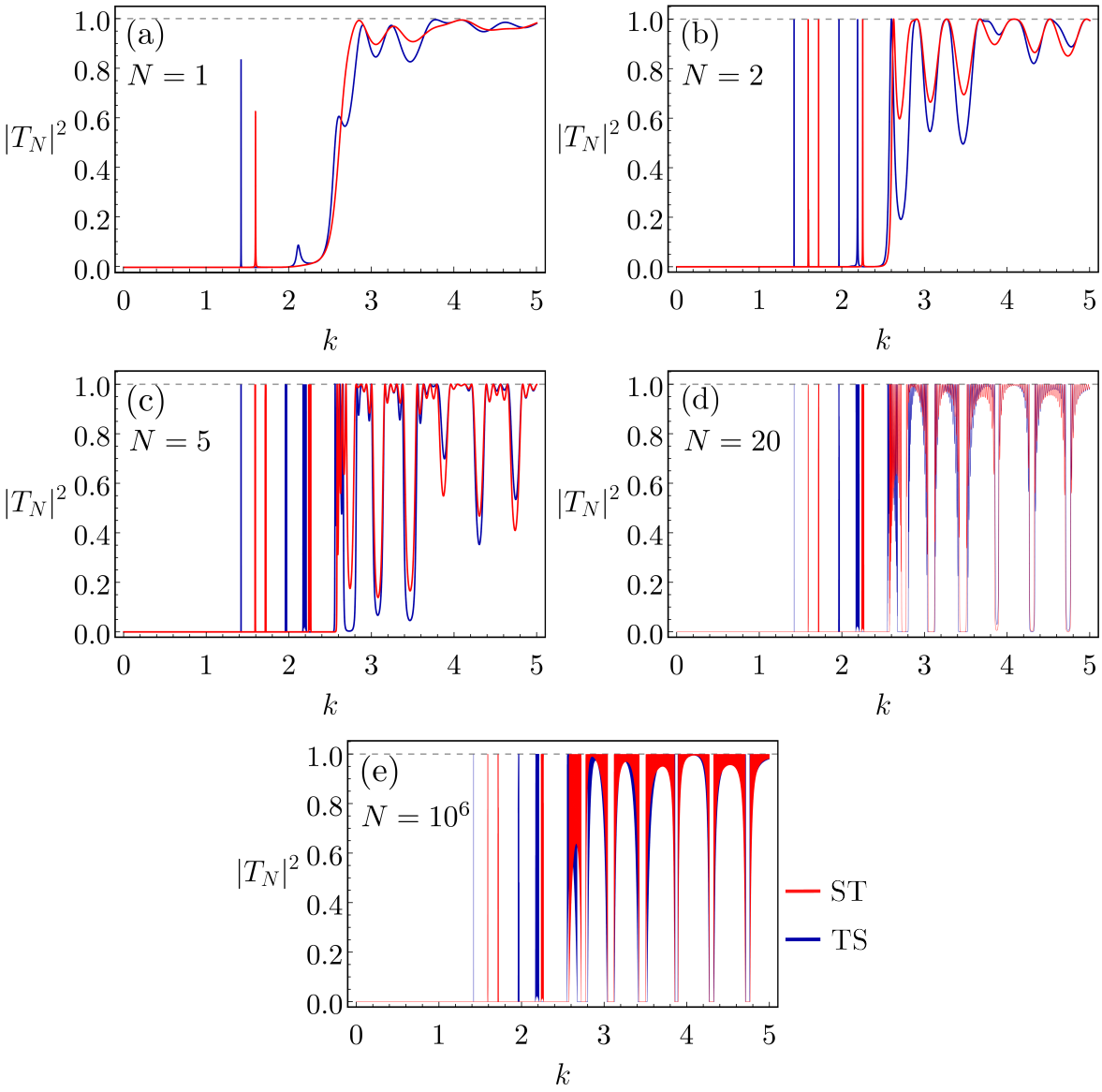

Figure 4.26: Transmission probability graphics for ST and TS BBs when (a) $N = 1$, (b) $N = 2$, (c) $N = 5$, (d) $N = 20$, and (e) $N = 10^6$ with $d = 1$ and $L = 0.5$ (and the square parameters: $V_0 = 6$, $2f = 2$ (width), and the trapezoidal parameters $(b - a) = 3$, $V_a = 5$, and $V_b = 2$).

To show that this result does not come from the fact that the distances between the individual potentials are different ($d \neq L$), in Figure 4.27(a) we present the transmission probabilities for a million of BBs when $d = L = 1$ (the lattices of Figure 4.25(b)). Again, the curves do not agree. In Figure 4.27(b) we show the same graphic of Figure 4.26(e),

but with the changed parameters ($d = 0.5$ and $L = 1$, Figure 4.25(c)). Once again the curves differ from each other. The last outcome from this analysis is that if $d = L$ the allowed bands are overlapping, and if $d \neq L$ they are not.

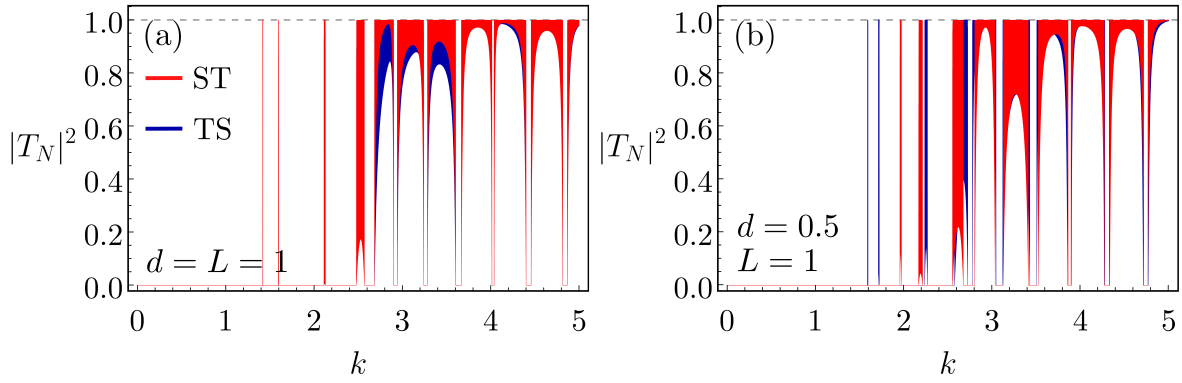

Figure 4.27: Transmission probability graphics for ST and TS BBs when (a) $d = L = 1$, (b) $d = 0.5$ and $L = 1$ (with the square parameters: $V_0 = 6$, $2f = 2$ (width), and the trapezoidal parameters: $(b - a) = 3$, $V_a = 5$ and $V_b = 2$).

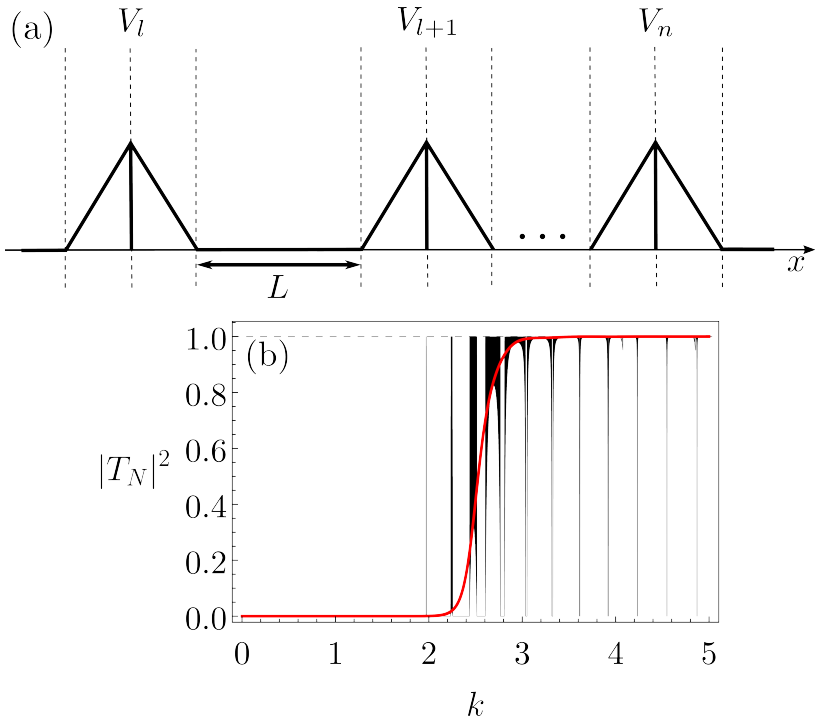

Figure 4.28: (a) System formed by $N = n - l + 1$ sharp potentials, spaced by a length L. (b) Transmission probability for one (in red) and $N = 10^6$ sharp barriers (in black). If the first triangular potential is such that $V(x) = V_b[(x - a)/(b - a)]$ and the second is $V(x) = V_c[(d - x)/(d - c)]$, in this case, $a = 1$, $b = c = 5$, $d = 9$, $V_a = V_d = 0$, $V_b = V_c = \sqrt{48} \cong 6.93$, and $L = 1$ (i.e. the BB corresponds to an equilateral triangle of size 8).

There is another intriguing network constituted of a double building block to be inspected. Combining two triangular potentials such that there is no space between them

($d = 0$), and the right height of the first one is equal to the left height of the second one ($V_b = V_c$ and $V_a = V_d = 0$), we obtain a *sharp barrier*[10], as shown in the Figure 4.28(a). The transmission probability of this BB is similar to the Dirac delta or the triangular barrier, obviously due to the "sharp" format, as present in Figure 4.28(b)[11]. Although in Figure 4.28 the potential is exemplified by an equilateral case, an isosceles or scalene triangle can be investigated as well.

4.2.2 A triple building block

There are several possible *triple BBs* (twenty-seven to be exact). Here, in order to compare it with the sharp BB, we will focus on the TST, a building block formed by a trapezoidal followed by, respectively, a square and another trapezoidal barrier, as schematized in Figure 4.29. Notice that, in this case, it is needed to employ the recurrence relations (Equations (3.15) to (3.18)) first for the TS, where the variable d_{12} appear[12]. After that, the recurrence relations are reused for the $(TS)T$, and the parameter d_{23} emerges.

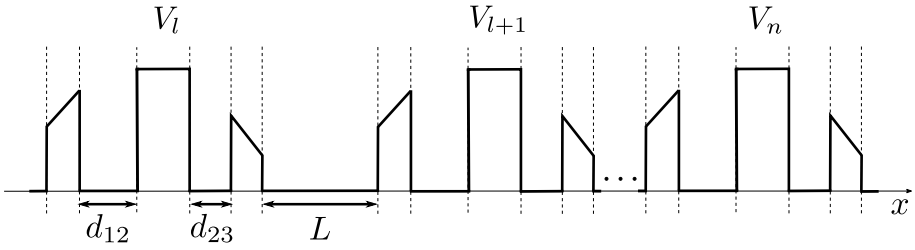

Figure 4.29: System formed by $N = n - l + 1$ TST potentials, spaced by a length L.

An interesting TST is the one where $d_{12} = d_{23} = 0$ and the Ts are triangles. Then, for instance, we can form a BB that is *half of a regular hexagon*, as schematized in Figure 4.30(a). The transmission probability for the periodic lattice composed of this building block is shown in Figure 4.30(b), where the size of the regular hexagon is equal to 8 (to compare it with Figure 4.28). Notice how different the curves of Figures 4.28(b) and 4.30(b) are, although the BBs have the same height (in addition $L = 1$ in both cases), showing how important is the shape of the cell for the transmission across lattices. Furthermore, notice that the lattice of Figure 4.30(a) acts like a filter, because there is transmission only for approximately $k > 2.6$ (see Figure 4.30(b))[13].

[10]Triangular double barriers were studied in [85], where the transfer matrix method was employed. In addition, the current density for triangular multi-barrier structure in a constant electric field was investigated in [86].

[11]The curve for $N = 1$ is a sigmoid function defined as $1/\{1+\exp[-\nu(k-\xi)]\}$ or as $1/2+1/2\tanh[\nu(k-\xi)/2]$ where $\nu \cong 11.56$ and $\xi \cong 2.54$, such functions are related to the growth theory [87] and in neural networks [88, 89].

[12]The index suggests that $d_{i\,i+1}$ is the space between the i-th and the $(i+1)$-th potentials. These indexes do not depend on the direction of the incident particle, just are chosen from the left to the right by convection.

[13]Besides that, the allowed bands of the solid-black curve of Figure 4.30(b) are thin.

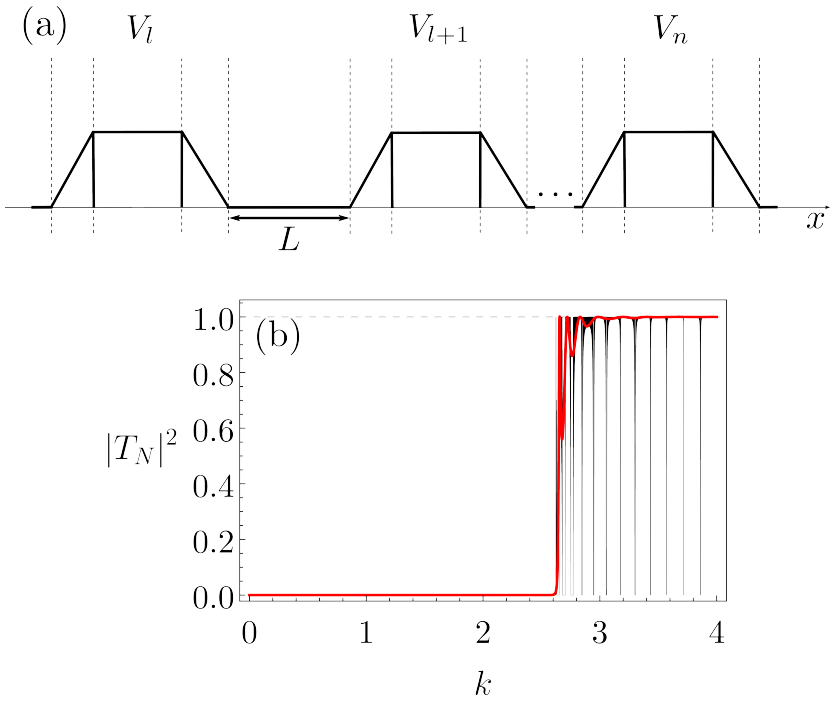

Figure 4.30: (a) System formed by $N = n - l + 1$ TST building blocks, spaced by a length L, such that the BB shape is half of a regular hexagon (of size equal to 8). (b) Transmission probability for one (in red) and $N = 10^6$ TST barriers (in black). If the first triangular potential is such that $V(x) = V_b[(x-a)/(b-a)]$, the square is $V(x) = V_0$ (with width $2f$), and the last triangular is $V(x) = V_c[(d-x)/(d-c)]$, in this case: $a = 1$, $b = 5$, $c = 13$, $d = 17$, $2f = 8$, $V_a = V_d = 0$, $V_b = V_c = V_0 = \sqrt{48} \cong 6.93$, $L = 1$ and $d_{12} = d_{23} = 0$.

The comparison between the graphs for a sharp and a TST BB can be interpret as follows. Consider the movement of an electron in a crystal lattice, whose sites are represented by a localized potential. We may assume that the center of mass (CM) of each site (atom, ion, etc.) coincides with the middle of the potential. Therefore, if the potential is a sharp building block as in Figure 4.28(a), on the x axis the electron finds (coming from the left or right) two different regions in the BB: where $V(x)$ is increasing until reaching a peak, to then become decreasing. However, if the potential is a TST cell, as in Figure 4.30(a), a third region appears: near the CM the $V(x)$ is constant[14]. The width of this region plays an important role in the transmission probability spectra.

As said before, continuous potentials can always be modeled by segmented potentials [62]. For example, using specific parameters, the TST building block can be adopted to study the transmission behavior of a continuous potential such that $V(x) = \sin^2(x/2)$. This continuous potential was investigated in [90] using the WKB approximation, and in [91] employing super-symmetry. In Figure 4.31(a), we see a dashed curve that is the $\sin^2(x/2)$ graphic, and a solid curve that is the corresponding TST. The transmission probability of this TST is shown in Figure 4.31(b), where we observe that the curves are

[14]This constant region could illustrate the site core, for example, the nucleus of an atom.

very different from the ones of Figure 4.30(b). For instance, the allowed bands (in black, for $N = 10^6$) of Figure 4.31(b) are larger and present even for low ks (this behavior is explained by the different parameters used in both figures). Moreover, in Figure 4.31(b), the black curve corresponds to the transmission probability when the scattering potential is modeled as a squared sine of half x function for a wide range, whereas the red curve models the same scattering potential but for a short range.

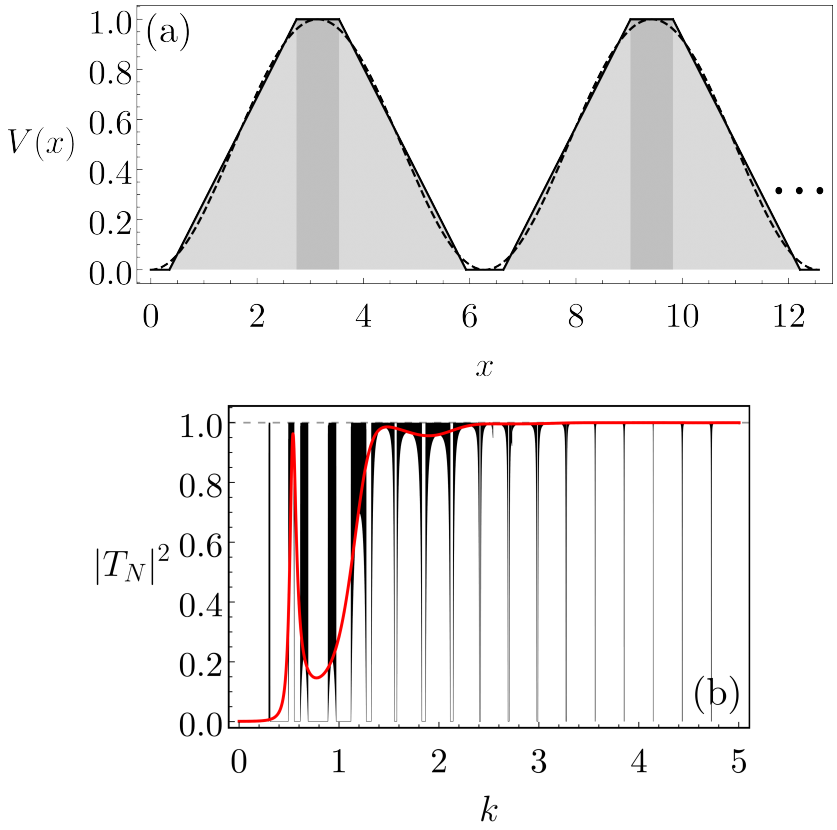

Figure 4.31: (a) Simulating the continuous potential $V(x) = \sin^2(x/2)$ (the dashed curve) with a lattice composed of TST building blocks (the solid curves). (b) Transmission probability for one (in red) and $N = 10^6$ TST barriers (in black). If the first triangular potential is such that $V(x) = V_b[(x-a)/(b-a)]$, the square is $V(x) = V_0$ (with width $2f$), and the last triangular is $V(x) = V_c[(d-x)/(d-c)]$, in this case: $a = 0.35$, $b \cong 2.74$, $c \cong 3.54$, $d \cong 5.93$, $2f = 0.8$, $V_a = V_d = 0$, $V_b = V_c = V_0 = 1$, $L = 0.35$ and $d_{12} = d_{23} = 0$.

4.2.3 A quintuple building block

Other intriguing continuous potentials can be simulated by a composed BB as well. For now, consider that the potential in question has a Gaussian distribution-like shape, i.e., the potential is such that

$$V(x) = \exp\left[-\frac{(x-\mu)^2}{2\sigma^2}\right], \tag{4.61}$$

where μ and σ are analogous to the mean and the standard deviation. Employing a *quintuple building block*, TTSTT, the simulation can be made as schematized in Figure 4.32. Notice that this potential has a format *similar* to a Gaussian distribution, moreover, μ and σ are not statistic quantities but they are related, respectively, to the position center and the height and width of the BB[15]. It is clear that to obtain the scattering coefficients for this BB (the general TTSTT) it is required to use the recurrence relations four times, given rise to d_{12}, d_{23}, d_{34} and d_{45} when analyzing the sets TT, (TT)S, (TTS)T and (TTST)T, respectively (see Figure 4.33). To reproduce the format of a Gaussian distribution, we have to do $d_{12} = d_{23} = d_{34} = d_{45} = 0$ and then choose the correct parameters for the elementary potentials.

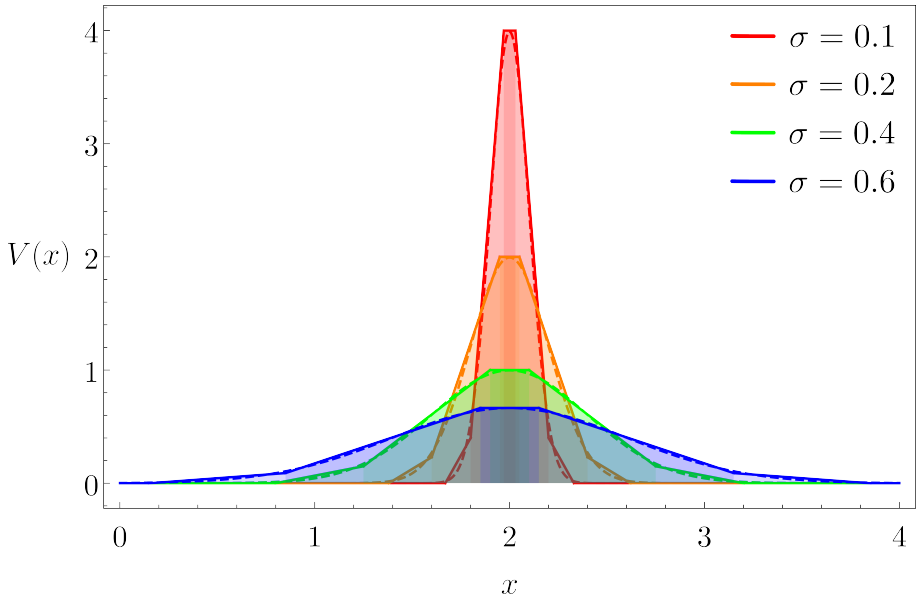

Figure 4.32: Modeling the Gaussian distribution for $\mu = 2$ and different standard deviations (the dashed curves) with TTSTT building blocks (the solid curves). Notice that for all standard deviation values, it is needed the following sequence of elementary potentials: triangular, trapezoidal, square, trapezoidal, and triangular, all represented by different opacities of the corresponding color.

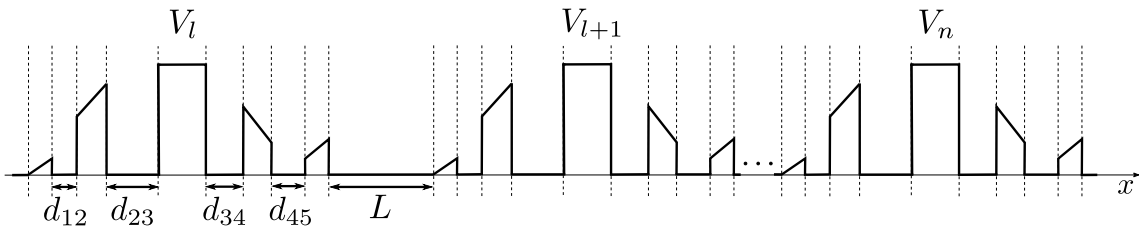

Figure 4.33: System composed of $N = n - l + 1$ TTSTT potentials, spaced by a length L.

Figure 4.34 shows the graphics of transmission probability for the TTSTT associated with the Gaussian distributions presented in Figure 4.32. The colorful curves are the

[15]The Equation (4.61) defines the potential such that the areas inside the barrier are always equal to one, thus, when σ increases the barrier width also increases while the barrier height decreases.

transmission probabilities for just one barrier, and we notice that as the standard deviation increases the curve converges more quickly to one. The black curves represent the transmission probability for a hundred BBs. Although we can analyze more significant lattices with the approach of this work (as seen before) this number of TTSTT ($N = 100$) was chosen to show how the allowed bands get thinner (and therefore more fulfilled) as the standard deviation increases (that is, the cells become wider and lower). The study of the scattering by one Gaussian barrier was made in [92, 93, 94], with different approaches, where the curves for the transmission probabilities are similar to those we present here. For comparison purposes, unfortunately, we do not know any work that investigates scattering by more than one Gaussian barrier.

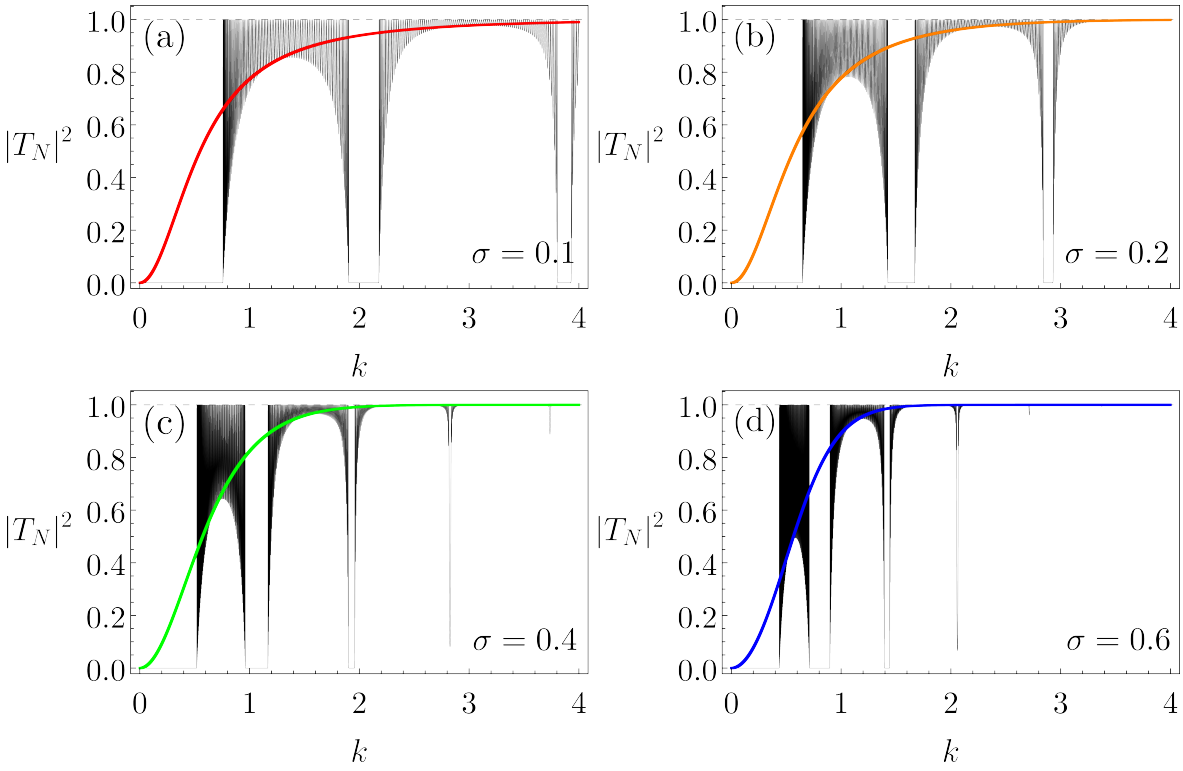

Figure 4.34: Transmission probability for the TTSTT associated with different values of standard deviation. The colorful and black curves correspond, respectively, to the plots for $N = 1$ and $N = 100$ TTSTT building blocks.

If the Gaussian distribution represents the interaction of a crystal lattice site with an incident electron, the center of mass of each site coincides with the mean and the standard deviation with the range and intensity of interaction. If the interaction loses intensity (i.e. loses height), increasing the range of the interaction (that is, its width) is not enough to keep the transmission probability constant in this case, although the area of the sites is kept constant (equal to one). Lastly, note that the employment of the trapezoidal walls makes the modeling of continuous potentials straightforward. If only square potentials were used, as in [62], peak shape continuous potentials would require more barriers in each BB, making the calculations complicated.

Chapter 5

Conclusion

In this work we have proposed a novel approach for the one-dimensional quantum scattering problem in periodic structures. The key idea has been to employ the exact Green's function for a single (localized) building block (or unit cell) of such structure, as already discussed in the literature. Hence we have found recurrence relations for the reflections and transmission coefficients. Such relations have been demonstrated rigorously and can be applied to the most general case: an arbitrary set of compact support potentials. This has enabled the study of more complex lattices since with the recurrence relations the scattering amplitudes for the most diverse building blocks can be calculated.

Since the reflections and transmission coefficients can be written in terms of an auxiliary function, $C_N(k)$, which is a continued fraction depending only on the amplitudes of the unit cell, the behavior of a lattice formed by any number of building blocks (N) has been unraveled. To simplify the calculations, an additional strategy has been adopted: the properties of the continued fractions have made it possible to write $C_N(k)$ in a reduced form, where the number of BBs in the periodic potential become exponents of functions. Although $C_N(k)$ is an auxiliary function, since we are often interested in the reflection and transmission coefficients of the lattice, we have showed that $C_N(k)$ also carries the scattering properties.

To restrict ourselves to an analytical study, exact solved compact support potentials have been used as a basis: the Dirac delta, the square wall, and trapezoidal wall. The lattices composed of these three single building blocks have been deeply analyzed, especially the associated transmission probabilities, and the results have been successfully compared with the literature. Indeed the filling of allowed energy bands with the increase of BB's number has been observed. Moreover, we have noticed that the number of peaks — where the transmission probability is equal to one — in each allowed band is equal to $N - 1$, as expected.

In addition, we have applied our method to situations where the building blocks are compositions of two or more basic localized potentials, including the cases that may simulate a continuous potential — as the square sine of half x function and the Gaussian

distribution. The use of the trapezoidal wall has proved to be essential, since it has made the modeling of peak shape continuous potentials more straightforward. We reinforce that all the results have been obtained in a very intuitive form, and that large lattices have been scrutinized — with N in the order of a million, so we conclude that our methodology is reliable and fruitful.

As a future study, we intend to apply our approach to the materials area, aiming to predict some properties that could be calculated with the scattering amplitudes. Previous experimental works, that used the transfer matrix method as theoretical modeling, could be improved with our technique. Some examples are the study of conductance, transmittance, or absorption in multi-junction solar cells [57], graphene layer materials [50, 95], conjugated polymers [96, 97], and organic semiconductors [98].

An investigation about the potential shape and the intrinsic characteristics of the material also could be realized. Another possible application of our method is the study of a few impurities or defects in a periodic lattice, aiming to study the impact of their shape and lattice position. In addition, the impact of periodicity break, so present in gap solitons [99, 100, 101, 102], could be studied as well.

Moreover, there are papers in diverse fields that employed the transfer matrix method and could be advanced, as in acoustics [103, 104, 105, 106, 107], electromagnetics and optics [108, 109], nanophotonics [110], organic thin films [111], multibody systems (Rui method) [112], and even in the identification of bacteria [113].

Focusing on the theoretical area, another further (and simpler) work could be the analysis of electron transmission through semiconductor superlattices, especially the coupling of different modes with the unit cell, similarly as done in [77]. We also could study the scattering by Cantor-like potentials, that are known to present multifractality in the transmission probability [114]. We suspect that multifractality is present also in not multifractal potentials (the Cantor-like potentials have a multifractal shape).

We could also consider potentials that have no analytic solution and then couple our method with numerical solution approaches to create a more general mixed technique. Our approach can be used to calculate the density of states, i.e., the number of modes per energy too. A final future work could be to expand our technique to scattering problems where the spreader is a well (an attractive potential) and not a barrier (a repulsive potential, as it was done in this work).

Appendix A

Demonstration of the scattering coefficients for the trapezoidal barrier

We aim to calculate the scattering amplitudes for the case of a particle (with mass m) that is spread by a potential such that

$$V(x) = -\frac{(V_a - V_b)}{(b-a)}x + \frac{(V_a b - V_b a)}{(b-a)}, \tag{A.1}$$

which corresponds to a trapezoidal potential as shown in Figure 4.15. Notice that $V(a) = V_a$ and $V(b) = V_b$.

Dividing the space problem into the regions: (I) $x < a$, (II) $a < x < b$, and (III) $x > b$, the Schrödinger equation in the region (II) is $[-(\hbar^2/2m)(d^2/dx^2) + V(x)]\psi(x) = E\psi(x)$, or yet,

$$\Big[-\frac{\hbar^2}{2m}\frac{d^2}{dx^2} - \frac{(V_a - V_b)}{(b-a)}x + \frac{(V_a b - V_b a)}{(b-a)}\Big]\psi(x) = E\psi(x). \tag{A.2}$$

Defining

$$\alpha = \frac{2m}{\hbar^2}\frac{(V_a - V_b)}{(b-a)}, \quad \beta = \frac{2m}{\hbar^2}\frac{(V_a b - V_b a)}{(b-a)} \text{ and } k^2 = \frac{2mE}{\hbar^2}, \tag{A.3}$$

we find,

$$\Big(-\frac{d^2}{dx^2} - \alpha x + \beta - k^2\Big)\psi(x) = 0. \tag{A.4}$$

The Equation (A.4) can be rewritten strategically as

$$\Big\{-\frac{1}{\alpha}\frac{d^2}{dx^2} + \Big[-x + \frac{(\beta - k^2)}{\alpha}\Big]\Big\}\psi(x) = \Big\{-\alpha^{-\frac{2}{3}}\frac{d^2}{dx^2} + \Big[-x + \frac{(\beta - k^2)}{\alpha}\Big]\alpha^{\frac{1}{3}}\Big\}\psi(x) = 0. \tag{A.5}$$

Setting $y = [-x + (\beta - k^2)/\alpha]\alpha^{1/3}$, it is easy to see that

$$\frac{d^2}{dy^2} = \alpha^{-\frac{2}{3}}\frac{d^2}{dx^2}, \tag{A.6}$$

so the Equation (A.5) reduces to

$$\Big(-\frac{d^2}{dy^2} + y \Big)\varphi(y) = 0, \tag{A.7}$$

where $\psi(x) = \varphi(y)$. The Equation (A.7) is the Airy equation and the possible solutions are the Airy functions $\mathrm{Ai}(y)$ and $\mathrm{Bi}(y)$ [115]. In other words, the general solution for the equation above is

$$\varphi(y) = \mathcal{A}\mathrm{Ai}(y) + \mathcal{B}\mathrm{Bi}(y), \tag{A.8}$$

in the region (II), where $a < x < b$.

At this point, it is necessary to examine two cases separately, since the incident wave can come from **(i)** left and **(ii)** right.

(i) For an incident wave coming from the left, once in the regions (I) and (III) the particle is free, the general solution for the whole problem is

$$\psi(x) = \begin{cases} \exp[ikx] + \mathcal{R}^{(+)}\exp[-ikx], & x < a \\ \mathcal{A}^{(+)}\mathrm{Ai}[y(x)] + \mathcal{B}^{(+)}\mathrm{Bi}[y(x)], & a < x < b \\ \mathcal{T}^{(+)}\exp[ikx], & x > b \end{cases} \tag{A.9}$$

with the boundary conditions: **(a)** $\psi_I(x=a) = \psi_{II}(x=a)$, **(b)** $\psi_{II}(x=b) = \psi_{III}(x=b)$, **(c)** $\psi'_I(x=a) = \psi'_{II}(x=a)$, and **(d)** $\psi'_{II}(x=b) = \psi'_{III}(x=b)$, where $\psi' = d\psi/dx$.

Applying the boundary conditions described above, we obtain the following system of equations:

$$\begin{cases} \mathcal{A}^{(+)}\mathrm{Ai}(y_a) + \mathcal{B}^{(+)}\mathrm{Bi}(y_a) - \exp[ika] - \mathcal{R}^{(+)}\exp[-ika] = 0 & \textbf{(a)} \\ \mathcal{A}^{(+)}\mathrm{Ai}(y_b) + \mathcal{B}^{(+)}\mathrm{Bi}(y_b) - \mathcal{T}^{(+)}\exp[ikb] = 0 & \textbf{(b)} \\ \Big[\mathcal{A}^{(+)}\mathrm{Ai}'(y_a) + \mathcal{B}^{(+)}\mathrm{Bi}'(y_a)\Big]\alpha^{\frac{1}{3}} + ik(\exp[ika] - \mathcal{R}^{(+)}\exp[-ika]) = 0 & \textbf{(c)} \\ \Big[\mathcal{A}^{(+)}\mathrm{Ai}'(y_b) + \mathcal{B}^{(+)}\mathrm{Bi}'(y_b)\Big]\alpha^{\frac{1}{3}} + ik\mathcal{T}^{(+)}\exp[ikb] = 0 & \textbf{(d)} \end{cases} \tag{A.10}$$

where $y_c = y|_{x=c} = y(x=c)$ and $F'(y_c) = dF(y_c)/dy_c$, with $c = a, b$.

Solving this system, we have

$$\mathcal{T}^{(+)}(k) = -\exp[-(b-a)k]\frac{2\eta(k)}{\pi C^{(+)}(k)} \quad \text{and} \quad \mathcal{R}^{(+)}(k) = \exp[2iak]\frac{D^{(+)}(k)}{C^{(+)}(k)}, \tag{A.11}$$

where $\eta(k) = i\alpha^{1/3}/k$,

$$\begin{aligned} C^{(+)}(k) = {} & [\mathrm{Ai}(y_a) + \eta(k)\mathrm{Ai}'(y_a)][\mathrm{Bi}(y_b) - \eta(k)\mathrm{Bi}'(y_b)] \\ & - [\mathrm{Ai}(y_b) - \eta(k)\mathrm{Ai}'(y_b)][\mathrm{Bi}(y_a) + \eta(k)\mathrm{Bi}'(y_a)], \end{aligned} \tag{A.12}$$

and

$$\begin{aligned} D^{(+)}(k) = {} & [\mathrm{Ai}(y_a) - \eta(k)\mathrm{Ai}'(y_a)][\mathrm{Bi}(y_b) - \eta(k)\mathrm{Bi}'(y_b)] \\ & - [\mathrm{Ai}(y_b) - \eta(k)\mathrm{Ai}'(y_b)][\mathrm{Bi}(y_a) - \eta(k)\mathrm{Bi}'(y_a)]. \end{aligned} \tag{A.13}$$

Since $\mathcal{T}^{(+)}(k) = \exp[-(b-a)k]t^{(+)}(k)$ and $\mathcal{R}^{(+)}(k) = \exp[2iak]r^{(+)}(k)$, we conclude that

$$t^{(+)}(k) = -\frac{2\eta(k)}{\pi C^{(+)}(k)} \quad \text{and} \quad r^{(+)}(k) = \frac{D^{(+)}(k)}{C^{(+)}(k)}. \tag{A.14}$$

(ii) Now, for an incident wave coming from the right, the general solution is

$$\psi(x) = \begin{cases} \exp[-ikx] + \mathcal{R}^{(-)}\exp[ikx], & x > b \\ \mathcal{A}^{(-)}\mathrm{Ai}[y(x)] + \mathcal{B}^{(-)}\mathrm{Bi}[y(x)], & a < x < b \\ \mathcal{T}^{(-)}\exp[-ikx], & x < a \end{cases} \tag{A.15}$$

with the same boundary conditions — **(a)** to **(d)**.

Implementing the boundary conditions and solving the associated system, similarly to item **(i)**, we find

$$\mathcal{T}^{(-)}(k) = -\exp[-(b-a)k]\frac{2\eta(k)}{\pi C^{(-)}(k)} \quad \text{and} \quad \mathcal{R}^{(-)}(k) = \exp[-2ibk]\frac{D^{(-)}(k)}{C^{(-)}(k)}, \tag{A.16}$$

where $\eta(k) = i\alpha^{1/3}/k$,

$$\begin{aligned} C^{(-)}(k) = {} & [\mathrm{Ai}(y_a) + \eta(k)\mathrm{Ai}'(y_a)][\mathrm{Bi}(y_b) - \eta(k)\mathrm{Bi}'(y_b)] \\ & - [\mathrm{Ai}(y_b) - \eta(k)\mathrm{Ai}'(y_b)][\mathrm{Bi}(y_a) + \eta(k)\mathrm{Bi}'(y_a)], \end{aligned} \tag{A.17}$$

and

$$\begin{aligned} D^{(-)}(k) = {} & [\mathrm{Ai}(y_a) + \eta(k)\mathrm{Ai}'(y_a)][\mathrm{Bi}(y_b) + \eta(k)\mathrm{Bi}'(y_b)] \\ & - [\mathrm{Ai}(y_b) + \eta(k)\mathrm{Ai}'(y_b)][\mathrm{Bi}(y_a) + \eta(k)\mathrm{Bi}'(y_a)]. \end{aligned} \tag{A.18}$$

As $\mathcal{T}^{(-)}(k) = \exp[-(b-a)k]t^{(-)}(k)$ and $\mathcal{R}^{(-)}(k) = \exp[-2ibk]r^{(-)}(k)$, then

$$t^{(-)}(k) = -\frac{2\eta(k)}{\pi C^{(-)}(k)} \quad \text{and} \quad r^{(-)}(k) = \frac{D^{(-)}(k)}{C^{(-)}(k)}. \tag{A.19}$$

Comparing the Equations (A.12) and (A.17) we see that $C^{(+)}(k) = C^{(-)}(k) = C(k)$, so $t^{(+)}(k) = t^{(-)}(k) = t(k)$ (and $\mathcal{T}^{(+)}(k) = \mathcal{T}^{(-)}(k) = \mathcal{T}(k)$), as expected. Finally, with the Equations (A.12) to (A.19) we recover the Equations (4.57) to (4.59) from Section 4.1.

Appendix B

Technique of the exact Green's function: some examples

To understand more deeply the technique present in Equation (2.47), let us analyze some examples of scattering paths and the associated Green's function terms. For this, consider a wave that is spread by three compact support potentials, V_1, V_2, and V_3, as shown in Figure B.1. In the same figure, we represent three — of the infinitely possible — s.p. by colorful arrows. Assume that the individual scattering amplitudes for the potentials are t_j and $r_j^{(\pm)}$, with $j = 1, 2, 3$, where the index $(\pm)$ means that the wave is coming from the left (right) an instant before colliding with the barrier[1]. Moreover, consider that the Green's functions terms for the red, green, and blue s.p. are, respectively, $G_r(x_f, x_i; k)$, $G_g(x_f, x_i; k)$ and $G_b(x_f, x_i; k)$.

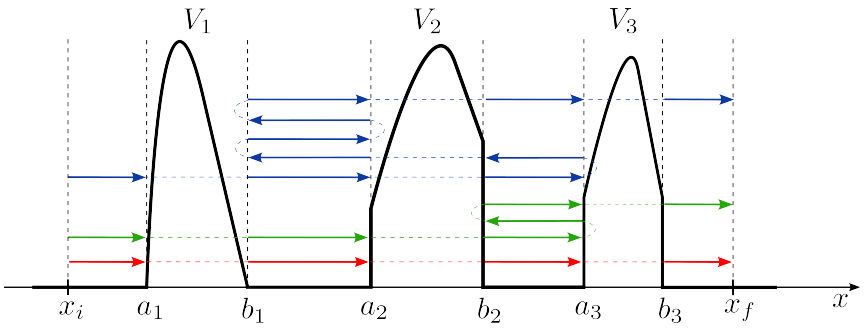

Figure B.1: System formed by three compact support potentials, where three — of the infinitely possible — different scattering paths are represented by the colorful arrows.

The red s.p. is the simplest one: the particle gets out of the position x_i and is transmitted by all the three potentials until reaches x_f. Therefore, the whole amplitude is $W_r = t_1 t_2 t_3$ and the classical action[2] is such that $S_r = k[(a_1 - x_i) + (a_2 - b_1) + (a_3 - b_2) +$

[1]We know that $t_j = t_j(k)$ and $r_j^{(\pm)} = r_j^{(\pm)}(k)$, but for simplicity, the wavenumber dependence will be suppressed here.

[2]Remember that the computed length only refers to the path outside the potentials.

$(x_f - b_3)]$. So, $G_r(x_f, x_i; k) = t_1 t_2 t_3 \exp\{ik/\hbar[(a_1 - x_i) + (a_2 - b_1) + (a_3 - b_2) + (x_f - b_3)]\}$. The green s.p. is a little different: after being transmitted by the two first potentials, the particle is reflected by V_3 (from the left) and by V_2 (from the right), for then be transmitted for V_3 and reaches the endpoint. Thus, we have: $W_g = t_1 t_2 r_3^{(+)} r_2^{(-)} t_3$ and $S_g = k[(a_1 - x_i) + (a_2 - b_1) + 3(a_3 - b_2) + (x_f - b_3)]$, and, of course, $G_g(x_f, x_i; k) = t_1 t_2 r_3^{(+)} r_2^{(-)} t_3 \exp\{ik/\hbar[(a_1 - x_i) + (a_2 - b_1) + 3(a_3 - b_2) + (x_f - b_3)]\}$.

In the blue s.p., the wave is transmitted by the first two barriers too, but then it is reflected by the last one, transmitted by V_2 (from the right), and "bounces" three times between potentials V_1 and V_2 for finally be transmitted by V_2 and V_3. Therefore, we have $W_b = t_1 (t_2)^3 r_3^{(+)} \left(r_1^{(-)}\right)^2 r_2^{(+)} t_3$ and $S_b = k[(a_1 - x_i) + 5(a_2 - b_1) + 3(a_3 - b_2) + (x_f - b_3)]$, what means that $G_g(x_f, x_i; k) = t_1 (t_2)^3 r_3^{(+)} \left(r_1^{(-)}\right)^2 r_2^{(+)} t_3 \exp\{ik/\hbar[(a_1 - x_i) + 5(a_2 - b_1) + 3(a_3 - b_2) + (x_f - b_3)]\}$. It is worth remembering that there are infinitely possible scattering paths, which fortunately converge to a geometric series, as seen in Chapter 3.

Bibliography

[1] E. S. Hedges, *Physico-Chemical Periodicity*. The University of Manchester (United Kingdom), 1930.

[2] C. Kittel and P. McEuen, *Introduction to solid state physics*. John Wiley & Sons, 2018.

[3] P. Pereyra, *Fundamentals of Quantum Physics: Textbook for Students of Science and Engineering*. Springer Science & Business Media, 2012.

[4] F. Bloch, "Über die quantenmechanik der elektronen in kristallgittern," *Zeitschrift für physik*, vol. 52, no. 7-8, pp. 555–600, 1929.

[5] R. L. Kronig and W. G. Penney, "Quantum mechanics of electrons in crystal lattices," *Proceedings of the royal society of London. Series A, containing papers of a mathematical and physical character*, vol. 130, no. 814, pp. 499–513, 1931.

[6] P. Pereyra, "The transfer matrix method and the theory of finite periodic systems: from heterostructures to superlattices," *Physica Status Solidi B*, vol. 259, no. 3, p. 2100405, 2022.

[7] D. Kiang, "Multiple scattering by a Dirac comb," *American Journal of Physics*, vol. 42, no. 9, pp. 785–787, 1974.

[8] D. J. Griffiths and N. F. Taussig, "Scattering from a locally periodic potential," *American journal of physics*, vol. 60, no. 10, pp. 883–888, 1992.

[9] D. W. L. Sprung, H. Wu, and J. Martorell, "Scattering by a finite periodic potential," *American Journal of Physics*, vol. 61, no. 12, pp. 1118–1124, 1993.

[10] J. P. Vigneron and P. Lambin, "Transmission coefficient for one-dimensional potential barriers using continued fractions," *Journal of Physics A: Mathematical and General*, vol. 13, no. 4, p. 1135, 1980.

[11] P. Lambin and J. P. Vigneron, "Improved continued fraction treatment of the one-dimensional scattering problem," *Journal of Physics A: Mathematical and General*, vol. 14, no. 7, p. 1815, 1981.

[12] J. Horáček and T. Sasakawa, "Method of continued fractions with application to atomic physics," *Physical Review A*, vol. 28, no. 4, p. 2151, 1983.

[13] J. Horáček and T. Sasakawa, "Method of continued fractions with application to atomic physics II," *Physical Review A*, vol. 30, no. 5, p. 2274, 1984.

[14] J. Horáček and T. Sasakawa, "Method of continued fractions for on-and off-shell T matrix of local and nonlocal potentials," *Physical Review C*, vol. 32, no. 1, p. 70, 1985.

[15] N. Ahmed, S. Z. Alamri, and M. Rassem, "Probing Schrödinger's equation with a continued fraction potential," *NRIAG Journal of Astronomy and Geophysics*, vol. 7, no. 1, pp. 1–3, 2018.

[16] H. Mori, "A continued-fraction representation of the time-correlation functions," *Progress of Theoretical Physics*, vol. 34, no. 3, pp. 399–416, 1965.

[17] M. W. Evans, P. Grigolini, and G. P. Parravicini, *Memory Function Approaches to Stochastic Problems in Condensed Matter*, vol. 62. John Wiley & Sons, 2009.

[18] P. Hänggi, F. Rösel, and D. Trautmann, "Continued fraction expansions in scattering theory and statistical non-equilibrium mechanics," *Zeitschrift Für Naturforschung A*, vol. 33, no. 4, pp. 402–417, 1978.

[19] E. R. Vrscay and J. Cizek, "Continued fractions and Rayleigh–Schrödinger perturbation theory at large order," *Journal of Mathematical Physics*, vol. 27, no. 1, pp. 185–201, 1986.

[20] D. V. Chudnovsky and G. V. Chudnovsky, "Explicit continued fractions and quantum gravity," *Acta Applicandae Mathematica*, vol. 36, no. 1, pp. 167–185, 1994.

[21] J. Bissell and A. Nagaitis, "Infinity, self-similarity, and continued fractions in physics: applications to resistor network puzzles," *Physics Education*, vol. 57, no. 5, p. 055014, 2022.

[22] A. Wierling, "Fitting the dielectric response of collisionless plasmas by continued fractions," *Physics of Plasmas*, vol. 16, no. 11, p. 112105, 2009.

[23] H. Müller, "Physics of irrational numbers," *Progress in Physics*, vol. 18, 2022.

[24] K. Hattori, T. Hattori, and H. Watanabe, "Block spin approach to the singularity properties of the continued fractions," *Communications in Mathematical Physics*, vol. 115, no. 1, pp. 31–48, 1988.

[25] C. Cohen-Tannoudji, B. Diu, and F. Laloë, *Quantum Mechanics*, vol. 2. John Wiley & Sons, 1986.

[26] R. Shankar, *Principles of quantum mechanics*. Springer Science, 1994.

[27] E. Merzbacher, *Quantum mechanics*. Jones & Bartlett Publishers, 1961.

[28] G. Baym, *Lectures on quantum mechanics*. ABP, 1990.

[29] D. J. Griffiths, *Introduction to quantum mechanics*, vol. 1. Prentice Hall, 2005.

[30] J. J. Sakurai and E. D. Commins, *Modern Quantum Mechanics*. American Association of Physics Teachers, 1995.

[31] M. G. E. da Luz, E. J. Heller, and B. K. Cheng, "Exact form of Green's functions for segmented potentials," *Journal of Physics A: Mathematical and General*, vol. 31, no. 13, p. 2975, 1998.

[32] H. Iwamoto, V. M. Aquino, and V. C. Aguilera-Navarro, "Scattering coefficients for a trapezoidal potential," *International Journal of Theoretical Physics*, vol. 42, no. 8, pp. 1795–1807, 2003.

[33] Q. Luo, Y. Jiang, L. Shen, W. Xu, and J. Han, "Calculation of the transmission coefficient for one-dimensional trapezoid potential barrier," *University Physics*, vol. 33, no. 12, pp. 42–42, 2014.

[34] T. M. Kalotas and A. R. Lee, "One-dimensional quantum interference," *European Journal of Physics*, vol. 12, no. 6, p. 275, 1991.

[35] D. J. Vezzetti and M. M. Cahay, "Transmission resonances in finite, repeated structures," *Journal of Physics D: Applied Physics*, vol. 19, no. 4, p. L53, 1986.

[36] D. Bar and L. P. Horwitz, "Dynamical effects of a one-dimensional multibarrier potential of finite range," *The European Physical Journal B-Condensed Matter and Complex Systems*, vol. 25, no. 4, pp. 505–518, 2002.

[37] P. R. Berman, "Transmission resonances and bloch states for a periodic array of delta function potentials," *American Journal of Physics*, vol. 81, no. 3, pp. 190–201, 2013.

[38] S. Das, "Tunneling through one-dimensional piecewise-constant potential barriers," *American Journal of Physics*, vol. 83, no. 7, pp. 590–599, 2015.

[39] P. Pereyra and E. Castillo, "Theory of finite periodic systems: general expressions and various simple and illustrative examples," *Physical Review B*, vol. 65, no. 20, p. 205120, 2002.

[40] P. Su, Z. Cao, K. Chen, C. Yin, and Q. Shen, "Explicit expression for the reflection and transmission probabilities through an arbitrary potential barrier," *Journal of Physics A: Mathematical and Theoretical*, vol. 41, no. 46, p. 465301, 2008.

[41] J. S. Walker and J. Gathright, "Exploring one-dimensional quantum mechanics with transfer matrices," *American Journal of Physics*, vol. 62, no. 5, pp. 408–422, 1994.

[42] P. H. Grossel and J. M. Vigoureux, "Calculation of wave functions and of energy levels: application to multiple quantum wells and continuous potential," *Physical Review A*, vol. 55, no. 1, p. 796, 1997.

[43] M.-T. Lee, I. Iga, M. M. Fujimoto, and O. Lara, "The method of continued fractions for electron (positron)-atom scattering," *Journal of Physics B: Atomic, Molecular and Optical Physics*, vol. 28, no. 9, p. L299, 1995.

[44] M.-T. Lee, I. Iga, M. M. Fujimoto, and O. Lara, "Application of the method of continued fractions for electron scattering by linear molecules," *Journal of Physics B: Atomic, Molecular and Optical Physics*, vol. 28, no. 15, p. 3325, 1995.

[45] M.-T. Lee, M. M. Fujimoto, and I. Iga, "Application of the method of continued fractions to low-energy electron scattering by the hydrogen molecule," *Journal of Molecular Structure: THEOCHEM*, vol. 394, no. 2-3, pp. 117–125, 1997.

[46] N. L. Harshman and P. Singh, "Entanglement mechanisms in one-dimensional potential scattering," *Journal of Physics A: Mathematical and Theoretical*, vol. 41, no. 15, p. 155304, 2008.

[47] J. R. Ott, N. A. Mortensen, and P. Lodahl, "Quantum interference and entanglement induced by multiple scattering of light," *Physical review letters*, vol. 105, no. 9, p. 090501, 2010.

[48] R. Ghosh and A. Das, "Disorder-induced enhancement of entanglement growth in one dimension: information leakage at the scale of the localization length," *Physical Review B*, vol. 103, no. 2, p. 024202, 2021.

[49] J. Dajka, M. Mierzejewski, and J. Łuczka, "Analytically solvable model for the entanglement via scattering-like mechanisms," *Quantum Information Processing*, vol. 8, no. 5, pp. 461–475, 2009.

[50] L. G. Wang and S. Y. Zhu, "Electronic band gaps and transport properties in graphene superlattices with one-dimensional periodic potentials of square barriers," *Physical Review B*, vol. 81, no. 20, p. 205444, 2010.

[51] P. A. Kalozoumis, G. Theocharis, V. Achilleos, S. Félix, O. Richoux, and V. Pagneux, "Finite-size effects on topological interface states in one-dimensional scattering systems," *Physical Review A*, vol. 98, no. 2, p. 023838, 2018.

[52] A. T. Tilke, F. C. Simmel, H. Lorenz, R. H. Blick, and J. P. Kotthaus, "Quantum interference in a one-dimensional silicon nanowire," *Physical Review B*, vol. 68, no. 7, p. 075311, 2003.

[53] G. Buchs, D. Bercioux, P. Ruffieux, P. Gröning, H. Grabert, and O. Gröning, "Electron scattering in intrananotube quantum dots," *Physical review letters*, vol. 102, no. 24, p. 245505, 2009.

[54] E. Glushkov, N. Glushkova, A. Eremin, and R. Lammering, "Trapped modes and resonance wave transmission in a plate with a system of notches," *Journal of Sound and Vibration*, vol. 412, pp. 360–371, 2018.

[55] O. Richoux, V. Tournat, and T. Le Van Suu, "Acoustic wave dispersion in a one-dimensional lattice of nonlinear resonant scatterers," *Physical Review E*, vol. 75, no. 2, p. 026615, 2007.

[56] X. Fang, Y. Bando, U. K. Gautam, T. Zhai, S. Gradečak, and D. Golberg, "Heterostructures and superlattices in one-dimensional nanoscale semiconductors," *Journal of Materials Chemistry*, vol. 19, no. 32, pp. 5683–5689, 2009.

[57] A. Gonzalo, A. D. Utrilla, D. F. Reyes, V. Braza, J. M. Llorens, D. Fuertes-Marrón, B. Alén, T. Ben, D. González, A. Guzman, *et al.*, "Strain-balanced type-II superlattices for efficient multi-junction solar cells," *Scientific Reports*, vol. 7, no. 1, pp. 1–10, 2017.

[58] J. D. Jackson, *Classical electrodynamics*. American Association of Physics Teachers, 1999.

[59] G. B. Arfken, H. J. Weber, and F. E. Harris, *Mathematical Methods for Physicists*. Elsevier, 2013.

[60] E. N. Economou, *Green's functions in quantum physics*, vol. 7. Springer Science & Business Media, 2006.

[61] M. C. Gutzwiller, *Chaos in classical and quantum mechanics*, vol. 1. Springer Science & Business Media, 2013.

[62] T. M. Kalotas and A. R. Lee, "A new approach to one-dimensional scattering," *American Journal of Physics*, vol. 59, no. 1, pp. 48–52, 1991.

[63] F. M. Zanetti, J. Kuhn, G. J. Delben, B. K. Cheng, and M. G. E. da Luz, "Classifying the general family of 1D point interactions: a scattering approach," *Journal of Physics A: Mathematical and General*, vol. 39, no. 10, p. 2493, 2006.

[64] Z. M. Ibran, E. A. Aljatlawi, and A. M. Awin, "On continued fractions and their applications," *Journal of Applied Mathematics and Physics*, vol. 10, no. 1, pp. 142–159, 2022.

[65] W. B. Jones and W. J. Thron, *Continued fractions: Analytic theory and applications*, vol. 11. Addison-Wesley Publishing Company, 1980.

[66] O. N. Karpenkov, "Geometric continued fractions," in *Geometry of Continued Fractions*, pp. 87–96, Springer, 2022.

[67] D. Hensley, *Continued fractions*. World Scientific, 2006.

[68] M. G. Rozman, P. Reineker, and R. Tehver, "One-dimensional scattering: Recurrence relations and differential equations for transmission and reflection amplitudes," *Physical Review A*, vol. 49, no. 5, p. 3310, 1994.

[69] A. Schmidt, B. K. Cheng, and M. G. E. da Luz, "Green's functions for generalized point interactions in one dimension: a scattering approach," *Physical Review A*, vol. 66, no. 6, p. 062712, 2002.

[70] K. Chadan and P. C. Sabatier, *Inverse problems in quantum scattering theory*. Springer Science & Business Media, 2012.

[71] D. H. Greene and D. E. Knuth, *Mathematics for the Analysis of Algorithms*, vol. 504. Springer, 1990.

[72] O. Levin, *Discrete mathematics: An open introduction*. 2021.

[73] B. Simon, "The bound state of weakly coupled schrödinger operators in one and two dimensions," *Annals of Physics*, vol. 97, no. 2, pp. 279–288, 1976.

[74] Y. D. Chong, "Quantum Mechanics III. Chapter 2: Resonances." http://www1.spms.ntu.edu.sg/~ydchong/teaching/PH4401_02_resonances.pdf. Online; accessed January 30, 2023.

[75] S. E. Ulloa, E. Castao, and G. Kirczenow, "Ballistic transport in a novel one-dimensional superlattice," *Physical Review B*, vol. 41, no. 17, p. 12350, 1990.

[76] G. A. Luna-Acosta, H. Schanze, U. Kuhl, and H. J. Stöckmann, "Impurity effects on the band structure of one-dimensional photonic crystals: experiment and theory," *New Journal of Physics*, vol. 10, no. 4, p. 043005, 2008.

[77] X. Luo, J. Shi, Y. Zhang, Z. Niu, D. Miao, H. Mi, and W. Huang, "Filtering electrons by mode coupling in finite semiconductor superlattices," *Scientific Reports*, vol. 12, no. 1, pp. 1–8, 2022.

[78] Y. He, Z. Cao, and Q. Shen, "Analytical formula of the transmission probabilities across arbitrary potential barriers," *Journal of Physics A: Mathematical and General*, vol. 38, no. 25, p. 5771, 2005.

[79] T. E. Hartman and J. S. Chivian, "Electron tunneling through thin aluminum oxide films," *Physical Review*, vol. 134, no. 4A, p. A1094, 1964.

[80] A. Schenk and G. Heiser, "Modeling and simulation of tunneling through ultra-thin gate dielectrics," *Journal of applied physics*, vol. 81, no. 12, pp. 7900–7908, 1997.

[81] L. Wei-Yi, R. Guo-Ping, J. Yu-Long, and R. Gang, "Trapezoid mesa trench metal-oxide semiconductor barrier schottky rectifier: an improved schottky rectifier with better reverse characteristics," *Chinese Physics B*, vol. 20, no. 8, p. 087304, 2011.

[82] F. Ambriz-Vargas, G. Kolhatkar, M. Broyer, A. Hadj-Youssef, R. Nouar, A. Sarkissian, R. Thomas, C. Gomez-Yáñez, M. A. Gauthier, and A. Ruediger, "A complementary metal oxide semiconductor process-compatible ferroelectric tunnel junction," *ACS applied materials & interfaces*, vol. 9, no. 15, pp. 13262–13268, 2017.

[83] M. Dessai and A. V. Kulkarni, "Calculation of tunneling current across trapezoidal potential barrier in a scanning tunneling microscope," *Journal of Applied Physics*, vol. 132, no. 24, p. 244901, 2022.

[84] R. Lefebvre, "Scattering by a triangular barrier," *International Journal of Quantum Chemistry*, vol. 107, no. 14, pp. 2643–2649, 2007.

[85] M. Ohmukai, "Triangular double barrier resonant tunneling," *Materials Science and Engineering: B*, vol. 116, no. 1, pp. 87–90, 2005.

[86] M. Luo, G. Yu, Y. Lin, and J. Su, "Calculation of current density for triangular multi-barrier structure in a constant electric field," *Superlattices and Microstructures*, vol. 74, pp. 78–84, 2014.

[87] N. Kyurkchiev, A. Iliev, and A. Rahnev, *Some Families of Sigmoid Functions: Applications to Growth Theory.* Lap Lambert Academic Publishing Saarbrucken, Germany, 2019.

[88] A. Menon, K. Mehrotra, C. K. Mohan, and S. Ranka, "Characterization of a class of sigmoid functions with applications to neural networks," *Neural networks*, vol. 9, no. 5, pp. 819–835, 1996.

[89] N. Kyurkchiev and S. Markov, "Sigmoid functions: some approximation and modelling aspects," *LAP LAMBERT Academic Publishing, Saarbrucken*, vol. 4, 2015.

[90] L. Shiyu and S. Mingzhu, "Sine-squared potential and semiclassical descriptio for dechanneting process," *Journal of Chongqing Jiaotong University (Natural Science)*, vol. 3, no. 4, p. 7, 1984.

[91] H. Rahbar, "Schrödinger equation with double cosine- and sine-squared potential by Darboux transformation method and super-symmetry," *The African Review of Physics*, vol. 12, 2017.

[92] F. M. Fernández, "Quantum gaussian wells and barriers," *American Journal of Physics*, vol. 79, no. 7, pp. 752–754, 2011.

[93] S. M. Al-Marzoug, "Scattering of solitons by complex PT symmetric gaussian potentials," *Optics Express*, vol. 22, no. 18, pp. 22080–22088, 2014.

[94] R. C. S. Bernardo and J. P. H. Esguerra, "Quantum scattering in one-dimensional systems satisfying the minimal length uncertainty relation," *Annals of Physics*, vol. 375, pp. 444–459, 2016.

[95] T. Zhan, X. Shi, Y. Dai, X. Liu, and J. Zi, "Transfer matrix method for optics in graphene layers," *Journal of Physics: Condensed Matter*, vol. 25, no. 21, p. 215301, 2013.

[96] J. Hwang, D. B. Tanner, I. Schwendeman, and J. R. Reynolds, "Optical properties of nondegenerate ground-state polymers: three dioxythiophene-based conjugated polymers," *Physical Review B*, vol. 67, no. 11, p. 115205, 2003.

[97] Z. Peng, Y. Zhang, Y. Xia, K. Xiong, C. Cai, L. Xia, Z. Hu, K. Zhang, F. Huang, and L. Hou, "One-step coating inverted polymer solar cells using a conjugated polymer as an electron extraction additive," *Journal of Materials Chemistry A*, vol. 3, no. 41, pp. 20500–20507, 2015.

[98] C. Kaiser, S. Zeiske, P. Meredith, and A. Armin, "Determining ultralow absorption coefficients of organic semiconductors from the sub-bandgap photovoltaic external quantum efficiency," *Advanced Optical Materials*, vol. 8, no. 1, p. 1901542, 2020.

[99] Y. S. Kivshar and N. Flytzanis, "Gap solitons in diatomic lattices," *Physical Review A*, vol. 46, no. 12, p. 7972, 1992.

[100] S. O. Demokritov, A. A. Serga, V. E. Demidov, B. Hillebrands, M. P. Kostylev, and B. A. Kalinikos, "Experimental observation of symmetry-breaking nonlinear modes in an active ring," *Nature*, vol. 426, no. 6963, pp. 159–162, 2003.

[101] L. Zeng and J. Zeng, "One-dimensional gap solitons in quintic and cubic–quintic fractional nonlinear Schrödinger equations with a periodically modulated linear potential," *Nonlinear Dynamics*, vol. 98, pp. 985–995, 2019.

[102] N. Pernet, P. St-Jean, D. D. Solnyshkov, G. Malpuech, N. Carlon Zambon, Q. Fontaine, B. Real, O. Jamadi, A. Lemaitre, M. Morassi, *et al.*, "Gap solitons in a one-dimensional driven-dissipative topological lattice," *Nature Physics*, vol. 18, no. 6, pp. 678–684, 2022.

[103] G. Campa and S. M. Camporeale, "Application of transfer matrix method in acoustics," in *European COMSOL Conference*, 2010.

[104] O. Doutres, N. Atalla, and H. Osman, "Transfer matrix modeling and experimental validation of cellular porous material with resonant inclusions," *The Journal of the Acoustical Society of America*, vol. 137, no. 6, pp. 3502–3513, 2015.

[105] J. H. Han, Y. J. Kim, and M. Karkoub, "Modeling of wave propagation in drill strings using vibration transfer matrix methods," *The Journal of the Acoustical Society of America*, vol. 134, no. 3, pp. 1920–1931, 2013.

[106] D. H. Lee and Y. P. Kwon, "Estimation of the absorption performance of multiple layer perforated panel systems by transfer matrix method," *Journal of sound and vibration*, vol. 278, no. 4-5, pp. 847–860, 2004.

[107] K. Verdière, R. Panneton, S. Elkoun, T. Dupont, and P. Leclaire, "Transfer matrix method applied to the parallel assembly of sound absorbing materials," *The Journal of the Acoustical Society of America*, vol. 134, no. 6, pp. 4648–4658, 2013.

[108] T. G. Mackay and A. Lakhtakia, "The transfer-matrix method in electromagnetics and optics," *Synthesis lectures on electromagnetics*, vol. 1, no. 1, pp. 1–126, 2020.

[109] A. Menéndez-Manjón, P. Wagener, and S. Barcikowski, "Transfer-matrix method for efficient ablation by pulsed laser ablation and nanoparticle generation in liquids," *The Journal of Physical Chemistry C*, vol. 115, no. 12, pp. 5108–5114, 2011.

[110] R. B. Balili, "Transfer matrix method in nanophotonics," in *International Journal of Modern Physics: Conference Series*, vol. 17, pp. 159–168, World Scientific, 2012.

[111] L. A. A. Pettersson, L. S. Roman, and O. Inganäs, "Modeling photocurrent action spectra of photovoltaic devices based on organic thin films," *Journal of Applied Physics*, vol. 86, no. 1, pp. 487–496, 1999.

[112] X. Rui, X. Wang, Q. Zhou, and J. Zhang, "Transfer matrix method for multibody systems (Rui method) and its applications," *Science China Technological Sciences*, vol. 62, no. 5, pp. 712–720, 2019.

[113] A. N. Nilsson, G. Emilsson, L. K. Nyberg, C. Noble, L. S. Stadler, J. Fritzsche, E. R. Moore, J. O. Tegenfeldt, T. Ambjörnsson, and F. Westerlund, "Competitive binding-based optical DNA mapping for fast identification of bacteria-multi-ligand transfer matrix theory and experimental applications on Escherichia coli," *Nucleic acids research*, vol. 42, no. 15, pp. e118–e118, 2014.

[114] T. Ogawana and H. Sakaguchi, "Transmission coefficient from generalized Cantor-like potentials and its multifractality," *Physical Review E*, vol. 97, no. 1, p. 012205, 2018.

[115] M. Abramowitz and I. A. Stegun, *Handbook of mathematical functions with formulas, graphs, and mathematical tables*, vol. 55. US Government printing office, 1970.